5-2010

From Mouse Mammary Tumor Model to New Therapeutic Method ---Mammary Tumor Development in Balb/c-Trp53+/- Mice and Magnetic Nanoparticle Induced Heating for Cancer Treatment

Haoheng Yan
University of Massachusetts Amherst

FROM MOUSE MAMMARY TUMOR MODEL TO NEW THERAPEUTIC METHOD

---MAMMARY TUMOR DEVELOPMENT IN BALB/c-*Trp53*+/- MICE AND MAGNETIC NANOPARTICLE INDUCED HEATING FOR CANCER TREATMENT

A Dissertation Presented

by

HAOHENG YAN

Submitted to the Graduate School of the
University of Massachusetts Amherst in partial fulfillment
of the requirements for the degree of

DOCTOR OF PHILOSOPHY

MAY 2010

Molecular and Cellular Biology Program

FROM MOUSE MAMMARY TUMOR MODEL
TO NEW THERAPEUTIC METHOD

---MAMMARY TUMOR DEVELOPMENT IN BALB/c-*Trp53+/-* MICE AND MAGNETIC NANOPARITLCE INDUCED HEATING FOR CANCER TREATMENT

A Dissertation Presented

by

HAOHENG YAN

Approved as to style and content by:

_____
D. Joseph Jerry, Chair

_____
Vincent M. Rotello, Member

_____
Richard B. Arenas, Member

_____
Barbara A. Osborne, Member

_____
David J. Gross, Interim Director
Molecular and Cellular Biology Program

DEDICATION

To my parents

ACKNOWLEDGMENTS

I am most grateful to my mentor, Dr. D. Joseph Jerry. His scientific vision and open-minded view enabled me to develop a good understanding of my projects. His encouragement, guidance, and support helped me move forward research, explore new ideas and start my career. Joe never pushed me for results. On a few occasions, he would casually ask how this or that is going, simply to offer help if there was any technical problem. I can only conclude that he fully grasped the idea of "individual medicine", and I was grouped into the "leave her alone" subtype. Joe never laughed at my wacky research ideas, instead, he challenged them. In the process, I think I became a better thinker, a better researcher.

Dr. Richard Arenas introduced me to my first tumor research project. Though that project didn't work out, Rick continually helped me on my nanoparticle project giving me new ideas, pointing out new directions, and helping me with career choices.

I did my first lab rotation in Dr. Vincent Rotello's lab characterizing gold nanoparticles. Little did I know that nanoparticles would become a topic of my thesis work. Vince gave me very clear instructions and knew exactly what the status was, even though he had 20+ project going on in his lab. He steered Bappa and me out of dead ends many times throughout the project. I couldn't be luckier.

I thank Dr. Barbara Osborne for taking her time away from her lab and students helping me achieve my degree. I also need to thank the whole Osborne lab. From "borrowing" chemicals, to learning techniques and methods, the Osborne lab has been so generous and warm-hearted to me.

I am would like to express my gratitude to everyone who has helped me along the way; to Dr. Nick Fischer for getting me involved in the NP project, giving me suggestions and his friendship; to Dr. Bappaditya Samanta, a person I couldn't ask any more of as a lab partner; to Dr. Shaolei Lu for helping me fit in in the lab; to Luwei Tao whose discussion and companionship I will always treasure; to Dr. Mary Hagen who helped me with array analysis; to Ellen Dickenson who taught me breeding mice and much much more; to Amy Roberts for being somebody I can always count on; to Dr. Jae Hong Seo for encouraging me to become a medical oncologist like him; to Dr. Karen Dunphy, Dr. Linda Hill, Dr. Erick Roman, Jeff Kane, Nick Griner, Dr. Trevor Baptiste for being great lab colleagues. A few UMass undergraduate students lent me their able hands during my study, they are Beth Pelletier, Kelly Summerhayes, Yves Mukanya, Amy Straut, Ama Boadu. I thank them.

The BALB/c *Trp53*+/- mouse project required a great deal of efforts from multiple institutes. I would like to thank Dr. Anneke Blackburn for starting the project and reviewing the manuscript, Dr. Daniel Medina for reviewing the manuscript, Dr. Christopher Otis, Dr. Q. Jackie Cao, Dr. Giovanna Crisi for reviewing my pathology slides.

Aside from colleagues and collaborators, I'm lucky to have friends and family supporting and taking care of me along the way. My special thanks to June Hinton who opened her heart and her home to me, to my dear Matthew Allen who brightens my days, months, and years to come.

I owe all my achievements, if any, to my parents, none of them would have been possible without their unconditional support and forgiveness.

ABSTRACTS

FROM MOUSE MAMMARY TUMOR MODEL TO NEW THERAPEUTIC METHOD

---MAMMARY TUMOR DEVELOPMENT IN BALB/c *Trp53*+/- MICE AND MAGNETIC NANOPARTICLE INDUCED HEATING FOR CANCER TREATMENT

MAY 2010

HAOHENG YAN, M.D., PEKING UNION MEDICAL COLLEGE

Ph.D., UNIVERSITY OF MASSACHUSETTS AMHERST

Directed by: Professor D. Joseph Jerry

PATHWAYS CONTRIBUTING TO DEVELOPMENT OF SPONTANEOUS MAMMARY TUMORS IN BALB/c-*Trp53*+/- MICE

Mutation and loss of *p53* function are common features among human breast cancers. We use BALB/c-*Trp53*+/- mice as a model to examine the sequence of events leading to mammary tumors. Mammary epithelium proliferation rates were similar in both BALB/c-*Trp53*+/- mice and wild type controls. Among the 28 mammary tumors collected from BALB/c-*Trp53*+/- mice, loss of heterozygosity for *Trp53* was detected in more than 90% of invasive mammary tumors. Transplantation of *Trp53*+/- ductal hyperplasias indicated an association between loss of the wild type allele of *Trp53* and progression to invasive carcinomas. Expression of biomarkers such as ERα, PR, Her2/Neu and activated Notch1 varied among the tumors suggesting that multiple oncogenic events collaborate with loss of p53 function. The majority of the tumors expressed both luminal and basal cytokeratins (59%). Gene expression analysis showed

ligands and receptors of stem cell related pathways, such as Notch and Wnt, were increased in the tumors. These results indicate that mammary tumors in BALB/c *Trp53+/-* mice might initiate from bipotent mammary progenitor cells.

USING MAGNETIC NANOPARTICLES FOR CANCER THERMOTHERAPY

Alternating magnetic field (AMF) heating of magnetic nanomaterials provides a promising method for executing therapeutic thermal treatment for cancer patients. In order to explore the potential of magnetic nanoparticles (MNPs) for hyperthermia treatment, we synthesized iron oxide MNPs with various passivation by citric acid, folate, trimethylamine carboxylic acid, or albumin. The albumin passivated MNP (MNP-A) surpassed other MNPs, showing efficient heating with very low inherent cytotoxicity. Confocal microscopy located MNP-A (FITC tagged) accumulation in both cell nucleus and cytosol after 24hr incubation with HeLa cells. The quantity of cell bound MNP-A (including internalized and cell membrane bound MNP-A) was positively associated with MNP-A concentration and incubation time with cells. The MNP-A bound to cells was sufficient to increase the temperature in the cell pellet $\Delta 7°C$ after 8min exposure to AMF. No significant temperature increase or cell death was detected in control groups. Our data demonstrate that MNP-A provides a selective tool for AMF-induced thermal treatment, as well as useful dosing information for future preclinical animal studies.

TABLE OF CONTENTS

Page

LIST OF TABLES

Table Page

LIST OF FIGURES

Figure Page

CHAPTER 1

INTRODUCTION

An estimated 192,370 new cases of invasive breast cancer and 62,280 new cases of in situ breast cancer are expected to occur among women in the US during 2009 (1). Excluding cancers of the skin, breast cancer is the most frequently diagnosed cancer in women. An estimated 40,610 breast cancer deaths are expected in 2009. Breast cancer ranks second as a cause of cancer death in women (after lung cancer). Death rates for breast cancer have steadily decreased in women at 2.0-3.2% per year since 1990. The improvement is largely due to progress in both earlier detection and improved treatment.

The exact mechanism that drives the normal mammary gland towards malignancy is still not clear, but new molecular biology techniques are enabling us to have better understanding of breast tumor cell biology and its molecular genetics during the process of tumorigenesis.

Multistep Model of Breast Cancer Progression

There are many models of human breast cancer evolution. One of the most well-established models, published by Wellings and Jensen over 30 years ago, proposed that the cellular origin of most breast cancers occurs in the normal terminal duct lobular unit (TDLU) and that there is an apparently continuous but nonobligatory progression from TDLUs to cancer through a series of increasingly abnormal stages over long periods of time (2;3) (Figure 1.1). The key stages in this progression are called atypical ductal hyperplasia (ADH), ductal carcinoma in situ (DCIS), and invasive breast cancer (IBC) in today's terminology (4). This model was originally based on the evidence of gradual

histological continuity. Confirmatory evidence that precursors and preinvasive lesions are clonal processes arises from studies showing similar genetic changes in low-grade DCIS and ADH and the shared genetic alterations between the precursors and IBC from the same patients (5-9).

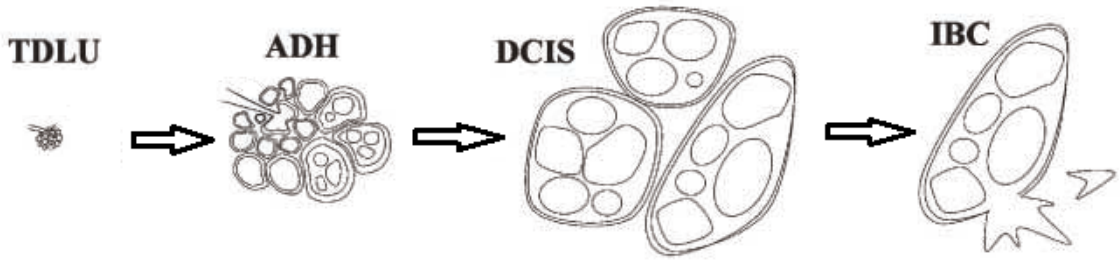

Figure 1.1 Multi-step model of breast cancer progression.
Adapted from (4)

On this spectrum, the diversity of histological features largely expands from premalignant lesions to malignancy. ADHs usually show quite well-differentiated histological and biological features, whereas IBCs show enormous diversity, ranging from very well to very poorly differentiated. DCIS reside between these extremes and are divided into three (e.g., low versus intermediate versus high grade) categories reflecting variations in the degree of differentiation (10).

Changes in the expression of molecular markers also accompany the pathological change. In the normal pre-menopausal breast, estrogen receptor positive (ER+) cells are luminal epithelial cells, evenly distributed and comprise 7% of the total epithelial cell population (11). ER positivity and proliferation (Ki67+) are almost mutually exclusive in normal epithelial breast tissue. It is thought that ER(+) cells secrete paracrine factors that influence proliferation of the adjacent ER(-) cells (12). In ADH and DCIS, contrary to

the normal breast, ER(+) cells are surrounded by contiguous cells that are also ER(+). Moreover, ER(+)/Ki-67(+) cells are commonly seen in DCIS (12-14). In general, ER (+) IBC exhibit more frequent ER positivity in the tumor (15). On the other hand, there are approximately 35-60% of primary breast cancer are ER negative.

Similar to estrogen receptors, progesterone receptors (PR) have been found elevated very early in premalignant breast lesions (16). In DCIS and IBC, PR positivity is usually associated with ER positivity (17;18).

The *Her2/Neu* oncogene encodes a transmembrane tyrosine kinase receptor with extensive homology to the epidermal growth factor receptor (19). It is commonly overexpressed/amplified in human breast cancer. According to a variety of studies, Her2/Neu has not been found overexpressed at the protein level in benign proliferative breast disease or ADH (20-22). However, amplification of *Her2/Neu* has been documented with the use of fluorescent *in situ* hybridization (FISH) in ADH (21). In DCIS, Her2/Neu overexpression has been primarily associated with DCIS of higher grade, with (23) or without (24) IBC present. Approximately 30% of IBC has Her2/Neu overexpression/amplification (25).

It is important to point out that deregulated expression of ER, PR, and Her2/Neu are not only the oncogenic driving force, but also therapeutic targets for hormone therapy or anti-Her2/neu monoclonal antibody therapy (1).

Recently, comprehensive gene expression profiling of large sets of tumors by multiple independent groups and technologies have revealed five major molecular subtypes of breast cancer: luminal A, luminal B, Her2/Neu overexpressing, basal-like, and normal-like (26;27). The molecular differences result in distinct clinical outcomes

and responses to treatment: the basal-like breast cancers have the worst outcomes, and within the estrogen receptor ER positive subtypes the luminal B cohort has a significantly worse prognosis than luminal A. These five subtypes are already present in DCIS (28)

Although these data provide invaluable information about molecular epidemiology in each stage of the human breast cancer, it is difficult to follow sequential molecular changes in human breast cancer. Spontaneous mammary tumors from genetically engineered mice provide a model to individually examine the sequence of phenotypic and genetic alterations during mammary tumorigenesis.

Genetically Engineered Mouse Mammary Tumor Model

The initial studies of mouse mammary tumors focused on searching for the cause of cancer in high mammary tumor strains. These studies eventually led to the discovery of mammary tumor virus (MMTV) (29). Though the comparable virus has not been identified in human or other species, the study of MMTV put down the foundation of the genetically engineered mice (GEM) mammary tumor model. The first genetically engineered mouse mammary tumor model used MMTV-LTR to promote *Myc* gene expression in the mouse mammary gland (30). These mice developed mammary tumors with a very short latency. Soon, transgenic mice with other oncogenes were created (31-33). In addition to transgenic mice, conditional knockout mice from which the gene of interest (e.g. *BRCA1* or *Trp53*) was removed from most cells in mammary gland, were generated for studying mammary tumor biology (34;35). Today, there are probably more than 100 GEM mammary tumor models covering almost all known tumor-related genes. Researchers use these models to study every aspect of tumor biology. Unlike MMTV induced tumors which are morphologically distinct from human breast cancer, many of

the mammary tumors in GEM mice mimic morphological features that resemble human breast cancers (36). In addition to morphological features, many of the defining molecular characteristics of human breast cancer subtypes (defined by gene expression profiling) were conserved among the GEM mouse models (37).

Roles of Stem Cells in Cancer

Among the five intrinsic subtypes of human breast cancer, basal-like breast cancers have drawn particular attention because they are associated with aggressive behavior, poor prognosis and typically do not express ER, PR or Her2/Neu ("triple-negative"). Therefore, patients with basal-like cancers are unlikely to benefit from currently available targeted systemic therapy. This basal-like subtype of breast cancer preferentially overexpresses genes normally enriched in embryonic stem cells (38). In fact, many researchers support the hypothesis that breast cancer can initiate from stem cells (39).

Embryonic stem cells have the potential to develop into all cell types in the body during early life and growth. Tissue specific stem cells remain in many adult tissues providing a reservoir for regeneration and repair of tissues, dividing when necessary to replenish dead cells. Stem cells account for a very tiny proportion of total adult tissue cells and may remain quiescent for long periods of time until they are recruited to fulfill the needs to maintain tissues due to normal turnover of cells or resulting from disease or tissue injury (40).

The unique self-renewal feature shared between stem cells and cancer cells inspired an interesting hypothesis that cancer arises from stem cells (39;41;42). Many adult tissues are thought to be maintained by a hierarchical system in which a very small

population of self-renewing adult stem cells gives rise to proliferating progenitor cells that undergo limited rounds of mitotic division and then terminally differentiate, losing their ability to proliferate further. In this hierarchical system, only the stem cells are long-lived (42). Malignant transformation comes from series of gene mutations which require long cellular life span or self-renewal ability to pass on the mutations. Fully differentiated tissue cells have short life spans and no ability to self-renew, whereas stem cells have long life span and large replicative potential which enable them to accumulate mutations over an extended period of time.

Early evidence started with studies on acute myelogenous leukemia where leukemia initiating cells possessed characteristic features of normal primitive cells (43). Later research on non-hematopoietic systems discovered genes that are commonly found aberrantly expressed in tumor samples are also key players in stem cell regulation, such as genes involved in Wnt, Notch and Hedgehog pathways (44-46). MMTV-*Wnt1* mammary tissue harbors an increased number of stem cells and develops mammary tumors preferentially from these cells (47-49). Recently, Barker et al. used lineage tracing methods to directly demonstrate that colon crypt stem cells were the cellular target of transformation for intestinal cancer (50). In their study, deletion of *Apc* (adenomatous polyposis coli, negative regulator of Wnt pathway) in these stem cells leads to their transformation within days and they develop into adenomas within 3-5 weeks. Meanwhile, the same deletion in non-stem cell populations fails to drive malignant transformation (50).

Parallel to the studies on the role of stem cells in tumorigenesis, a cancer stem cell concept prevails based on transplanted tumor formation tests from separate populations

of tumor cells. It postulates that a small reservoir of self-sustaining cells (cancer stem cells) are exclusively able to self-renew and give rise to the majority of tumor cells which are non-tumorigenic (51-56). Whether all cancer stem cells are transformed from normal tissue stem cells is still under debate, tumors initiate from stem cells do show the hierarchic cell organization (43). Analysis of tumors arising from transformed stem cells revealed that differentiation capacity of these cancer initiating stem cells is partially retained during tumor development (47-50). The aberrant differentiation, generating most of the cells within a tumor, most likely defines phenotypic features of each tumor.

p53 Regulates Stem Cells

Recently, p53 function has been linked to stem cells.

p53 is a well know tumor suppressor gene. Mutation of the p53 tumor suppressor gene is one of the most common alterations identified in invasive tumors (57;58). The mechanisms by which p53 suppresses tumors are diverse. The roles of p53 in mediating cell cycle arrest and apoptosis have been described extensively (59). More recently, the activities of p53 have been expanded to include regulation of DNA repair, senescence, autophagy, cellular metabolism and microRNA processing (60-65). Overall, p53 is a central stress response protein that keeps the machinery of cell in control, preventing the proliferation of damaged cells which may ultimately leads to tumorigenesis (59).

Recent evidence suggest p53 may affect how stem cells replicate *in vivo*. Tissue stem cells are usually quiescent. When needed, a stem cell can undergo asymmetric division, giving rise to one daughter stem cell (self-renewal) plus one cell that is destined to differentiate to normal tissue cells within a few divisions. In some cases, stem cells can execute symmetric division to generate two daughter stem cells, resulting in the

expansion of stem cell numbers (66). The p53 protein plays a fundamental role in restricting the pool of stem cells in embryonic stem cells (67-69) as well as adult tissues including hematopoietic system (70;71), neuronal system (72;73) and mammary gland (74;75). *p53* null stem cells from mouse mammary glands undergo symmetric self-renewal division (75%) *in vitro* while the WT control uses asymmetric division (80%). *In vivo*, the number of stem cells in mammary glands of *p53* null mice was higher than WT controls and increased progressively over time (74). Recently, five different labs independently identified p53 as an important checkpoint during the multifactor reprogramming process in which induced pluripotent stem cells (iPS-cell) are derived from differentiated adult cells (76-80). In each case, inactivation of p53 enhanced the efficiency of iPS-cell production, suggesting p53 may be a major gatekeeper of self renewal function of stem cells. Overall, p53 is a key player in regulating stem cell replication, and loss of p53 function may result in abnormal expansion of the stem cell pool in normal tissue.

p53 and Mammary Tumors

Although disruption of p53 function predisposes the human body to a broad spectrum of malignancies, the breast epithelium appears exquisitely sensitive to proper p53 function. Polymorphisms in MDM2, CHK2 and ATM alter the stability and activity of p53 and have been linked to breast cancer risk in women. Breast cancer is the most prevalent tumor among women with Li-Fraumeni syndrome which is most commonly associated with heterozygous mutations in *TP53* (81-83). In animal models, high incidence of mammary tumors develops after transplantation of *p53* null mammary epithelium into fat pads of wild type mice (84) or somatic inactivation of p53 (35).

As *p53* null mammary epithelium contains increasing numbers of stem cells and stem cells are potential targets to malignant transformation, tumorigenesis in the *p53* null mammary epithelium may start with expanding the pool of putative tumor target cells. A few recent studies showed direct tumorigenesis from p53 deficient neutral stem/progenitor cells, osteoblast, and mesenchymal stem cells (85-87). These transformed stem cells (tumor initiating cells) partially retain their original differentiation *in vitro* and *in vivo* giving rise to the heterogeneous mass tumor cell population.

As a Li-Fraumeni syndrome animal model, BALB/c-*Trp53*+/- female mice spontaneously develop a high incidence of mammary tumors (88;89). Compared to total function loss in *p53* null mice, reduced dosage of the *p53* gene has been associated with haploinsufficiency with respect to levels of p53 protein and activity, cell cycle arrest, apoptosis and homology-directed DNA repair (90-92). Recent investigation of astrocytomas further suggested that *p53* heterozygous stem/progenitor cells display abnormal growth and differentiation properties *in vitro* before any gross morphological abnormality occurs (86). Therefore, the level of p53 activity appears to be a critical regulator of tumor suppressor pathways and breast cancer risk.

The sequential changes occurring in normal tissue and in premalignant mammary lesions as a consequence of heterozygous mutations in *TP53* would provide clues to the mechanisms that initiate the carcinogenic cascade as well as the cellular origins of breast cancer. While it is difficult to monitor sequential changes in human breast cancers, spontaneous mammary tumors of BALB/c-*Trp53*+/- female mice (89;93) provide a model to examine the sequence of phenotypic and genetic alterations during mammary tumorigenesis.

Role of p53 in Parity-Induced Protection from Breast Cancer

Development of the mammary gland is tightly regulated by ovarian hormones throughout puberty and pregnancy. Mammary epithelium progresses through proliferation, differentiation, and regression as circulating levels of ovarian hormones change during the menstrual cycle and are most dramatic during pregnancy, lactation and involution. Estrogens and progestins stimulate proliferation through their receptors on mammary epithelium and long term exposure to these hormones are associated with increased breast cancer risk (94). However, estrogens and progestins also mediate the protection from breast cancer afforded by parity. A full-term pregnancy early in reproductive life reduces breast cancer incidence by up to 50% (95).

The activity of p53 has been shown to be responsive to hormones in rodent models (96-98). Exogenous estrogen and progesterone are sufficient to render the mammary epithelium resistant to carcinogen-induced tumors mimicking the protective effect afforded by a full-term pregnancy (99) and the p53 pathway participates in the hormone-induced protection by increasing p53 mediated apoptosis in mammary epithelium (84;100).

Recent findings using mice have suggested that an early pregnancy (5 weeks) is associated with a small decrease in mammary stem cell number, although their capacity to repopulate the fat pad was unaffected (101). A later pregnancy (9 weeks) was shown to have no effect on the mammary stem cell pool (102). Further direct comparison is needed to provide convincing evidence regarding whether pregnancy protects via a persistent decrease in mammary stem cell activity (103). Considering the role of p53 in expanding

the stem cell pool, comparison between tumorigenesis in nulliparous and parous p53 deficient mice may provide new supporting evidence on this issue.

CHAPTER 2

PATHWAYS CONTRIBUTING TO DEVELOPMENT OF SPONTANEOUS MAMMARY TUMORS IN BALB/c-*Trp53*+/- MICE

Introduction

Compromised function of the p53 tumor suppressor pathway remains among the most common alterations found in cancers (104). Although disruption of p53 function predisposes to a broad spectrum of malignancies, the breast epithelium appears exquisitely sensitive to proper p53 function. Polymorphisms in *MDM2*, *CHK2* and *ATM* alter the stability and activity of p53 and have been linked to breast cancer risk in women. The activity of p53 has also been shown to be responsive to hormones in rodent models (105-107). Exogenous estrogen and progesterone are sufficient to render the mammary epithelium resistant to carcinogen-induced tumors mimicking the protective effect afforded by a full-term pregnancy (108) and the p53 pathway participates in the hormone-induced protection (84;109). Furthermore, breast cancer is the most prevalent tumor among women with Li-Fraumeni syndrome which is most commonly associated with heterozygous mutations in *TP53* (110-112). Reduced dosage of the p53 gene has been associated with haploinsufficiency with respect to levels of p53 protein and activity, cell cycle arrest, apoptosis and homology-directed DNA repair (90-92). Therefore, the level of p53 activity is a critical regulator of tumor suppressor pathways and breast cancer risk.

The mechanisms by which p53 suppresses tumors are diverse. The roles of p53 in mediating cell cycle arrest and apoptosis have been described extensively (59). More

recently, the activities of p53 have been expanded to include regulation of DNA repair, senescence, autophagy, cellular metabolism and microRNA processing (60;64;113-116). Additionally, loss of p53 was shown to permit expansion of the pool of pluripotent embryonic stem cells (67;117) and cancer stem cells (117-119). The activities of p53 that are critical for suppression of tumors vary among tissues. In the thymus, the pro-apoptotic activity of p53 was necessary to suppress lymphomas while the cell cycle checkpoint function was dispensable (120). In contrast, senescence is the principal pathway leading to regression of liver tumors following restoration of p53 function (121) and appears to be the prominent pathway in sarcomas as well (122). Among the known breast cancer susceptibility genes there is a convergence of function highlighting the central role of homology-directed repair of DNA double strand breaks in breast cancer risk (123). Thus, fidelity of double strand break repair may be a critical pathway controlled by p53 in breast tissue.

The sequential changes that occurring in normal tissue and in premalignant mammary lesions as a consequence of heterozygous mutations in *TP53* provide clues to the mechanisms that initiate the carcinogenic cascade as well as the cellular origins of breast cancer. While it is difficult to monitor sequential changes in human breast cancers, spontaneous mammary tumors are common in BALB/c-*Trp53*+/- female mice (89;93) providing a model to examine the sequence of phenotypic and genetic alterations during mammary tumorigenesis. Using this model, we demonstrate that heterozygosity for *Trp53* does not increase proliferation of the epithelium or the incidence of precancerous lesions. However, loss of the wild type allele of *Trp53* was associated with the transition from hyperplastic to invasive phenotypes. In a set of 28 spontaneous tumors, histologic

phenotypes and expression of oncogenes were heterogeneous. The majority of tumors expressed markers of both luminal and basal epithelia (59%) suggesting that progenitor cells are the most common origin. However, significant numbers of tumors expressed purely luminal keratins (27%) or basal keratins (11%). Although distinct patterns of keratins were observed, stem cell markers were expressed similarly in tumors with only keratins associated with luminal cells (K8/18) as well as tumors expressing both luminal and basal cell keratins (K8/18 and K5/6). Therefore, it appears that tumors arise most frequently from progenitor cells which then commit toward more differentiated lineages during progression. Lineage decisions were not associated with specific activation of either Notch1 or Her2. As tumor phenotypes were stable after transplantation, this panel of tumors can be used to speed preclinical testing of chemotherapeutic agents.

Material and Methods

Mice

BALB/c-*Trp53*+/- mice were generated, described previously (124), by backcrossing (C57BL/6 x 129/Sv) *Trp53*-/- mice onto the BALB/cMed strain for 11 generations. Mice were genotyped by multiplex PCR as described previously (125). BALB/c-*Trp53*+/+ and *Trp53*+/- mice were monitored weekly for tumor development or morbidity, and were palpated for mammary tumors. 97 virgin female BALB/c-*Trp53*+/- mice and 30 *Trp53*+/+ mice, and 52 parous BALB/c-*Trp53*+/- mice were included in the study.

Estrous Stage Determination

Stages of estrous were determined by cytological evaluation of vaginal smears. Vaginal smears of adult female nulliparous mice age 35-37 weeks were taken daily. Once the estrous stages were determined, mice were injected intraperitoneally with 30µg 5-bromo-2-deoxyuridine (BrdU; Sigma, St. Louis, MO) per gram of body weight and sacrificed 2 hours later. Mammary glands were isolated and processed for immunohistological analysis.

Mammary Gland Wholemount

Mammary glands were removed and spread on glass slides and fixed in Carnoy's fixative (60% ethanol, 30% chloroform, 10% glacial acetic acid) for 3 hours. The glands were washed in 70% ethanol for 15 minutes followed by brief rinse in distilled water. The tissues were then stained in carmine alum solution (1 gm carmine, 2.5 gm aluminum potassium sulfate/500 ml of water) at 4°C overnight. The tissues was dehydrated by soaking it in a series of solutions with increasing concentrations of ethanol (70-100%), washed in xylene twice, and mounted on a slide.

Isolation and Culture of Transplantable Mammary Tumor Cells

For transplantable tumor fragments: each mammary tumor from BALB/c-*Trp53*+/- mice was minced and frozen in DMEM:F12 medium with 10%FBS, 7% DMSO following general cell freezing method and kept in liquid nitrogen. To isolate tumor cells, mammary tumors were removed from mice, rinsed in PBS, minced and incubated 3hrs at 37ºC in medium containing DMEM:F12 supplemented with 25mM Hepes, 1.2g/L $NaHCO_3$, 10µg/ml insulin, 5ng/ml EGF, 2% adult bovine serum(ABS), 100U/ml

penicillin, 100µg/ml streptomycin, 0.25µg/ml amphotericin B and 0.2% collagenase type 3 (Worthington 4182, 223U/mg). After dissociation and centrifugation, cells were grown in DMEM:F12 medium containing 2% ABS, 10µg/ml insulin, 5ng/ml EGF, 100u/ml penicillin, 100µg/ml streptomycin and 0.25µg/ml amphotericin B. The cells were expanded for 6 passages before freezing in liquid nitrogen.

Transplantation of Mammary Hyperplasias, Tumor Fragments and Tumor Cell Lines

Procedures for transplantation of tissues into cleared mammary fat pads has been described previously (126). In brief, 21-24-day old BALB/c wild type females were used as transplant recipients. The endogenous mammary epithelium was surgically removed from the 4^{th} inguinal glands to provide a cleared mammary fat pad. Fragments of PH1b and PH2 hyperplastic outgrowth lines (127) or spontaneous mammary tumors were inserted into the cleared mammary fat pads. Tumor cell lines were injected, $5x10^5$ cells in 10µL saline, into each cleared fat pad. Mice were palpated 3 times/week to monitor for tumor development. To test hormone dependence, tumor fragments were transplanted into recipients, then ovariectomized when tumors were palpable.

Histology and Immunohistochemistry

All collected tissues were fixed overnight at 4ºC in 10% neutral-buffered formalin, then stored in 70% ethanol until they were embedded in paraffin. Sections (4µm thick) were deparaffinized in xylene, then hydrated through a series of graded ethanol. The sections used for histopathological evaluation were stained with hematoxylin and eosin (H.E.). Immunohistochemical staining was performed using the

Dakocytomation Envision+System-HRP kit after antigen retrieval. The antibodies used were anti-ERα (1:200, MC 20, Santa Cruz Biotechnology), anti-PR (C-19, 1:50, Santa Cruz Biotechnology) and anti-mouse cytokeratin 6 (PRB-169P, 1:5000, Covance, Berkeley, CA, USA). BrdU staining was performed using BrdU staining kit (Zymed, Invitrogen, Carlsbad, CA). Immunofluorescence staining followed published procedures (37). Briefly, hydrated slides were boiled in sodium citrate (10mM) for 15min. After the slides cooled, they were incubated in blocking buffer (5%BSA/0.5%Tween-20 in PBS) for 1hr at room temperature. Then the slides were incubated in primary antibodies, anti-*cytokeratin 5* (1:8000, PRB-160P, Covance, Berkeley, CA, USA) and anti-*Cytokeratin 8/18* (1:400, GP11, Progen Biotechnick, Heidelberg, Germany) in a humid chamber at room temperature overnight. After series of washing steps, Texas Red® or Cy™2 conjugated secondary antibodies (1:200, Jackson ImmunoResearch Laboratories, West Grove, PA) and DAPI (1µg/ml Sigma, St. Louis, MO) were added to the samples for 1hr at room temperature. Slides were mounted in mounting medium (2.5% Dabco/ 50mM Tris-HCl pH8.0/ 90% glycerol) and sealed with clear nail polish.

Trp53 Genotyping and Loss of Heterozygosity

Loss of heterozygosity (LOH) at *Trp53* in hyperplastic outgrowths and tumors was determined by Southern blotting as described previously (88). The epithelium in hyperplastic outgrowths (PH1b, PH2) was enriched by digestion in DMEM:F12 supplemented with 25mM Hepes, 1.2g/L $NaHCO_3$, 10µg/ml insulin, 5ng/ml EGF, 2% adult bovine serum(ABS), 100U/ml penicillin, 100µg/ml streptomycin, 0.25µg/ml amphotericin B and 0.2% collagenase type 3 (Worthington 4182, 223U/mg) as described

for cell lines followed by centrifugation. Genomic DNA was extracted from the enriched epithelial pellet. For tumors, DNA was extracted directly from frozen tissue. Genomic DNA was digested with *Stu*I and *Eco*R1. Southern blots were hybridized with a probe spanning exons 7-9 of the *Trp53* gene. The intensity of the wild-type and null bands was quantified using a phosphorimager (Cyclone; Packard Bioscience, Boston MA) and the OptiQuant software package. The ratios of wild-type:null band hybridization values were calculated. Loss of the wild-type allele was defined as the ratio of wild-type:null alleles <0.5.

Western Blot

Flash-frozen tissues were homogenized in buffer (50mM Tris, 150mM NaCl, 1% TritonX-100, 1mM sodium vanadate, 10mM sodium fluoride, 10mM β-glycerol phosphate, 1x protease inhibitor from Sigma P8340) using 200 µl buffer/50 mg tissue. The protein concentration was determined using BCA reagent (Pierce, Rockford, IL, USA). Lysates (50 μg) were separated by 6% gel electrophoresis and electrophoretically transferred to nitrocellulose membrane. The membrane was incubated with anti-Her2/Neu (1:250 C20, Santa Cruz Biotechnology), anti-Phospho Her2/Neu (Tyr1248, 1:1000, Stressgen), anti-Notch1 (mN1A, 1:1000, eBioscience) or anti-β-actin (1:1000, Sigma A3853), followed by incubation with horseradish peroxidase conjugated secondary antibodies, and developed using an enhanced chemiluminescence (ECL) solution (Amersham, GE Healthcare UK, Buckinghamshire, United Kingdom).

Isolation of Mammary Gland Organoids

Isolation of mammary gland organoids (enrichment of epithelium cells) was performed essentially as previously described (128). Briefly, mammary glands were removed from mice, rinsed in PBS, minced and incubated on a shaker for 1hr at 37ºC in medium containing DMEM:F12 supplemented with 25mM Hepes, 1.2g/L $NaHCO_3$, 5% fetal bovine serum(ABS), 100u/ml penicillin, 100µg/ml streptomycin, 2mg/ml collagenase type 3 (Worthington 4182, 223U/mg), and 100U/ml hyaluronidase (Sigma H3506). Following enzyme digestion the fat layer was decanted and the remaining organoids were centrifuged and washed three times with PBS. The organoid pellets were subject to RNA extraction immediately after the washes.

RNA Isolation and PCR Array Analysis

Total RNA from mammary gland organoid and tumor samples were extracted by Qiazol Lysis Reagent (Qiagen, CA) and further purified using Qiagen RNeasy Mini Kit (Qiagen, CA). PCR array analysis was performed by using 1µg of total RNA of each sample and the RT² Profiler™ PCR Array for mouse stem cells (SABiosciences, Frederick, MD) according to the recommendations of the manufacturer. Expression levels on each array plate were normalized using two housekeeping genes: *Hprt1* and *Hsp90ab1*. Tumor samples were compared to mammary gland organoids from age matched BALB/c-*Trp53*+/- mice. Analysis of ΔCt and fold changes was conducted using the online data analysis tool supported by the array manufacturer. Genes were considered to be differentially expressed if the fold-change between tumor and mammary epithelial organoids was >2.5. Genes that are differentially expressed between the “mixed keratin”

tumors (V06, V22) and “luminal keratin” tumors (V07, V14) were selected if the ratio differed by >4-fold.

Results [§]

Analysis of Preneoplastic Changes in BALB/c-*Trp53*+/- Mammary Tissues

Previously, Kuperwasser C. etc from our lab has developed a mammary tumor model in BALB/c *Trp53*+/- mice (89). In order to further dissect the role of p53 and examine the sequential events during mammary tumorigenesis, tissues were collected from BALB/c-*Trp53*+/+ and BALB/c-*Trp53*+/- nulliparous female mice at 8 week intervals up to 52 weeks. The overall ductal structure showed no difference in branching or alveologenesis between the two groups (Figure 2.1A). Proliferation rates were also similar for both genotypes at 36wks (Figure 2.1B). Sporadic hyperplastic foci were seen in BALB/c-*Trp53*+/- mice (Figure 2.1C), but the incidence was too low to compare between the groups. Thus, heterozygosity for *Trp53* did not increase proliferation or appearance of precancerous lesions.

[§] *Most of the data in this chapter is published in American Journal of Pathology, 2010 Mar;176(3):1421-32*

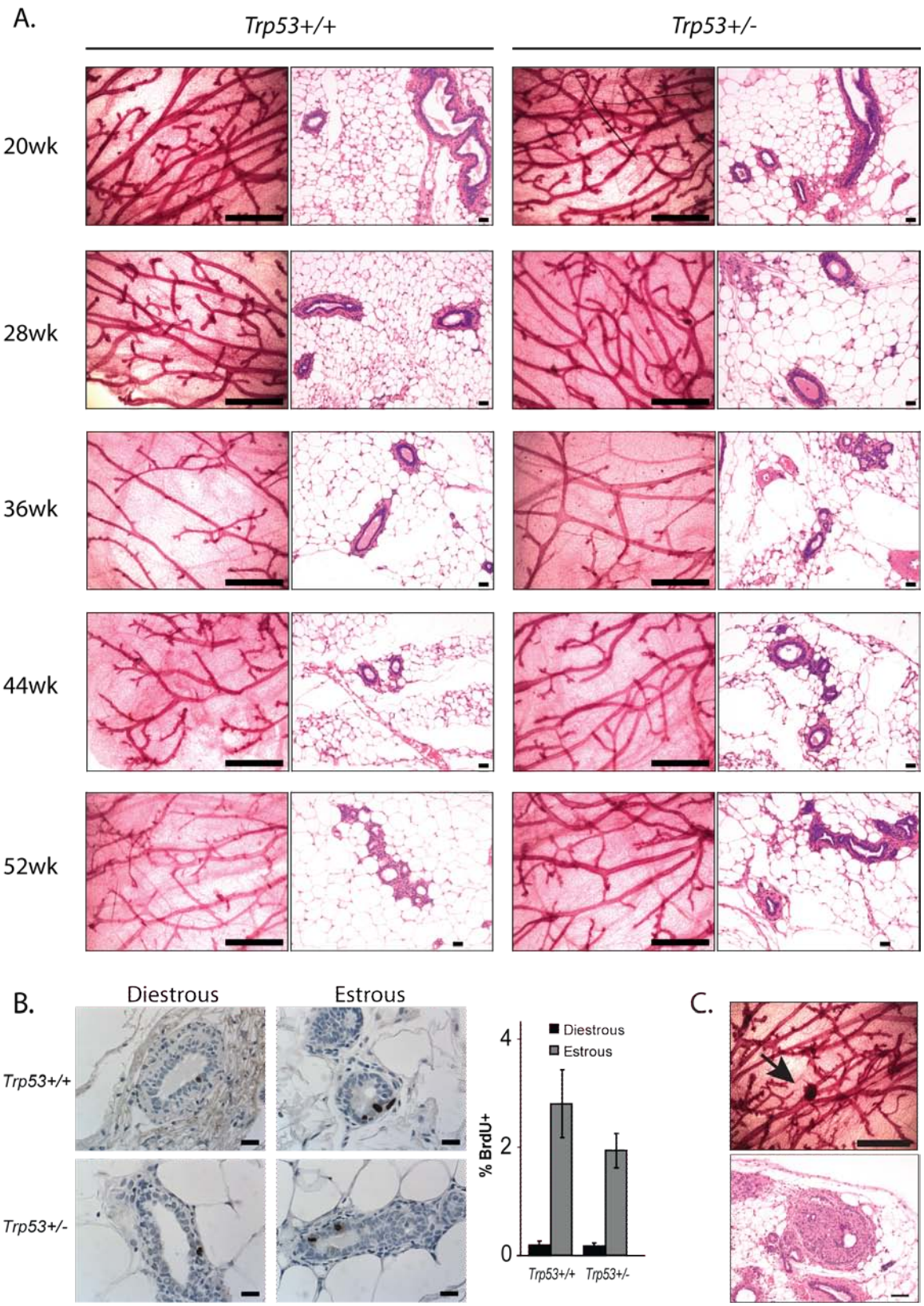

Figure 2.1 Mammary gland morphology in BALB/c-*Trp53*+/+ and -*Trp53*+/- mice.

(**A**) Wholemount and H&E staining of mammary glands from 20-52wk-old mice. (**B**) Proliferation of mammary epithelial cells was determined at different estrous phases by BrdU incorporation. The histogram shows the average percentage of BrdU positive cells. No significance was detected between the *Trp53* genotypes in either stage. At least 2500 epithelial cells were counted per slide for a minimum of three mice per genotype. (**C**) Hyperplastic foci appeared at low incidence in wholemounts (left) and H.E (right) from *Trp53*+/- mice. Scale bars: 1mm in wholemounts; 40µm in H.E; 20µm in BrdU staining.

Loss of heterozygosity (LOH) for *Trp53* is observed frequently in breast cancers and was also observed in 90% of spontaneous mammary tumors from BALB/c-*Trp53*+/- mice (88). In this panel, well-differentiated lesions such as mammary intraepithelial neoplasias (MIN) retained the wild type allele of *Trp53*, while poorly differentiated adenocarcinomas had near complete LOH (Figure 2.2A). To explore the timing of *Trp53* LOH, two transplantable hyperplastic lines (PH1b & PH2) derived from BALB/c-*Trp53*+/- mice (127) were transplanted into cleared mammary fat pads in BALB/c-*Trp53*+/+ hosts. The PH outgrowths displayed abnormal ductal morphologies in the recipient glands and later developed into invasive carcinomas with latencies of 16-26 weeks. Despite the *Trp53* heterozygous status of the PH lines, 8/9 of the resulting tumors lost the wild type allele of *Trp53* (Figure 2.2B). These results suggested that complete loss of *Trp53* is not necessary to establish premalignant lesions such as hyperplasias or mammary intraepithelial neoplasias (MIN), but LOH is strongly associated with the transition into invasive tumor.

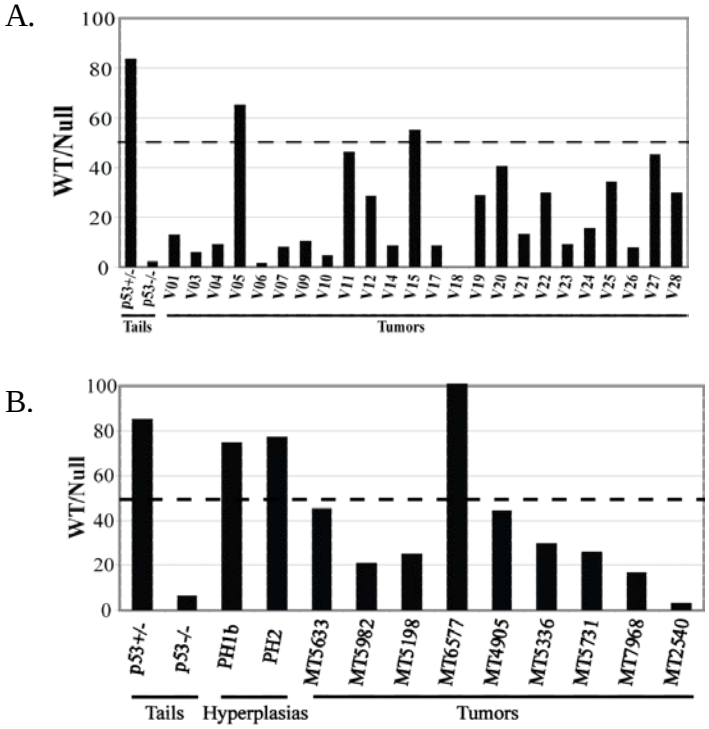

Figure 2.2 Loss of heterozygosity during mammary tumorigenesis in BALB/c-*Trp53*+/- mice.

The proportions of wild type (WT) and null (Null) alleles in tumors were determined by Southern blot hybridization and were compared with the ratios for tail DNAs from mice that were homozygous for the wild type allele or heterozygous (*Trp53*+/+ and *Trp53*+/-, respectively). Reductions in the WT allele below 50% (indicated by the dashed line) were considered significant loss of heterozygosity. (**A**) The majority of tumors showed loss of wild-type allele. (**B)** The transplanted ductal hyperplasias (PH1b, PH2) used for transplantation retained the WT allele at levels equivalent to tail DNA controls. However, tumors developing from the hyperplasias showed severe loss of heterozygosity in all cases except MT6577.

Pathological and Genetic Alterations Associated with BALB/c-*Trp53*+/- Mammary Tumors

We next explored whether mammary tumorigenesis in BALB/c-*Trp53*+/- mice follows a restricted set of pathological or molecular pathways. The histological features of the total 28 spontaneous mammary lesions collected ranged from intraepithelial neoplasia to invasive carcinomas (Figure 2.3). As collections were focused on large palpable lesions, the majority of tumors were poorly differentiated invasive ductal adenocarcinomas. A minority of tumors (2/28) underwent transdifferentiation into adenosquamous carcinoma or had focal squamous differentiation. A complete summary of tumor characteristics is provided in Table 2.1.

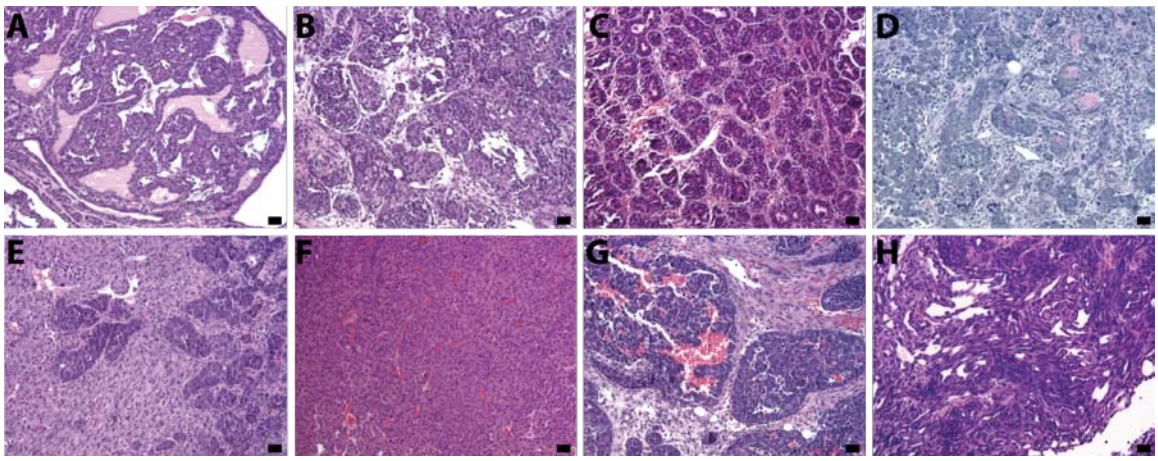

Figure 2.3 Histological characterization of BALB/c-*Trp53*+/- mammary lesions. Mammary lesions from BALB/c-*Trp53*+/- mice showed diverse histological features including (**A**) intra-epithelial neoplasia (MIN, V05), (**B**) ductal adenocarcinoma (V03), (**C**) adenocarcinoma with acinar morphology (V23), (**D**) adenocarcinoma with squamous differentiation (V01), (**E**) carcinosarcoma (V08), (**F**) solid sheets of tumors with little stroma (V26), (**G**) adenocarcinoma with strong stromal reaction (V13) and (**H**) adenocarcinoma with spindle cell feature (V28). Scale bar: 20µm.

Table 2.1 Features of mammary tumors from nulliparous BALB/c-*Trp53*+/- mice.

Sample	Tumor Type	Latency (weeks)	LOH WT/Null	PR	ER	Her2 /neu	K8/ 18	K5	K6	Met$^{\Delta}$
V01	adenocarcinoma	30	12.6	-	-	-	-	+	+	-
V02	adenocarcinoma	30	lost null signal	-	-	-	+	+	+	-
V03	adenocarcinoma	40.7	5.9	+	+	-	+	+	+	
V04	adenocarcinoma	46.7	8.8	-	-	-	+	+	+	
V05	MIN*	47.1	64.9	+	+	-	+	+	+	
V06	adenocarcinoma	46.3	1.4	-	-	-	+	+	+	-
V07	adenocarcinoma	48.9	7.7	-	-		+	-	-	+
V08	carcinosarcoma	49.1		-	-		+	+	+	
V09	adenocarcinoma	42	10.2	+	+	-	+	+	+	-
V10	adenocarcinoma	42	4.5	-	-	+++	+	+	+	
V11	adenocarcinoma	53.9	46	-	-		+	-	-	
V12	adenocarcinoma	53.9	28.2	+	+					
V13	adenocarcinoma	52		-	-		-	+	+	
V14	adenocarcinoma	39.7	8.2	-	-	+++	+	-	-	-
V15	adenocarcinoma	50.4	54.8	-	-	-	+	-	-	
V16	adenocarcinoma	50.4		-	-		+	+	+	
V17	adenocarcinoma	50.9	8.2	-	-	++	+	+	+	
V18	adenocarcinoma	47.4	0	-	-	++	+	+	+	
V19	adenosquamous carcinoma	50.1	28.6	-	-	-	+	+	+	
V20	adenocarcinoma	52.9	40	-	-	+	-	+	+	+
V21	adenocarcinoma	47.1	12.8	-	-	+	+	+	+	
V22	adenocarcinoma	48.1	29.7	-	-	-	+	+	+	
V23	adenocarcinoma	47.9	8.7	-	-	-	+	-	-	
V24	adenocarcinoma	50.4	15.5	-	-	-	-	-	+	
V25	adenosquamous carcinoma	48.6	34.1	-	-	++	+	+	+	
V26	adenocarcinoma	40.7	7.4	-	-	++	+	-	-	
V27	adenocarcinoma	49.1	44.7	-	-	-	+	+	+	
V28	adenocarcinoma	48.7	29.7	-	-	-	+	-	-	

* MIN: Mammary intraepithelial neoplasia; $^{\Delta}$Met: Metastasis; N/A: Not available

Deregulation of estrogen receptor alpha (ERα) and progesterone receptor (PR) expression was observed during progression of the mammary gland lesions in BALB/c-*Trp53*+/- mice. Individual ERα and PR positive cells are distributed in normal ducts throughout *Trp53*+/- mammary glands (Figure 2.4A-C). An increase in clusters of ERα and PR positive cells was detected in ductal hyperplasias from BALB/c-*Trp53*+/- mice (Figure 2.4D-F). Expression of ERα and PR was retained in the majority of early lesions (MIN; Figure 2.4G-I) but lost in most invasive carcinomas (Figure 2.4M-O). In this panel, 3 of 27 malignant tumors were ERα+/PR+ (Figure 2.4J-L). The expression of ovarian steroid receptors during tumorigenesis in BALB/c-*Trp53*+/- mammary tissues mimics the pattern during progression of human breast cancers (14).

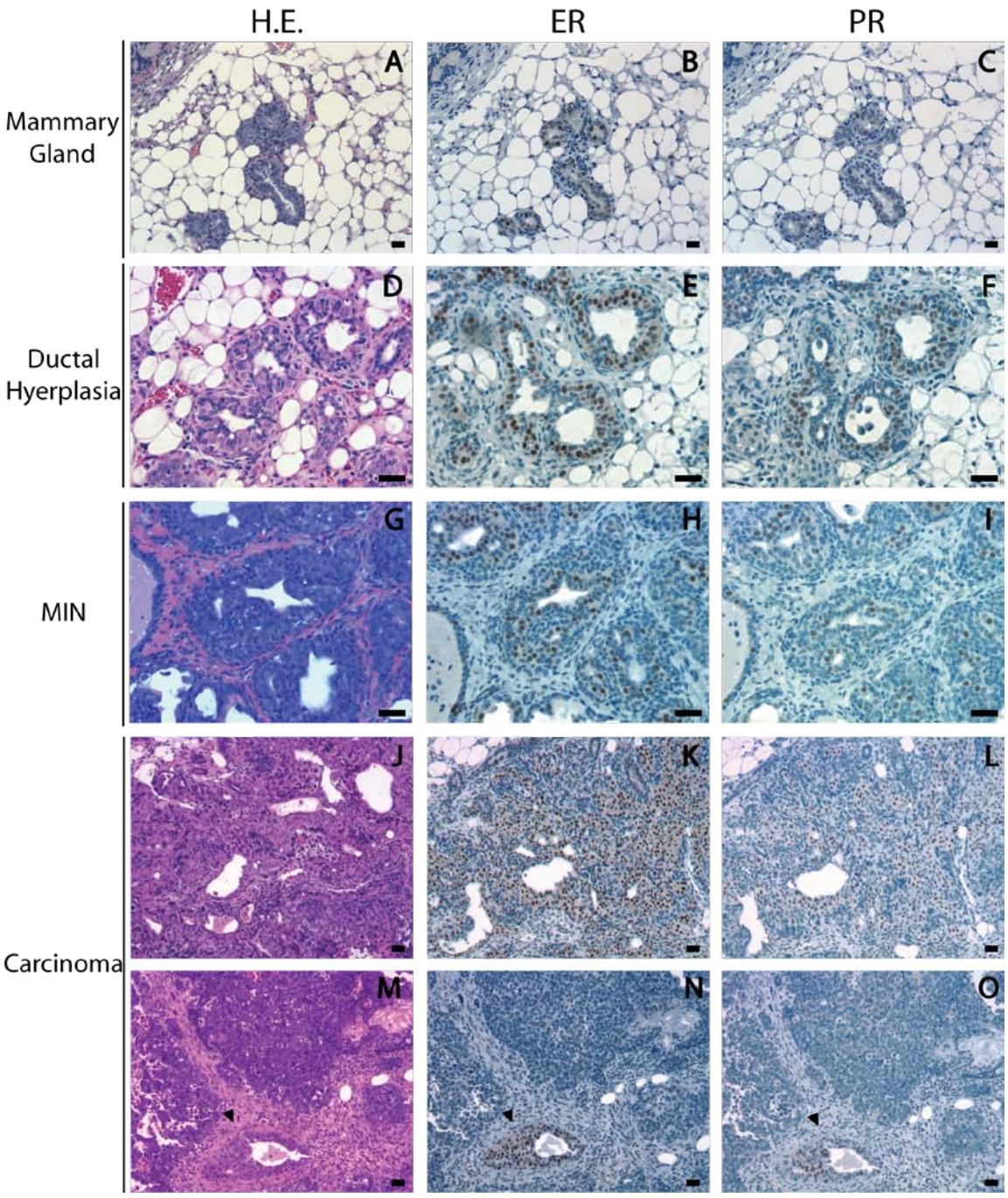

Figure 2.4 Expression of ERα and PR in mammary tissues and tumors.
Consecutive sections were stained with either H.E. or antibodies detecting estrogen receptor alpha or progesterone receptor. Pre-invasive lesions (Hyperplasias and MIN) retained expression of the steroid hormone receptors while the expression in tumors was variable. (**A-C**) Mammary duct; (**D-F**) ductal hyperplasia; (**G-I**) mammary intraepithelial neoplasia (V05); (**J-L**) ERα+/PR+ mammary adenocarcinoma (V09); (**M-O**) ERα-/PR- mammary adenocarcinoma (V13). Arrow head indicates entrapped mammary duct. Scale bar: 20µm.

Selected oncogenic alterations may collaborate with loss of p53 to stimulate progression of tumors in specific cellular compartments yielding tumors with distinct phenotypes. Her2/Neu expression was examined as it is commonly overexpressed in human breast cancers, often in conjunction with mutations in p53 (25). Similar to breast cancers, levels of Her2/Neu protein were elevated in 36% (8/22) of the BALB/c-*Trp53*+/- mammary tumors. The Her2/Neu protein appeared to be active as it was phosphorylated (Figure 2.5). Although protein levels were elevated, it was not associated with amplification of the *Her2/Neu* gene as determined by Southern blot (data not shown). Recent findings have suggested that p53 regulates Notch1 receptor activities, though the effect seems to differ among tissues (130;131). Activated Notch-1 expression was identified in BALB/c-*Trp53*+/- mammary tumors (Figure 2.5). Levels of activated Notch1 varied among BALB/c-*Trp53*+/- mammary tumors, but were independent of histopathological types or expression of other biomarkers. These results revealed the heterogeneous molecular alterations among mammary tumors from BALB/c-*Trp53*+/- mice.

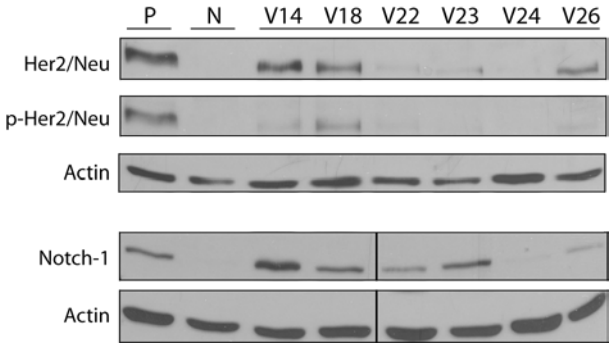

Figure 2.5 Expression of Her2/Neu and Notch1 oncogenes in mammary tumors. Western analysis using anti-Her2/Neu, anti-phospho-Her2/Neu (p-Her2/Neu) antibodies and antibody against intracellular domain of Notch1 were used to examine expression in tumors. Nulliparous mammary tissue (N) from *Trp53*+/- mice was used for comparison. Lysates from A431 cells and mice spleenocytes cells (stimulated with CD3 & CD28) were used as positive controls (P) for Her2/Neu and Notch1, respectively.

Mammary Tumor Fragment and Cell Line Banks from BALB/c-*Trp53*+/- Mice.

Based on the 28 spontaneous mammary tumors from BALB/c *Trp53*+/- mice, we established a mouse tumor bank including transplantable tumor fragments from 20 tumors and tumor cell lines from 10 tumors.

Cryopreserved tumor fragment (barely visible by eye) can be transplanted into mammary fat pad of wild type BALB/c mice. Palpable tumors can be detected within 2-3 weeks in most cases. The tumor outgrowths retained the histological features of the primary tumors. In the case of the V09 tumor, both primary tumor and outgrowths after transplantation expressed ERα (Figure 2.6A-D). However, the tumor transplants expressed ERα at levels greater than the endogenous epithelium, their growth was unaffected by ovariectomy (Figure 2.6E)

The tumor fragment bank expanded the depth and possibility of our study on metastasis. Although all original mammary tumors exhibited highly invasive phenotypes, distant metastases were not detected during the observation period up to 14 months. The metastatic potential of these mammary tumors could be masked, as mice were sacrificed due to large mammary tumors or coincident lymphomas. To further address the metastatic potential of the mammary tumors, tumor fragments from 8 of the primary BALB/c-*Trp53*+/- mammary tumors (V01, V02, V06, V07, V09, V14, V20, V22) were transplanted into mammary fat pads that had been cleared of endogenous epithelium in BALB/c-*Trp53*+/+ hosts. The tumor outgrowths were resected to allow longer periods of observation. Two outgrowth lines, V07 (ERα-/PR-) and V20 (ERα-/PR-, Her2/Neu+), among the eight tested tumors formed metastases in the lungs (Figure 2.6F).

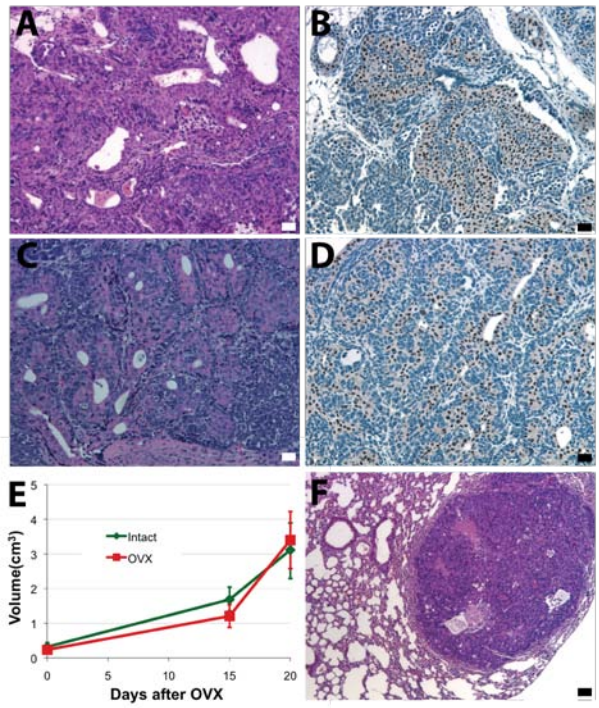

Figure 2.6 Outgrowths from transplanted tumor fragments.
ERα+ adenocarcinoma V09 (**A,B**) fragments were transplanted into mammary fat pads that had been cleared of endogenous epithelium in BALB/c-*Trp53*+/+ hosts. The tumor outgrowth in recipient BALB/c wild type mouse remained ERα+ adenocarcinoma (**C,D**). Half of the recipient mice were ovariectomized (OVX) when tumors were palpable. Tumor growth (**E**) was compared between ovary intact group and OVX group. Metastasis was seen in mice bearing transplants of tumor fragment from the V07 tumor (**F**). Scale bar: 20µm.

Compared to outgrowth from tumor fragments, outgrowth from tumor cell injection resemble less of original tumor yet more homogenous structure (Figure 2.7). It might be due to the culture condition while cells were isolated from minced tumor samples. The culture conditions favors growth of epithelial cells, consequently stromal cells were selected against during cell passaging. Before stable tumor cell lines were established, each line had also endured massive cell death and senescence during the initial transition to 2D culture and the first few passages. When stable cell replication and

regular cell passaging were achieved on each line, the culture may consist of only a few clones of tumor cells from the original sample.

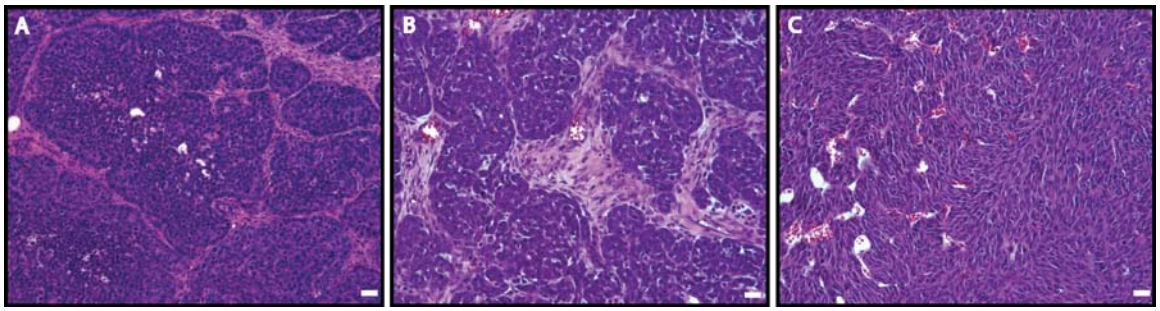

Figure 2.7 Outgrowth of transplanted tumor fragments and tumor cells isolated from spontaneous tumor.
Tumor fragments and cell line isolated from Adenocarcinoma V14 (**A**) were transplanted into mammary fat pads that had been cleared of endogenous epithelium in BALB/c-*Trp53*+/+ hosts. (**B**) Outgrowth from V14 tumor fragment. (**C**) Outgrowth from V14 tumor cell line. Scale bar: 20µm.

Origins of Mammary Tumors

To investigate the cellular origins, tumors from BALB/c-*Trp53*+/- mice were stained for markers of basal and luminal epithelial lineages (cytokeratins 5 or 8/18, respectively). A mixture of cells expressing either K5 or K8/18 (Figure 2.8A) was observed in 59% of the tumors, but co-expression of K5 and K8/18 in individual cells was rare. Both of the K5-positive cells and K8/18-positive cells were pleomorphic, disorganized, and in large quantities within each tumor. 26% of the tumors expressed only luminal cytokeratins (K8/18, Figure 2.8D) and 11% of the tumors expressed only K5-positive cells (Figure 2.8G). Tumors were also stained with cytokeratin 6 (K6) because it was found to be preferentially expressed in mammary stem/progenitor cells (132) and expanded in mammary tumors originating from progenitor cells (47;133;134). None of the K8/18-positive-only tumors contained K6 positive cells (Figure 2.8E-F),

whereas all of the double positive tumors and K5-positive tumors show K6 positive cells (Figure 2.8B-C, H-I). As the majority of tumors contained both luminal and basal cell lineages, it appears that tumors most often originate within the population of bipotent progenitors.

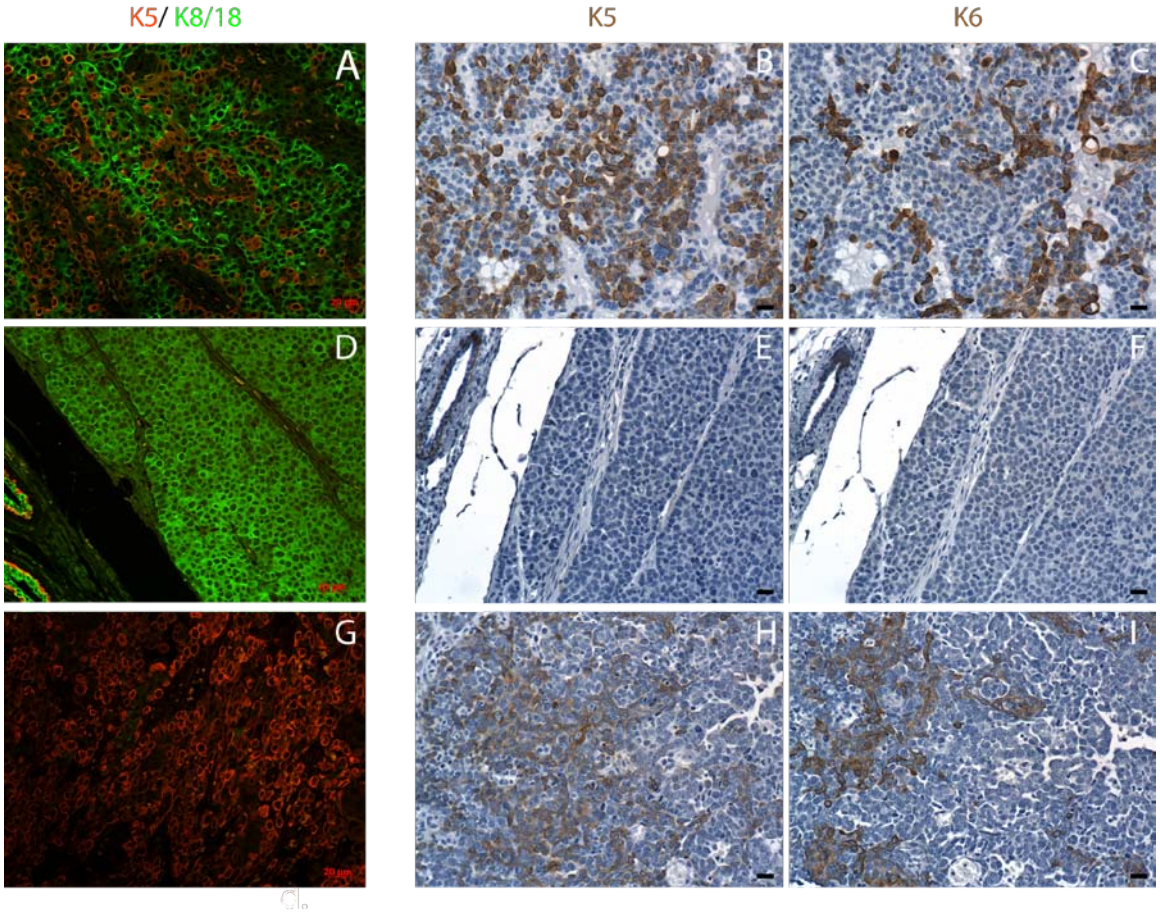

Figure 2.8 Heterogeneous patterns of keratin expression in mammary tumors from BALB/c-*Trp53*+/- mice.
Mammary ducts from BALB/c-*Trp53*+/- mice expressed cytokeratins normally with K5 localized to the basal/myoepithelium and K8/18 restricted to the luminal epithelium. (**A**) Most of the mammary tumors express a mixture of cells expressing K8/18 (green) with K5 (red). Though both cell populations were similarly abundant, cells expressing both luminal and basal keratins were rare. A smaller number of tumors have only K8/18 expressing cells (**D**) or only K5 expressing cells (**G**). Serial sections were also stained for K6 confirming the expanded populations of cells with basal-like cytokeratins among tumors composed of mixed populations of cells (**A, C**) and tumors expressing only K5 (**G, I**). In contrast, K8/18-only expressing tumors contain no K6 expressing cells (**A, C**). Although basal-like tumors contained cells that were positive for K5 and K6, individual cells do not necessarily express both (see **B vs C, H vs I**). Scale bar: 20µm.

Stem cell-related genes were shown to be enriched in aggressive breast cancers and have been suggested to reflect the origins of cancers within the progenitor cells of the breast epithelium (38). Therefore, expression of a panel of 84 stem cell-related genes was profiled in tumors that expressed either mixed luminal and basal keratins (V06, V22) and tumors expressing only luminal keratins (V07, V14). Distinct differences were observed for 9 genes (Figure 2.9, upper panel). N-cadherin (*Cdh2*) was elevated 22-fold in the "mixed keratin tumors" compared to normal mammary epithelial organoids while the "luminal-only keratin tumors" showed a 4-fold decrease compared to the normal mammary epithelial organoids. Expression of *Krt15* was also specifically elevated in the mixed keratin tumors along with cyclins D2 and E1 (*Ccnd2*, *Ccne1*). However, the overwhelming majority of genes showed similar patterns in both the tumors with mixed keratins as well as the tumors with luminal-only keratins (Figure 2.9, lower panel). While it is not surprising that both sets of tumors had elevations in proliferation-associated genes (Figure 2.9-I) compared to the normal mammary epithelium, levels of cytokines and growth factors were decreased (Figure 2.9-II). Both Notch and Wnt pathways have been implicated in maintenance of mammary stem cells (45;135;136). In both sets of tumors, ligands and receptors for Notch and Wnt were increased indicating that signaling through these pathways is increased dramatically compared to the normal mammary epithelium (Figure 2.9-V,VI). Therefore, there is broad overlap in the signaling pathways found in the tumors suggesting a common origin of the tumors regardless of the pattern of keratins expressed.

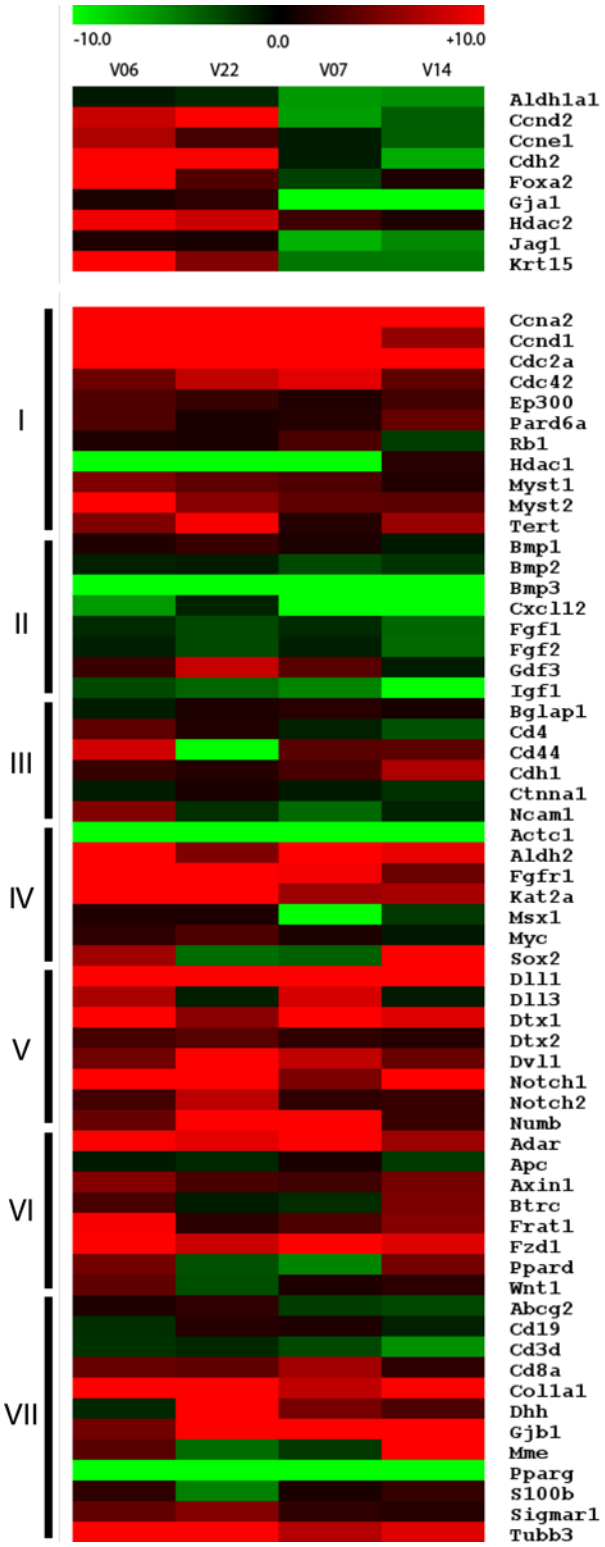

Figure 2.9 Expression of stem cell related genes in tumor samples differing in keratins expressed.

Expression of stem cell related genes was examined in tumors expressing "mixed keratins" (V06, V22) and tumors with "luminal-only keratins" (V07, V14). The

expression of each gene is presented as a ratio compared to the levels in normal mammary epithelium obtained by enzymatic digestion. A set of 9 genes are differently expressed between the two groups (top panel). However, 69 genes showed similar patterns of expression between the groups (bottom panel). The genes are grouped according to functions or pathways. (I) Cell cycle regulators, chromosome modulators and cell division related genes; (II) Cytokines and growth factors; (III) Cell adhesion molecule; (IV) Embryonic stem cell related genes; (V) Notch pathway related genes; (VI) Wnt pathway related genes; (VII) Tissue specific stem cell markers.

Parity is Protective in the BALB/c-*Trp53*+/- Mice

Parity is protective against breast cancer in human (95). We tested the protective effects in BALB/c-*Trp53*+/- mice by comparing tumor incidences and latencies between nulliparous *Trp53*+/- group and parous *Trp53*+/- group. Mammary tumors occurred in 43.2% of the nulliparous mice and 34.6% of the parous mice. Mammary tumor-free survival time was increased by 15 weeks in the parous group (Figure 2.10A, $P < 0.0001$) (90). So parity is effective in protecting from mammary tumors in this mouse model of Li-Fraumeni syndrome.

A few markers were used to detect possible molecular difference between the tumor from nulliparous mice and parous mice. There is an increase of ER+ tumors from parous mice (5/22, Table 2.2) compared to nulliparous mice (3/27, Table 2.2). So far it is hard to explain the increased proportion of ER+ tumors from parous mice. Since BALB/c-*Trp53*+/- mammary tumors appear to progress from ER+ to ER-, one of the explanations could be the earlier stage tumor collection in parous mice (older) due to co-morbidities (like lymphomas).

We applied lineage specific cytokeratin stain to the tumors from BALB/c-*Trp53*+/- parous mice (Figure 2.10). The majority of the parous tumors still contained a mixture of luminal (K8/18) and basal (K5) cytokeratin positive cells. Luminal (K8/18)

positive only tumors and basal (K5) positive only tumors were still proportionally in the minority. The fact that the proportion of each group of tumors (mixed, luminal or basal) remains similar between nulliparous and parous tumors supports the theory that parity protects against mammary tumors in BALB/c *Trp53*+/- mice by reducing the stem cell pool in those mice.

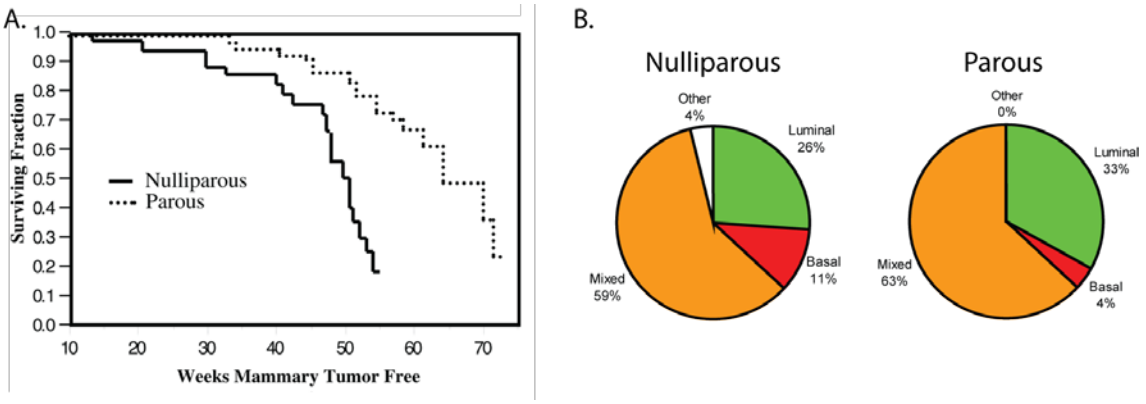

Figure 2.10 Parity is protective against mammary tumors in BALB/c-*Trp53*+/- mice. (A) The incidence of mammary tumors was monitored in both nulliparous and parous BALB/c-*Trp53*$^{+/-}$ female mice. The latency of spontaneous mammary tumors was increased in parous compared with nulliparous mice ($P < 0.001$) (90). (B) Cytokeratin (K8/18, K5) stain were compared between tumors from nulliparous and parous BALB/c-*Trp53*$^{+/-}$ female mice. Tumors contain mixed lineage cells dominant in both groups. There is a slight increase of luminal (K8/18) positive only tumors and a slight decrease of Basal (K5) positive only tumors in parous tumors compared to nulliparous ones. Tumor stained negative for both K8/18 and K5 was categorized as "Other".

Table 2.2 Features of mammary tumors from parous BALB/c-*Trp53*+/- mice.

Sample	Tumor type	ER	K8/18	K5
P01	adenocarcinoma	-	+	-
P02	MIN*	-	+	-
P03	adenocarcinoma	-	+	-
P04	adenocarcinoma	-	+	+
P05	adenocarcinoma	-	+	+
P06	adenocarcinoma	+	+	-
P07	adenocarcinoma	-	+	-
P08	adenocarcinoma	-	+	+
P09	adenocarcinoma	+	+	+
P10	adenocarcinoma	+	+	+
P11	adenocarcinoma	-	+	+
P12	adenocarcinoma	-	+	+
P13	adenocarcinoma		+	+
P14	adenocarcinoma	-	+	+
P15	adenocarcinoma	-	+	-
P16	adenocarcinoma	-	+	+
P17	adenocarcinoma	-	+	+
P18	adenocarcinoma	+	+	+
P19	adenocarcinoma	-	+	+
P20	adenocarcinoma	-	+	-
P21	adenocarcinoma	-	+	+
P22	adenocarcinoma	+	+	-
P23	adenosquamous carcinoma	-	-	+
P24	MIN	+	+	+

* MIN: Mammary intraepithelial neoplasia

Discussion

Although the p53 tumor suppressor pathway is commonly disrupted in a variety of cancers, breast tissue appears to be uniquely sensitive to the proper functioning of this pathway to prevent tumors. Heritable mutations in the *TP53* gene have been linked to Li-Fraumeni syndrome and breast cancer is the most common tumor type in women (81;83). Somatic mutation of *TP53* is also common in sporadic breast cancers (57;58) and may initiate tumorigenesis by pathways similar to those in Li-Fraumeni syndrome. Similar to Li-Fraumeni syndrome, BALB/c-*Trp53*+/- mice exhibit a prevalence of mammary tumors as well as lymphomas and sarcomas (89). The slow onset of mammary tumors allowed detailed analysis of the cellular targets and molecular events leading to mammary tumors. Although deficiency in p53 has been associated with impaired cell cycle control and apoptosis, there was no detectable difference in proliferation rates within the mammary epithelium of *Trp53*+/- and *Trp53*+/+ mice (Figure 2.1). In contrast, both basal and radiation-induced apoptosis in the mammary epithelium were decreased with *Trp53* gene dosage (90). Therefore, haploinsufficiency with respect to apoptosis, not proliferation, is associated with the susceptibility to mammary tumors in BALB/c-*Trp53*+/- mice. Haploinsufficiency in p53-mediated apoptosis has been observed in the involuting prostate of mice (137) and the pro-apoptotic role of p53 appears to be critical for suppression of lymphomas while cell cycle checkpoint function was dispensable (120). Thus, a decrease in p53 dosage was suggested to be sufficient to initiate breast tumors (138). However, in our study, the diminished spontaneous apoptosis in *Trp53*+/- mammary epithelium did not lead to a discernable increase in preneoplastic lesions

compared to the *Trp53*+/+ mice. The glands were normal with respect to ductal branching and alveologenesis. Therefore, *Trp53* haploinsufficiency alone did not permit initiation of preneoplasia.

Although *TP53* LOH is frequently observed in breast tumors among Li-Fraumeni patients (139), it has been unclear whether loss of the wild type allele of *TP53* initiates preneoplasia or it accompanies the transition to invasive cancers. In BALB/c-*Trp53*+/- mammary tissues, LOH was prevalent in invasive tumors, but not hyperplasia or MIN. Although rates of LOH in tumors differs between strains of mice and segregates with the predisposition to mammary tumors (88), LOH at *Trp53* was also observed in *K14-cre,Trp53*$^{fl/+}$ mice in a mixed 129xFVB background (140). Therefore, LOH appears to be a rate-limiting step in the genesis of mammary tumors. As p53 plays an important role in responding to oncogenic stimuli and the DNA damage response (DDR), it has been proposed that p53 function limits growth of preneoplastic cells and loss is necessary for progression (141). These results favor a model of carcinogenesis in which activation of oncogenes stimulate preneoplasia in both *Trp53*+/- and *Trp53*+/+ tissues. Though progression is limited by p53, the pro-apoptotic activity and double strand break repair pathways are impaired in *Trp53*+/- tissues allowing illegitimate mitotic recombination (88) which can abolish the wild type allele of *Trp53* eliminating the rate limiting step in the tumor progression.

While the requirement for loss of p53 function appears uniform, the histological appearance of the tumors in p53-deficient mice suggests divergent cellular origins. Oncogene-specific tumor phenotypes have been reported in transgenic mice expressing Her2/Neu or Ras (33;36;142), and thus, the heterogeneity of the tumors may reflect the

collaborating oncogenes. Alternatively, the tumor phenotypes may depend on the cellular origins. Selective deletion of *Trp53* in basal or luminal compartments using the Cre recombinase under control of K14, MMTV or WAP promoters resulted in heterogeneous tumor phenotypes (35;140;143) suggesting that tumors can arise from both luminal and basal cells. However, the origins were not definitive as Cre activity was evident in both the luminal and basal cells in these experiments. A WAP-cre that is restricted to the luminal epithelium and is pregnancy-dependent to drive activation of a point-mutation of *Trp53* (R270H) yielded tumors that were positive, as well as negative for ERα (144) suggesting that the luminal lineage can yield both ERα-positive and –negative tumors. Using more extensive immunophenotyping, we found that 59% of spontaneous mammary tumors in BALB/c-*Trp53*+/- mice expressed both luminal and basal keratins (K8/18 and either K5 or K6) suggesting origin of the tumors within bipotent progenitors (summarized in Figure 2.11). A smaller fraction of tumors expressed only luminal or basal keratins. There was no association between the oncogenes expressed and tumor phenotypes as Her2/Neu and Notch1 were detected in tumors with either luminal or basal keratins while the ERα-positive tumors were positive for both luminal and basal keratins. Although tumor V09 expresses high levels of ERα and PR and the phenotype was stable when tumor fragments were transplanted, its growth was estrogen-independent (Figure 2.7). This underscores the challenge of predicting origins or behavior of tumors based on a limited number of biomarkers.

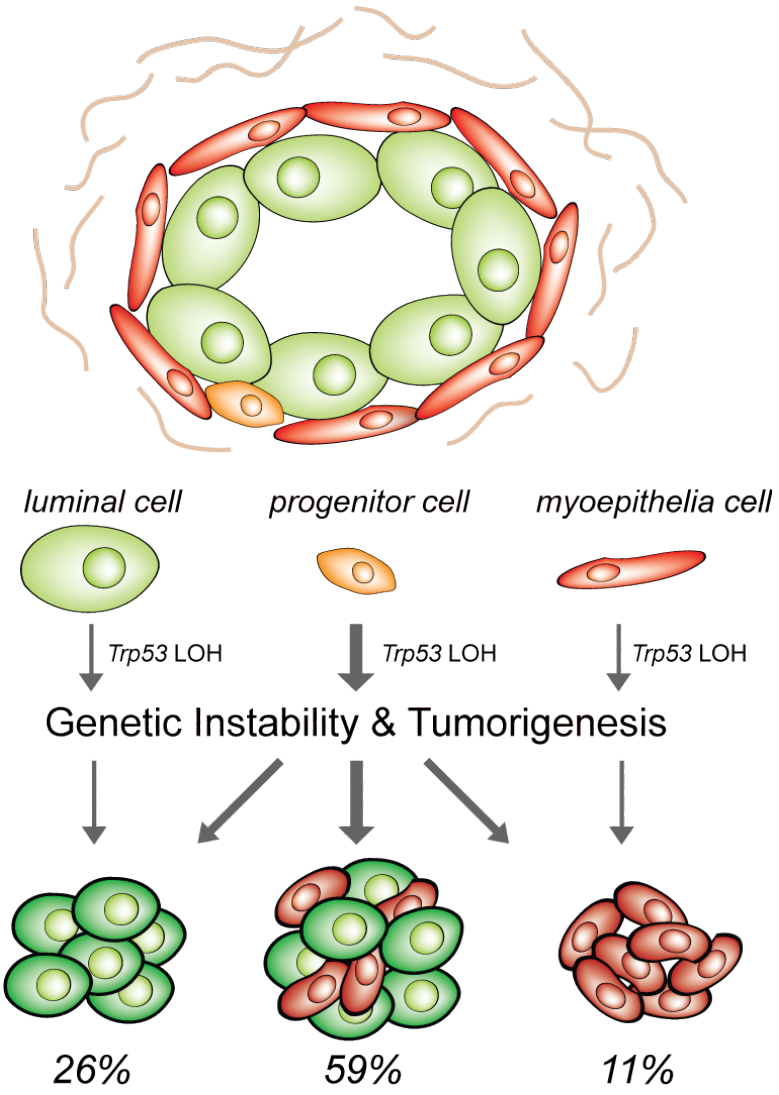

Figure 2.11 Cellular origins of mammary tumors in BALB/c-*Trp53*+/- mice
Mammary glands in BALB/c-*Trp53*+/- mice display normal ductal and alveolar structures composed of luminal (green) and basal cells (red). Progenitor cells (orange) with a potential to differentiate into both epithelial lineages also reside in the normal structure. Loss of the wild type allele of *Trp53* in any of these cells would abolish the rate limiting step in tumorigenesis resulting in invasive mammary tumors. As the majority of mammary tumors contain tumor cells expressing luminal and basal markers, a clonal origin within bipotent cells is suggested as the most common pathway. For tumors expressing only luminal or basal markers, there could be two possibilities. They may originate from bipotent progenitors and later partially-differentiate into tumors with single lineage cells or they could originate within the lineage-restricted cells. The overall similarity of the stem cell gene expression pattern of tumors suggested the former path.

As the majority of tumors expressed both luminal and basal keratins, it would appear that tumors initiate most often within stem cell/progenitor cells, and later differentiate into two (or more) distinct populations. It is possible that progenitor cells may be most susceptible to transformation, but decreased p53 function may also lead to expansion of the progenitor cell pool. The p53 protein plays a fundamental role in restricting the pool of stem cells in embryonic stem cells (67-69) as well as adult tissues including neuronal (73;145), hematopoietic systems (70;71) and mammary glands (74;75). In mammosphere culture of BALB/c *Trp53+/+, Trp53+/- and Trp53-/-* mice, haploinsufficiency is reflected on both the size of the mammospheres and the count of mammosphere initiating cells (unpublished data, L.Tao and D.J. Jerry). These results suggest an *in vivo* expansion of stem cell/progenitor pool in BALB/c *Trp53+/-* mice. Loss of p53 allows expansion of cancer stem cells either through asymmetric division or by promoting phenotypic plasticity and the acquisition of stem cell characteristics (119;146). Mammary tumors from BALB/c-*Trp53*+/- mice showed evidence of activated Wnt and Notch signaling. Aberrant signaling in these pathways could result in stem cell expansion and tumorigenesis in mammary glands (45;135;136). However, it remains possible that the tumors initiate within lineage-restricted cells and acquire the stem cell signature during progression.

Basal-like tumors are among the five mammary tumor subtypes identified recently by microarray profiling of human invasive breast carcinomas. It frequently harbors *p53* mutation and has poor clinical outcome (26;27). Microarray profiles on murine mammary tumor models reveals that tumors from *Trp53* deficient models showed basal like features and shared significant association with the human basal-like tumor

subtype (37). We are the first to show parity is protective against mammary tumor from *Trp53* heterozygous mice though human data is still unavailable (probably due to the early tumor incidence in Li-Fraumeni syndrome patients). Like *Trp53*-deficient mammary tumors, BRCA1-related hereditary breast cancers are also most commonly basal type (147;148). Up to 90% of *BRCA1*-associated tumors harbor TP53 alteration (149). Parity is protective against breast cancer in carriers of *BRCA1* mutation (150). More interestingly, *BRCA1* plays a critical role in the differentiation of ER-negative stem/progenitor cells to ER-positive luminal cells, and loss of BRCA1 function results in aberrant expansion of the stem cell pool in the human breast (151). Expanded bipotent progenitor cells were identified in breast tissues from *BRCA1* mutation carriers and showed abnormal growth *in vitro* (140). Evidence is accumulating that an expanded stem/progenitor cell pool resides in histologically normal mammary glands in both p53 deficient models and *BRCA1* deficient models. While the hypothesis that parity alters mammary stem cell numbers to provide protection against breast cancer is still under investigation, the similarity of lineages markers in tumors from nulliparous and parous BALB/c *Trp53*+/- supports the progenitor origin. Better lineage markers and lineage tracing techniques are required to prove the stem/progenitor origin of malignant transformation. On the other hand, one should never exclude differentiated cells as tumor initiating cells. The multi-step tumorigenesis (accumulation of gene mutations) may accompany each step of replication/differentiation, while the last straw can just happen in any position of the cellular hierarchy.

CHAPTER 3

USING MAGNETIC NANOPARTICLES FOR CANCER THERMOTHERAPY

Introduction:

Conventional cancer treatment involves a combination of surgery, chemotherapy and radiation therapy. Although often effective, significant damage is inflicted on healthy tissues and patients suffer from systemic side effects. Two types of targeting can be used to improve the current tumor therapy. First, tumors can be targeted spatially, with the toxic effect of the therapeutic agent localized to the tumor site only. The second type of targeting is to specifically direct treatment on tumor cells, sparing all normal cells in the vicinity. To achieve both of the goals, recent research has focused on regional heating of tumors using magnetic particles.

Thermotherapy as Cancer Treatment

Thermotherapy is a type of cancer treatment in which tumor tissues are damaged by exposing them to elevated temperatures. Under low pO_2 and low pH conditions in most solid tumors, tumor cells are more vulnerable to modest temperature rise (up to 46°C) while normal tissues are usually less sensitive (152). Elevation of tissue temperature above 40-41°C alters the function of many structural and enzymatic proteins within cells that can lead to apoptosis within hours or necrosis, if the temperature is higher than 46°C. Loss of membrane integrity, protein denaturation and inhibition of biochemical pathways have been implicated as the causes of cellular death (152;153). A few clinical trials have been conducted using hyperthermia as adjuvant therapy

(combined with traditional chemotherapy or radiation) for various types of cancers, including sarcoma, melanoma, and cancers of the head and neck, brain, lung, esophagus, breast, bladder, rectum, liver, appendix and cervix. Many of these studies have shown a significant reduction in tumor size compared to using traditional therapy alone (152;154).

Common thermotherapy techniques include electromagnetic waves radiated by antennas (microwave or radiofrequency probes) (155;156), laser (157), focused ultrasound (158;159) and magnetically excited metal thermoseeds (160;161). While effective in producing heat, the macroscopic heating systems perform poorly on heat distribution, thus have limited efficacy with larger tumor volumes. Insufficient temperature rise in parts of the tumor results in treatment failure. However, extensive intratumoral temperature rise can induce damage to adjacent normal tissues.

Two new approaches use nano-materials as a heating source to achieve better heat distribution: near-infrared laser induced thermotherapy and magentic field induced thermotherapy. In the former technique, metal nanoshells (162;163), nanorods(164), carbon nanotubes (165) provide selective heating to tissues upon exposure to intense near-infrared laser irradiation (NIR) from outside the body. The moderate penetration depth of NIR, however, limits the utility of this method in treating deep lesions in the body. Magnetic field induced thermotherapy uses alternating magnetic field (AMF, energy source) to heat nanoparticles (heat source) embedded within tissue (Figure 3.1). Animal tissue is essentially transparent to magnetic fields, and even quite strong fields are harmless to the human body (166). Furthermore, it can reach high cellular selectivity via tailored surface modification of the nanoparticle. In other words, thermotherapy using

AMF induced heating of nanoparticle can achieve localized, controlled heating in deep tumor tissue without damaging adjacent normal tissue.

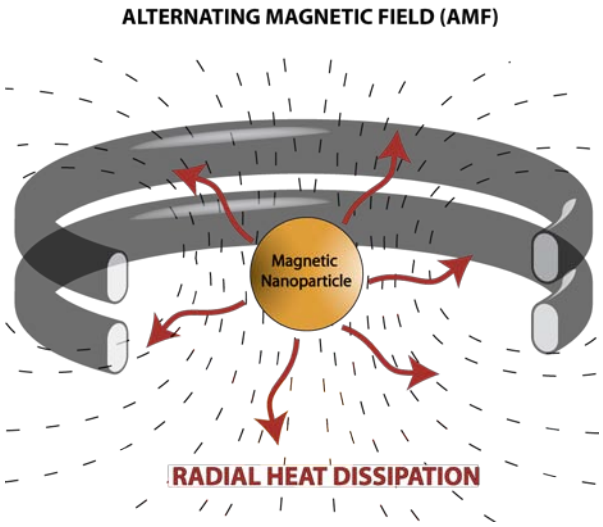

Figure 3.1 Inductive heating of magnetic nanoparticles
Heat is produced by the imposed alignment of magnetic dipoles in an alternating magnetic field produced in a coil. (courtesy of Fischer N.F.)

Heating of Magnetic Nanoparticles for Thermotherapy

Up to now, all magnetic nanoparticles intended to be used in vivo are composed of magnetic iron oxides (167). The main reason for this is their low toxicity and the known pathways of metabolism. Magnetic nanoparticles in an alternating magnetic field produce heat by Néel and Brownian relaxation. In the process of Néel relaxation, the AMF induces the rotation of magnetic moments within the magnetic core. Heat is then dissipated when the particle moment relaxes back to its equilibrium orientation. In addition, a portion of heat is generated due to rotational Brownian motion, namely the motion of the whole particle due to the exerted torque of the AMF (168).

Magnetic nanoparticle-loaded liposomes (169), magnetic fluids (ferrofluids)(170) and magnetite-doped microspheres (171), have been utilized in hyperthermia and ablation therapies with varying success. Hilger et al demonstrated the ablation of tumors by intratumoral injection of ferrofluid (magnetic particles suspended in a carrier fluid) followed by alternating magnetic field, whereby temperatures of up to 71ºC were achieved in as little as four minutes using biocompatible field strengths (170). However, these particles required liposome or anionic surfactant to keep them stable and/or solube which limited their further application in biological systems. Actually, many iron oxide nanoparticles have a high tendency to agglomerate and thus to build larger structure even in the absence of a magnetic field. It has a strong influence on the magnetic properties of the particle and its biomedical applications.

Water soluble superparamagnetic iron oxide nanoparticles (SPION), i.e. those that do not have a permanent dipole or domain wall which prevents undesired magnetic agglomeration even under the influence of an external magnetic field, are favored for biological applications. SPION coated and stabilized with hydrophilic polymers have been found to be quite thermodynamically stable under physiological conditions, not exerting obvious toxic effects (167). SPION with dextran or aminosilane coating have also been tested for thermotherapy (172). Aminosilane coated iron oxide nanoparticles (120 mg/ ml) were injected into transplanted prostate tumors in rats which then were exposed to 12.6 kA/m AMF for 60min. Intratumoral temperature reached 54.8ºC at maximal and 41-50% tumor growth inhibition was observed (173). DeNardo et al. reported the use of antibody conjugated dextran-coated iron oxide nanoparticle for targeted thermal cancer therapy (systemic injection) followed by application of a very

high magnetic field (700 Oe = 55.7 kA/m) (174). They observed a significant decrease in tumor growth. In these cases, heating capacity of these nanoparticles are largely reduced, due to polydispersity of the sizes of the nanoparticles, thus creating a need to use either high concentrations (with concomitant toxicity) or magnetic field strengths close to the lethal dose (173-175).

These studies illustrate the potential of using iron oxide nanoparticles for magnetic-mediated thermal ablation of tumors, but chemical and biological improvements are needed in order to achieve its full potential. First, the heating capacity of magnetic nanoparticle largely relies on its size and degree of monodispersity (176). Maximal heating of iron oxide nanoparticles require core size around 14 and 20nm (Fe_3O_4 and Fe_2O_3, respectively), according to theoretical calculation. Optimizing magnetic nanoparticle core size and decreasing size polydispersity will greatly help realizing its full heating potential. The second is to tailor the particle surface to promote biocompatibility and specific interaction with target tumor cells. The ideal passivation should confer the particle its stability on shelf, biocompatibiltity *in vivo* and selective targeting on tumor cells to various extents. For example, folate receptor is highly expressed on a variety of cancers, especially ovarian cancer. A few normal tissues also express folate receptor, but at a much lower level than folate receptor positive tumor samples. Folate can be engineered onto nanoparticle surface as part of passivation as well as target molecule. The same principle applies to antibodies against tumor specific antigens, e.g. Her2/Neu in human breast cancer.

Materials and Methods

Determination of the Particle Sizes

TEM images were acquired on a JEOL 100CX operating at 100keV. Samples were drop cast from water solution, onto a copper coated grid, dried, and imaged. The particles' size distribution, assigned as the standard deviation (SD), was measured using Image J software.

Experimental Setup for Magnetic Thermotherapy

An alternating magnetic field (AMF) heating system was purchased from MSI Automation, Inc. (Wichita, Kansas, USA). The experiment was performed inside a copper coil (diameter 10 cm), which produces an AMF at a fixed frequency of 400kHz and fixed amplitude of 6.3 kA/m. The experimental setup is depicted in Figure 3.2a. The temperature of the sample holder was maintained at 37±0.5ºC by using a thermal pad. The temperature for the experiments was measured by a DualLogR thermocouple thermometer (Eutech Instruments Pte Ltd, Singapore) with a TEF-30-T thermocouple (J-KEM Scientific, Inc. St. Louis, MO, USA). The initial linear rise in temperature versus time dependence, dT/dt, was measured as illustrated in Figure 3.2b. The specific absorption rate (SAR) is defined as follows.

SAR=(C_{water}/c)dT/dt, where C_{water} is the specific heat capacity of water and has the numeric value corresponding to 4185 J L/K, c is the sample concentration in g/L.

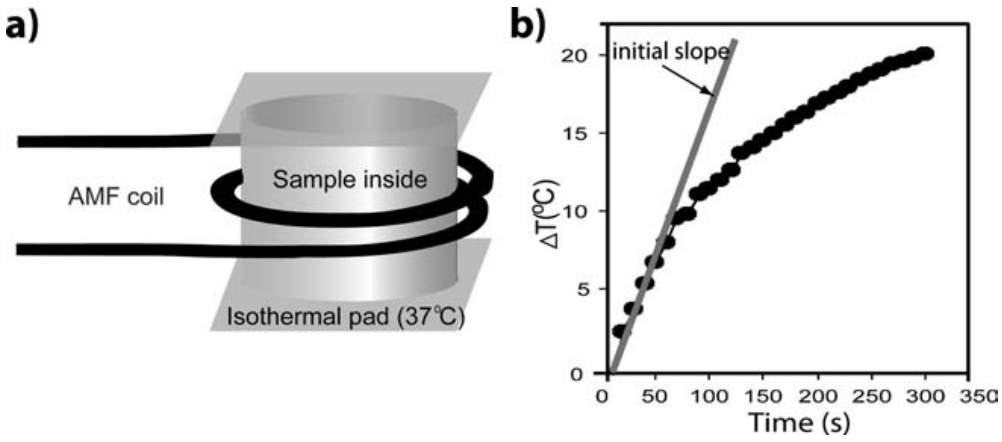

Figure 3.2 Experimental setup for magnetic thermotherapy
(a) Schematics of the AMF device for alternating magnetic field thermotherapy. **(b)** SAR was measured using the initial slop of dT/dt.

FT-Infrared Spectroscopy

Infrared spectra were taken of KBr pellets formed from dry powder samples of BSA, iron oxide precursor and MNP-A using a MIDAC M1200-SP3 spectrophotometer.

Dynamic Light Scattering (DLS)

DLS samples were prepared using 5 mM sodium phosphate buffer (pH=7.4) and in milliQ water filtered with Acrodisc 0.2 µm filters (Pall Gelman Laboratory, Ann Arbor, MI). The NPs' concentration was ~1 mg/mL. The measurement was performed on a Malvern Zetasizer Nano ZS instrument. Reported values of data are averages of nine measurements.

Thermogravimetric Analysis (TGA)

Thermogravimetric analysis was carried out using a TA Instruments (New Castle, DE) TGA 2050 thermogravimetric analyzer. 4.4 mg of MNP-A was placed in a open

platinum pan and heated from room temperature to 800°C with a heating rate of 10°C/min under acontinuous air purge of N_2.

Circular Dichroism (CD)

Far-UV CD spectra of BSA, thermally denatured BSA and MNP-A were measured on a JASCO J-720 spectropolarimeter with quartz cuvettes of 1mm path length at 25ºC. The spectra were recorded from 190 to 250 nm as an average of three scans at a rate of 10nm/min.

Stability Assays

100 µL of nanoparticles (10 mg/mL stock in distilled water) was added to 1900µL of deionized water, or cell culture medium. UV-visible absorbance spectra (HP 8452 spectrophotometer) were obtained for different time interval under room temperature.

Cell Culture

HeLa cells were grown in a RPMI1640 medium (Gibco BRL) supplemented with 10% fetal bovine serum (Gibco BRL), MEM non-essential amino acids (Sigma), sodium pyruvate (1mM), sodium bicarbonate (0.15%, w/v) and antibiotic–antimycotic solution (100 µg/mL penicillin + 100µg/mL streptomycin + 0.25µg/mL amphotericin B) in an atmosphere of 5% CO2 at 37ºC.

Thermal Effect of MNP-A on 2D Cell Culture

$8x10^4$ HeLa cells/well were seeded in 4 well plates ($200mm^2$/well) and incubated overnight. Then the culture medium was replaced by MNP-A containing medium for 2 h

followed by 45min magnetic field exposure. After AMF exposure, cells were immediately washed by PBS twice and subjected to cell viability assay.

Cell Viability Assay

Cell viability was measured by quantifying the reduction of a dye indicator alamar blue. Alamar blue is a dye that takes advantage of mitochondrial reductases to change from oxidized indigo blue state to reduced pink state. This dye has been successfully used in various cell cultures to measure cell viability (177;178). Briefly, cells in 4-well plates are loaded with 300µL culture medium containing 10% alamar blue (Biosource International) and incubated in 37ºC, 5% CO2 for 2 h. 100µL medium from each well was then transferred to a 96-well plate and subjected to measurement. The reduction of alamar blue was measured and calculated by a SpectroMax M5 micro-plate reader (Molecular Devices, Inc.) at 570 nm and 600 nm wavelengths.

Cell Staining

HeLa cells were incubated in MNP-A (4 mg/mL) containing medium for 2 h under cell culture conditions. After washing with PBS, cells were fixed with methanol at -20ºC, washed with PBS, incubated for 15 min in a solution of 2% potassium ferrocyanide (Sigma P9387) in 2% HCl, washed, and counter stained with eosin.

Quantification of Cell-bound MNP

Procedure for quantifying total cell-bound iron was based on published literature using Prussian blue reaction (179). Briefly, harvested MNP treated cells from 6-well plates were dissolved in 6N HCl (125µL/well) overnight. Then 125µL of 5%

K4[Fe(CN)6] was added into each sample. After 10min incubation, the absorbance was read at 690nm in SpectroMax M5 micro-plate reader. A standard curve of an aqueous $FeCl_3$ solution was treated in the same conditions to quantify the amount of cell-bound iron. Detailed protocol see Appendix.

Colony Formation Assay

After treatments, cell pellets were resuspended in 10mL culture medium and total live cells were counted using trypan blue staining. Cells were seeded into 60mm cell culture dishes at 1500 cells/dish. and culture for 7-10 days with no disturbance. Cell dishes were then fixed with 10% neutral-buffered formalin at room temperature for 10mins, washed with distilled water. Each dish was stained with 1% crystal violet for 5min followed by tap water rinse. Visible colonies were counted by G-box system.

Results [*]

Heating capacity and biocompatibility of iron oxide magnetic nanoparticles

The heating capacity of NPs was assessed by the surface absorption rate (SAR). When conditions of alternative magnetic field are fixed, SAR is mostly dependent on particle size and distribution. Numerous attempts were made in the chemistry lab (Dr. Rotello) during the course of the study to produce desired MNP.

Five iron oxide nanoparticles passed initial tests (SAR and water solubility) and were brought to in vitro biocompatibility test (Table 3.1). The albumin passivated

[*] *Most of the data in this chapter is published in Journal of Materials Chemistry, 2008 (180), except "Heating effects of cell bound MNP-A"*

magnetic nanoparticle (MNP-A) surpassed other nanoparticles showing efficient heating with very low inherent cytotoxicity.

Table 3.1 Features of magnetic nanoparticles in current study

Particle passivation	Core size (nm)	Surface charge	SAR* (W/g Fe)	Solubility in PBS	Solubility in cell culture medium w/ serum	Toxicity[§]
$-NH_2$	22	+	~10	yes	yes	high
-citrate	12	-	20[‡]	yes	visible aggregation	low
-folate	12	-	20	yes	partial aggregation in 24hrs	not tested
$-N(CH_3)_3$	12	+	36[±]	no	Yes (trace of precipitation)	low
-BSA[#]	12	-	36	yes	yes	very low

* SAR: specific absorption rate, heating capacity were measured under AMF (400kHz, 6.3kA/m)

[#] BSA: bovine serum albumin

[§] Toxicity test: Viability of HeLa cells tested after treating with culture medium containing MNP for 6hrs (Figure 3.3). Alamar Blue cell viability kit were used for viability test.

[±] Magnetic separation were performed to collect larger size nanoparticles.

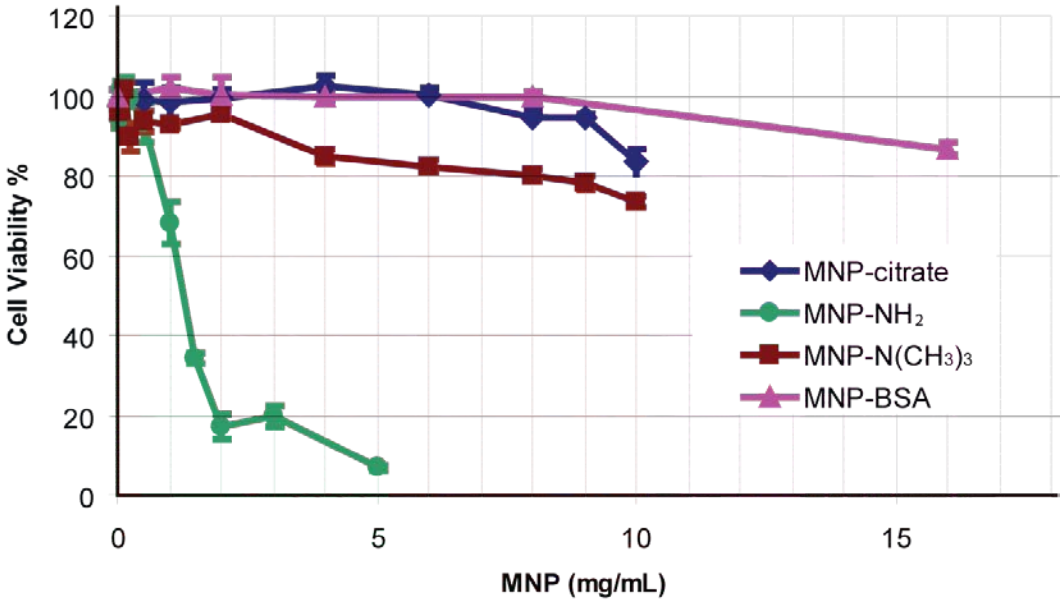

Figure 3.3 Toxicity test of MNPs.
HeLa cells were treated with various MNPs at different concentrations for 6hrs. After the treatment, cells were subjected to alamar blue cell viability test. Each testing point represents 4-6 replicates.

Features of albumin passivated magnetic nanoparticle (MNP-A)

The synthesis adopted a modified Massart's co-precipitation method to provide "naked" nanoparticles suitable for facile functionaliztion. Bovine serum albumin (BSA) passivation of the iron oxide core was performed via ultrasonication of the particle in the presence of excess BSA. BSA coated iron oxide (MNP-A) nanoparticles were isolated from excess BSA solution via ultracentrifugation (Figure 3.4a). The TEM micrograph of MNP-A revealed the NP core was 12.1±1.6 nm in diameter (Figure 3.4b).

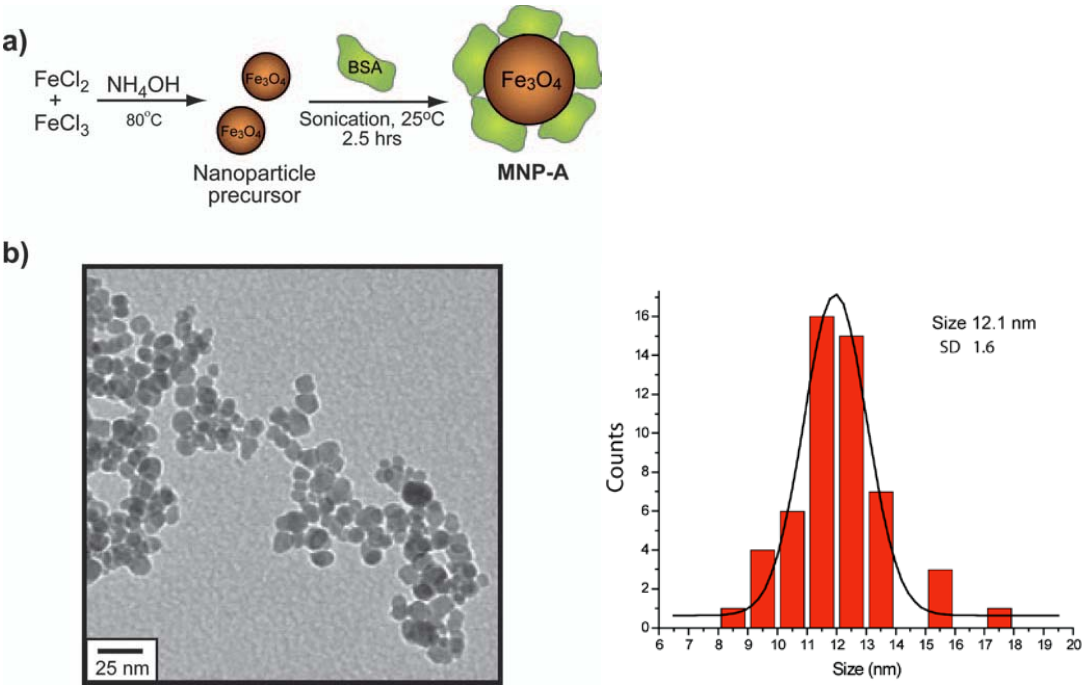

Figure 3.4 Synthesis, structure and size of MNP-A
(a) BSA was incorporated as MNP coating using ultrasonication; (b) Transmission electron microscopy (TEM, *left*) and histogram (*right*) of MNP-A core size (d=12.1±1.6 nm)

BSA is an anionic protein with a pI of 4.8, so it is likely that adsorption of the BSA onto the NP occurs through anionic functionality of the BSA. The presence of BSA on the NP surface was confirmed by Fourier transform infrared (FT-IR) spectroscopy, as the characteristic bands of the BSA protein at 1660 cm^{-1} and 1530 cm^{-1} are both present in the FT-IR spectra of MNP-A (Figure 3.5a). In addition, thermogravimetric analysis (TGA) was conducted to quantify the amount of adsorbed BSA (Figure 3.5b). The 22.5% weight loss observed from TGA of MNP-A corresponds to ~13 BSA molecules per iron oxide core. The adsorption of BSA to the NP core results in partial denaturation of the protein (Figure 3.5c). Considering the size of BSA (8.4nm), the thickness of the protein

shell on the nanoparticle would be ~8 nm, therefore the overall diameter of MNP-A would be ~28nm. In aqueous solution, the average hydrodynamic size of MNP-A is 50±5 nm, measured by dynamic light scattering (DLS) (Figure 3.5d). The increase in hydrodynamic diameter of MNP-A suggests that there is minor particle aggregation.

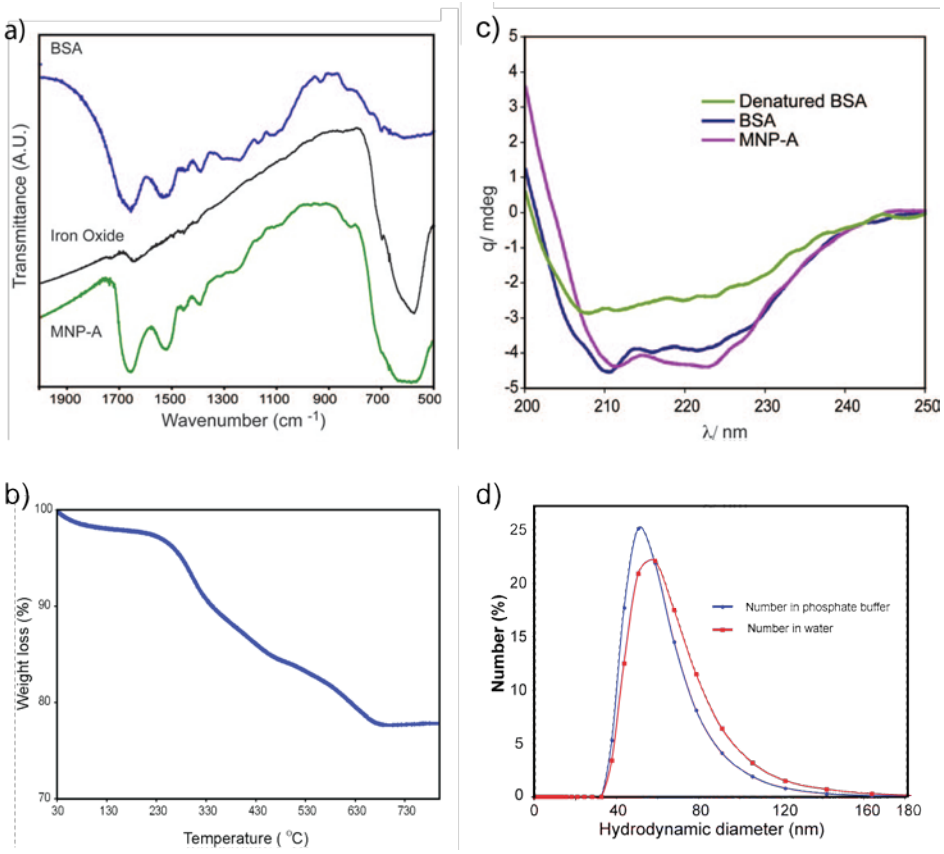

Figure 3.5 Characterization of MNP-A
(a) FT-IR spectrum of BSA (blue), iron oxide core (black) and MNP-A (green). b) MNP-A showed 22.5% weight loss on TGA test (c) Circular dichroism spectra of BSA, MNP-A and thermally denatured BSA. d) DLS analysis of MNP-A in H_2O and PBS.

MNP-A showed excellent long-term solution stability, remaining stable in deionized water for more than 2 months. No aggregation was observed under a variety of conditions, including deionzed water, and cell culture medium (Figure 3.6).

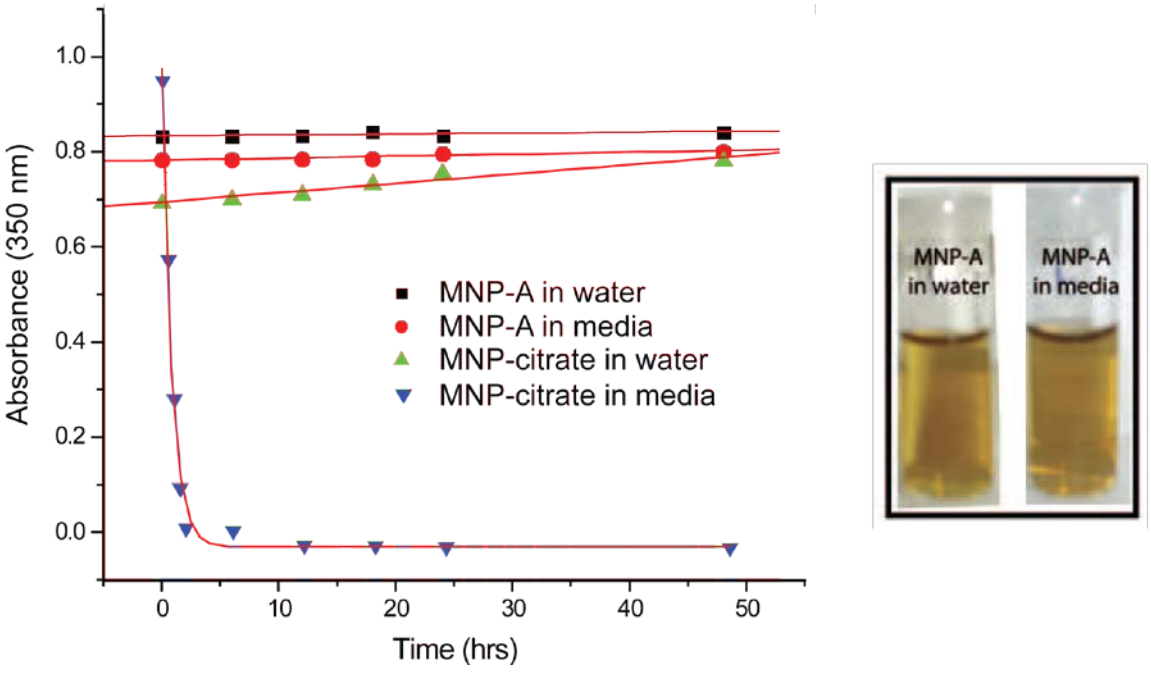

Figure 3.6 MNP-A showed stability in H_2O and cell culture medium.
Both MNP-A and MNP-citrate were prepared at 0.5mg/ml in water and cell culture medium. UV-visible absorbance spectra were obtained at different time points up to 50hrs under room temperature. MNP-A were stable in both solvent throughout the test, while MNP-citrate precipitated in cell culture medium.

Alternating magnetic field induced MNP-A heating on 2D cell culture

Thermal effects of MNP-A under AMF was first tested in cultured cancer cells. HeLa cells were incubated with MNP-A for 2 h followed by 45 min of magnetic field exposure (400 KHz, 6.3 kA/m). As a control, cells were also treated with MNP-A alone or AMF alone, or medium only. Immediately after treatment, cytotoxicity was measured among the treatments. The cells incubated with NP concentrations of more than 4 mg/mL subjected to the magnetic field showed total cell death after treatment, whereas cells that were treated with particles but without exposure to the magnetic field were unaffected, even at much higher NP concentrations (Figure 3.7). As expected, control cells that were

exposed to the magnetic field in the absence of NPs showed no decrease in the cell viability. In this experimental setup, cancers cells were abolished by the temperature rise due to the MNP-A heating under AMF. It demonstrates that MNP-A provides a selective tool for AMF-induced ablation, as well as useful dosing information for future animal study.

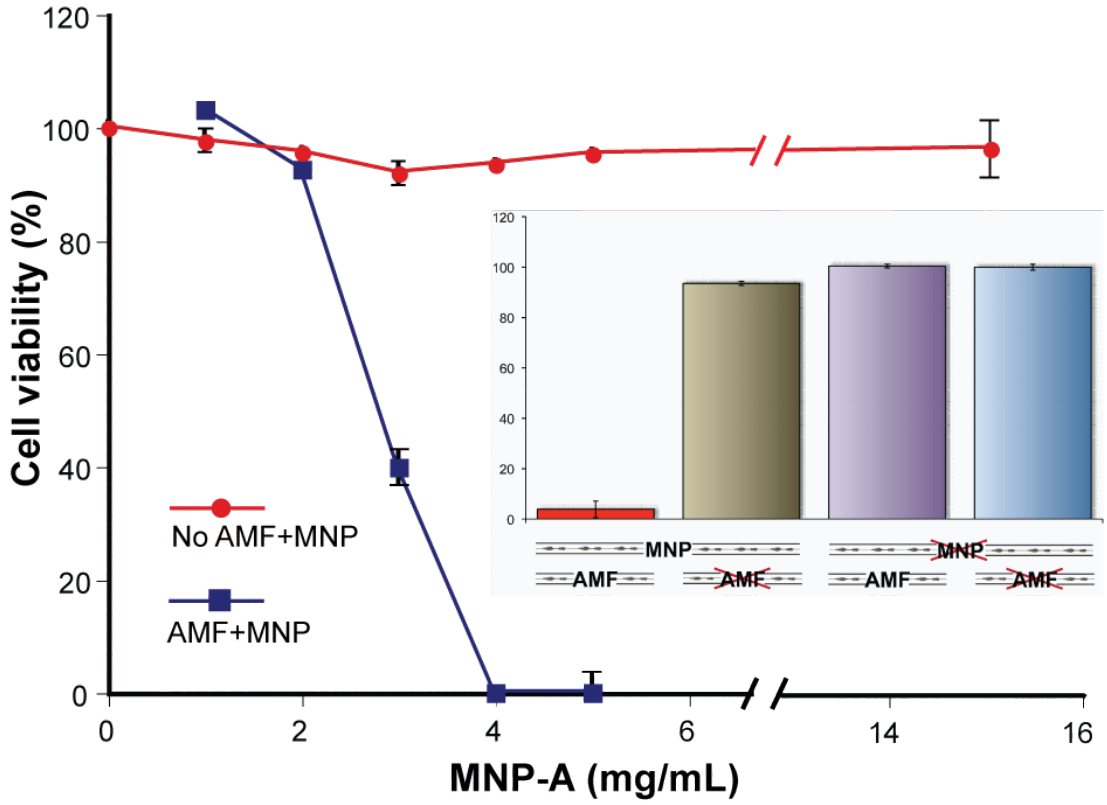

Figure 3.7 Thermal effect of MNP-A on cell culture
HeLa cells were incubated with MNP-A for 2 h followed by 45 min magnetic field exposure. After AMF exposure (400kHz, 6.3kA/m), cells were immediately washed by PBS twice and subjected to a cell viability (10% alamar blue reduction) assay, with cell death being confirmed by trypan blue staining (data not shown). Inset: Heating effects at 4mg/mL MNP-A.

Heating effects generated by cell-bound MNP-A under AMF

With prominent bulk heating effects established, MNP-A was further examined on its interaction with individual cells. Perls Prussian blue staining of MNP-A-treated HeLa cells revealed a high density of nanoparticles on the cell surface (Figure 3.8a). MNP-A was not only attached to the cell surface, they were also abundant in cytosol and cell nuclei (Figure 3.8b). We regard these MNPs as cell-bound MNPs which include particles that tightly attached to cell surface as well as internalized nanoparticles. It is likely that MNP-A is internalized into cells by endocytosis and phagocytosis (181). The amount of cell-bound MNP-A showed a tendency of MNP concentration dependence and incubation time dependence during the 48hrs study period. After the cells were treated with 2mg/ml MNP-A for 48hrs, cell bound MNP-A can reach as high as 12pg Fe/cell (Figure 3.8c).

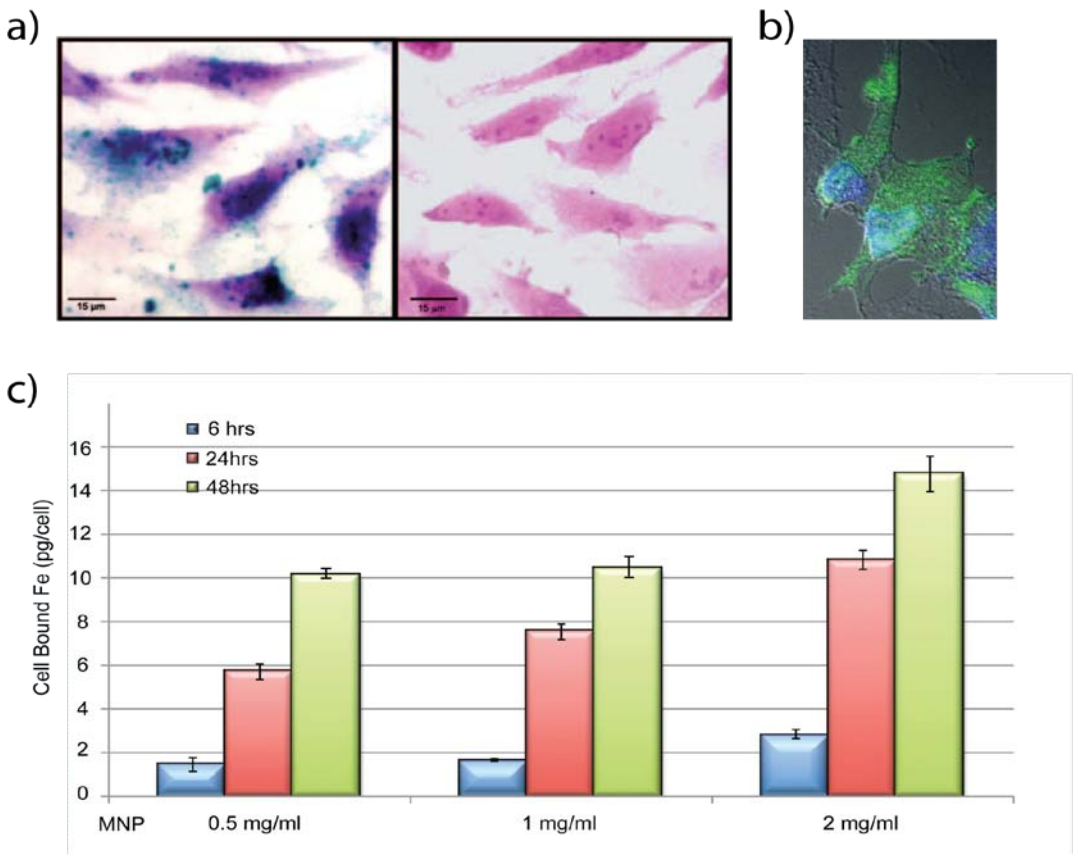

Figure 3.8 Interaction of MNP-A with cultured HeLa cells
(a) HeLa cells were incubated in medium with 4mg/mL MNP-A or without for 2hrs, followed by Perls Prussian blue staining. MNP-A appeared as blue precipitates on the cell cytoplasm (*left*) while no iron was detected in the control (*right*). **(b)** Confocal microscopic image of HeLa cells incubated with MNP-A-FITC (0.5mg/mL for 24hrs), cell nuclei were stained with DAPI. **(c)** HeLa cells were treated with MNP-A (0.5, 1.0, 2.0mg/mL) for 6, 24 or 48hrs. Cell bound MNP-A were quantified by the amount of Fe using Prussian blue reaction.

Will the amount of cell-bound MNP-A generate enough heating effect *in vivo* under biocompatible AMF? We used cell pellets (by centrifuging cultured cells) as *in vitro* model to mimic heating in solid tumors. After treating with 2mg/ml MNP-A for 48hrs, HeLa cells were washed with PBS, digested with trypsin and spun down into cell pellets. Cell pellets from MNP-A treated and MNP-A-untreated samples were then subject to AMF (400kHz, 6.3kA/m). The amount of MNP-A bound to HeLa cells

successfully produced rapid heating, sample temperature rose from 37ºC to 42ºC in 8 mins (Figure 3.9a). Instead of high temperature rise causing direct cytotoxic effects leading to necrosis, mild temperature rise usually impairs functions of cellular proteins, stops cell proliferation and ultimately causes apoptosis. To include this chronic cytotoxicity effect, we used colony formation assay to test cell-bound MNP-A heating effects on cell pellets. After the 60 mins AMF treatment, HeLa cells in pellets were well resuspended and further diluted for seeding in 6cm culture dish. After 7-10 days cell culture incubation, cell colonies were counted on each plate and compared among four treatment groups: MNP+AMF; MNP + No AMF; No MNP+ AMF; and No MNP+ No AMF (Figure 3.9b). The cells "bounded" with MNP-A and subjected to the magnetic field showed 70% fewer colonies compared to non-treatments group, whereas cells that were treated with particles but without exposing to the magnetic field were unaffected. However, the AMF only groups also showed 18% fewer colonies, suggesting weaker AMF strength is needed.

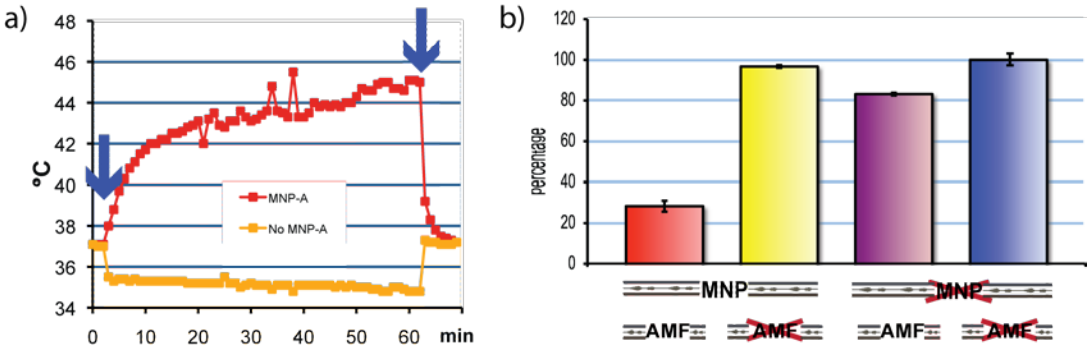

Figure 3.9 Heating effects generated by cell-bound MNP-A under AMF
HeLa cells were incubated with 2mg/ml MNP-A (or without) for 48hrs, followed by extensive PBS washes. Cells were then centrifuged into cell pellets before 1hr exposure to AMF(400kHz, 6.3kA/m). **(a)** Temperature record of the cell pellets. Arrows indicate the start and end of AMF. **(b)** After the treatments, cell pellets were re-suspended in

culture medium and subjected to colony forming assay. Cell colonies were counted 7-10 days after seeding.

Discussion

Current cancer thermotherapy is a physical therapy with fewer limitations than chemotherapy or radiation therapy. It is typically used in combination with both of these therapies. It potentially allows a greater number of repeated treatments without accumulation of systemic toxic side effects. Although successful in numerous clinical trials (152;154), thermotherapy is not yet established in clinical routines. This discrepancy is probably due to current technical limitations in achieving effective temperature distribution in the depth of the human body (154).

The heating of tissues using magnetic nanoparticles as a new technique for thermotherapy has the potential to overcome the shortcomings of current methods. The core task of this new technique for thermotherapy resides on developing biocompatible magnetic nanoparticles with high heating capacity.

Compared to organic polymer as nanoparticle coating, we have developed a non-toxic iron oxide NP that employs protein (BSA) as a biocompatible passivation agent. Among the handful of particles we studied, the heating capacity of MNP-A surpasses others without any magnetic separation and purification steps. The MNP coated by dextran or aminosilane are most commonly used in animal studies of magneticity induced thermotherapy. The SAR of dextran and aminosilane MNPs were reported at 120 and 146 W/g Fe respectively, under AMF 13.2kA/m, 520kHz (172;182;183). However, unless we can obtain these MNP samples, it is almost impossible to compare SAR with other

published data, as they were all reported under different AMF strength and amplitude. A brief feature comparison is provided in Table 3.2

Table 3.2 Comparison of MNP-A with dextran and aminosilane coated MNP

MNP features	MNP-A	#P6	#BU48
MNP coating	Albumin	Dextran	Aminosilane
Average core size (nm)	12	3.3	13.1
Core size distribution	monodispersed	polydispersed	N/A
Average hydrodynamic diameter	45-55	50-70	17
Surface charge	Negative	Negative	Highly positive
Cell toxicity	Very low	Very low	Very low
AMF condition	6.3kA/m, 420kHz	13.2kA/m, 520kHz	
SAR W/g	36	120	146

N/A: not available

MNP-A is stable in a variety of media, and shows very low inherent toxicity on cells. It provides very rapid and efficient heating under AMF conditions that the amount of cell-bound particles are sufficient to generate detectable heating and killing effects. Furthermore, the BSA coating provides a platform for future incorporating targeting molecules to realize targeted tumor thermal therapy for animal studies.

Various tumor targeting molecules have been proposed and even tested in animal models. These folate- (184), homing peptide- (185), or tumor specific antibody- (174;186) conjugated MNPs were intravenously injected into rodents bearing palpable tumors. The conjugation of these molecules largely enhanced the binding of MNP to tumor sites, which consequently delivered therapeutic heating effects under AMF. However, the equivalent MNP accumulation in liver, spleen and kidney cannot be

overlooked. Following intravenous injection, MNP are rapidly taken up by reticuloendothelial system (RES), mainly the kupffer cells in the liver and the spleen macrophages (187). These two organs accumulate more MNP than tumor site even in the presence of target molecules. Three strategies may be considered to lower collateral damage to liver, spleen and other organs during AMF induced thermotherapy. First, optimize MNP surface to reduce RES uptake. For example, smaller hydrodynamic size (<100nm) or hydrophilic surface evades RES uptake. Second, selectively treating tumors which can be spatially target by AMF. Tumors that are further away from abdomen can be good candidates, e.g. osteosarcomas in the limb, or brain tumors. The third strategy uses the inherent magnetic property of MNP. When MNP is injected in a selected artery supplying the region of interest (e.g. tumor site), under the influence of an external magnetic field, MNP will be held and concentrated in the targeted area (188;189). The localized accumulation of MNP-A and high permeability tumor vasculature will enable a much even distribution of MNP, thus better heating effects, and less systemic toxicity.

Overall, MNP-A potentially provides a versatile platform to achieve better treatment of solid tumor, addressing the need for minimally invasive treatment that is effective and has low systemic side effects.

APPENDICES

1. CYTOKERATIN EXPRESSION IN TUMORSPHERE CELLS FROM MAMMARY TUMORS IN BALB/c *Trp53*+/- MICE

Introduction

A variety of human malignancies, including breast cancer, are thought to be organized in a hierarchy, whereby a relatively minor population of tumor initiating cells (TIC) is responsible for tumor growth and the vast majority of remaining cells are nontumorigenic (51-56). As the majority of mammary tumors in the BALB/c *Trp53*+/- mice express both luminal and basal keratins, we proposed that the tumors initiated most often within stem cell/progenitor cells, and later differentiated into two (or more distinct) populations. Further gene expression array revealed a similar stem cell gene expression pattern between tumors with mixed cytokeratin expression and tumors expressing only luminal markers (Figure 2.9). It is likely that the tumors expressing only luminal or basal marker originate from similar progenitor cells.

Recently Zhang et al. identified tumor initiation cells in spontaneous mammary tumors from mice transplanted with synergetic *Trp53*-/- epithelium cells (119). Analysis of biomarkers suggested the tumor initiating cells population may arises from a bipotent mammary progenitor, and later differentiate into one or more lineage specific populations. Our data concurs with their finding.

To further explore the possible cellular hierarchy and path of differentiation within each type of tumor, we used in vitro tumorsphere method (190;191) to enrich the "tumor stem cells". Under low attachment culture condition, a small portion of tumor

cells survive and form floating cell balls (tumorspheres) consisting of 10-100 cells. Undifferentiated tumor stem cells are enriched in tumorspheres, and can be induced to differentiate when put into attachment culture.

Experiments and Results

Tumor fragments from V06 and V14 were transplanted into mouse (wild type) mammary fat pad cleared of endogenous epithelium. Mice were sacrificed when tumor growths reached 1cm in diameter. Cells were isolated from tumor outgrowths into single cell suspension and then cultured in low attachment cell culture flasks. Individual tumor cells grow into sphere like balls (mammary tumorsphere) and were passaged every 3-5 days. During each passage, a portion of the cells were plated into regular culture flasks (to induce differentiation). Mammary tumorspheres and induced cell cultures were subjected to immunofluorescent staining on K5 and K8/18.

The tumor growth from transplanted fragments (designated as T) expressed similar cytokeratin pattern as original tumors (data now shown). V06 tumor (and its outgrowth from transplanted fragments--V06T) expressed both K5 and K8/18. Most cells in V06T tumorspheres were negative for both K8/18 and K5. A small portion of the cells close to the surface of the spheres expressed K8/18 or K5 (Figure A.1, A-D). On the other hand, a majority of cells in attachment culture (induced differentiated cells) expressed K8/18, K5 or both (Figure A.1, E-G).

V14 tumor (and its outgrowth from transplanted fragments--V14T) expressed only K8/18. Cells in V14 tumorspheres were mostly negative for both K8/18 and K5 too. Surprisingly, not only K8/18 positive but also K5 positive cells were detected in V14T

tumorsphere (Figure A.1, K-N). In attachment culture, cells with positive cytokeratin stain largely increased. K8/18 positive, K5 positive, double positive and double negative cells were seen (Figure A.1, H-J).

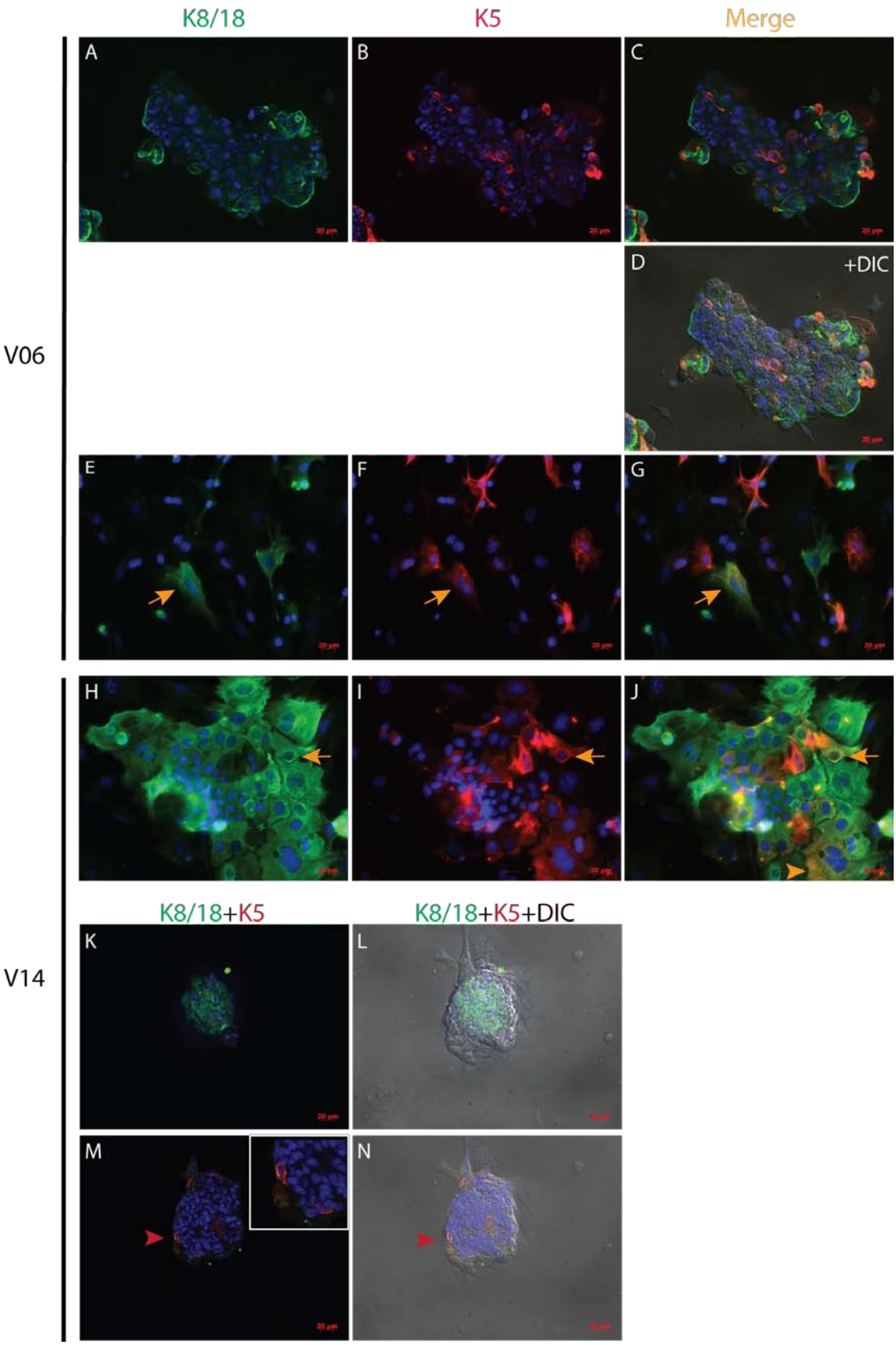
K8/18
K5
Merge
A
B
C
D
+DIC
V06
E
F
G
H
I
J
K8/18+K5
K8/18+K5+DIC
K
L
V14
M
N

Figure A.1 Cytokeratin expression in mammary tumorspheres.
V06 and V14 fragments were transplanted into mammary fat pads that had been cleared of endogenous epithelium in BALB/c-*Trp53*+/+ hosts. Isolated tumor cells from the outgrowth (V06T and V14T) were cultured in low attachment plates and formed mammary tumorsphere. Tumorspheres from V06T contained cells expressing K8/18, K5, both or neither (A-D, the structure of the sphere was shown in D). In regular attachment culture, cells from the V06T spheres attached to the bottom surface and expressed K8/18, K5, neither or both (E-G, orange arrow indicates a double positive cell). In regular attachment culture, cells from the V14T spheres expressed K8/18, K5, both (orange arrow) or neither (H-J). Though tumorspheres from V14T contained mostly cells negative for both K8/18 and K5, positive cells were occasionally seen near the surface of the spheres. In one tumorsphere, K and L shows a transverse plane near the top of the sphere, whereas M and N is a transverse plane in the middle of the sphere. K8/18 positive (K) and K5 positive (M, red arrowhead) cells are seen in the sphere.

Discussion

Based on epithelial lineage specific cytokeratin staining, we proposed that the majority of BALB/c *Trp53*+/- mammary tumor originate from bipotent mammary gland progenitors, and others from lineage-committed progenitors (Figure 2.11). As we have no means to trace tumorigenesis on single cell level, we cannot exclude the possibility that tumor initiating cells can be newly created from differentiated cells by certain mutations that reactivate genes regulating stem cell behavior (self-renewal and multipotential differentiation) (192-194). Cytokeratin expression pattern of mammary tumors in BALB/c *Trp53*+/- mice could be the outcome of random mutation and growth competition/selection within each tumor. The *in vitro* mammary tumorsphere assay supports this possibility, as the K8/18 positive, the K5 positive, the double positive and the double negative cells were all detected in both V14T and V06T.

Actually, creating tumor initiating cells by mutating normal stem cells or by reactivating stem cell properties in differentiated cells may not be mutually exclusive possibilities, and both could help explain the enormous biological diversity observed

within and between mammary tumors. Some cancers may even contain multiple stem cells, contributing to intratumor diversity. Depending on the accumulated gene mutations, transformed somatic cells may develop into heterogeneous tumors, too.

2. TESTING MAESTRO IN VIVO FLUORESCENCE IMAGE SYSTEM

Introduction

My original experimental plan involves using in vivo image system to track metastasis in mice transplanted with BALB/c *Trp53*+/- mammary tumors. I tested the Maestro system in vivo image system resided in Pioneer Valley Life Institute using a established metastasis cell line, but was unimpressed about the results. Here I quote from Maestro official website to introduce the key features of the system:

Maestro systems enable multiplexed in vivo *fluorescence imaging of small animals with unprecedented sensitivity. Maestro offers users the capability of removing autofluorescence emitted from images of skin and other tissues to reveal otherwise hard-to-detect labeled targets. The dramatic improvement in signal-to-noise can increase sensitivity up to several hundred-fold, enabling much smaller or fainter signals from biological targets to be detected earlier and accurately measured. The increased sensitivity over standard imaging techniques provided by Maestro's high-quality spectral imaging technology enable experiments and models which simply cannot be done with any other system.*

Experiment and Results

4T1 cell line is a established murine metastatic cell line. Palpable tumors can be detected within 2 weeks of subcutaneous injection (s.c.). Metastasis can be detected within a month after primary tumor is removed. So 4T1 cell line was perfect for preliminary test on Maestro system.

We were suggested by manufacturer to avoid using green fluorescent protein as it has strong interference with autofluorescence from mouse hair and skin. mOrange vector was obtained from Tsien R.Y. Lab. The fluorescence gene was reconstructed into a retrovirus vector generating *mOrange-pQCXIP* (*Pcmv-mOrange-IRES-Pur*^{r}). 4T1 cells were infected with the vector and placed in culture medium containing Puromycin for selection. Three weeks later, 4T1-mOrange cell line was established although I found there was only 60% of the cells are fluorescent (Figure A.2). Highly fluorescent cells were sorted out and plated in confluent density to avoid rapid replication which may result in losing fluorescence gene. These cells were harvested on the 2nd day after sorting to. injected s.c into wild type BALB/c mice ($5x10^4$/mouse).

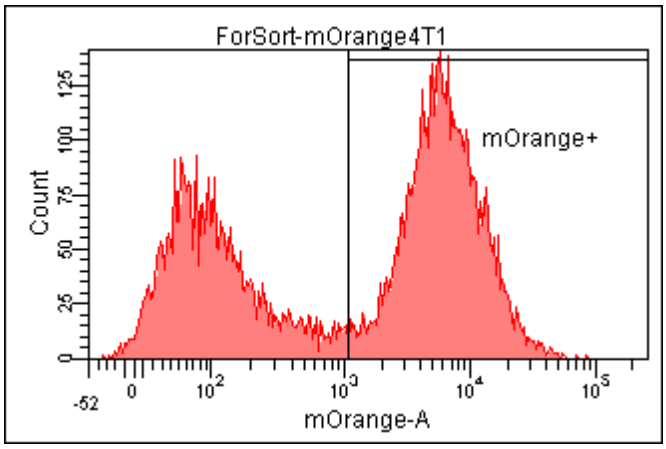

Figure A.2 4T1-mOrange
Highly florescent 4T1-mOrange cells were sorted for injection

Palpable tumors were detected two weeks after injection. On the day of imaging, mice were anesthetized using Tribromoethanol (Avertin®). They were then shaved and treated with Veet® hair removal foam for 10min to expose skin for imaging area. After

imaging, primary tumor were quickly removed and skin were sutured with absorbable suture. Mice were kept on heating pad whenever possible to keep body temperature.

Mice were monitored 2 times/week for signs of metastasis, such as visible or palpable lump, body weight lost, or any sick signs. When metastasis signs were observed, usually 4 weeks after primary tumor were removed, mice were taken to imaging following the same procedure during primary tumor imaging. After imaging, mice were sacrificed and autopsies were conducted to compare imaging results with autopsy results.

Maestro system can detect primary tumor very well as they are always right under the skin

Figure A.3.

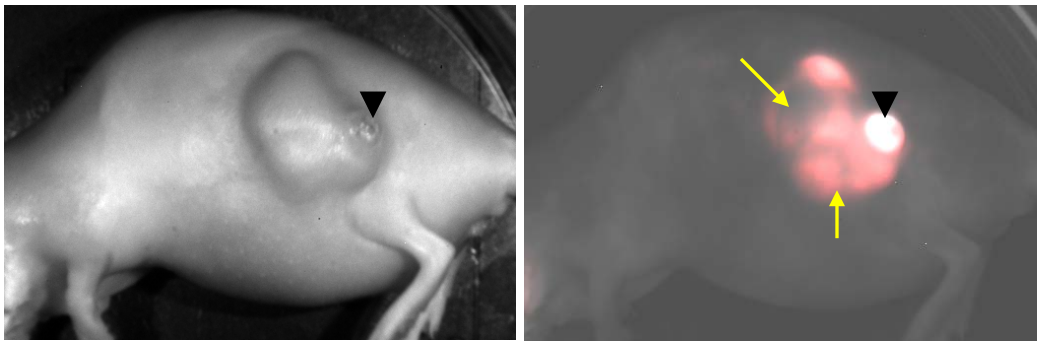

Figure A.3 Maestro system detecting primary tumor
Maestro image showed exact size and shape of primary tumor. There is a small skin rupture (arrowheads) on the tumor and the image system seems very sensitive to unevenness on the skin and gave out strong signal. The darker parts (arrows) of the image may be the vessels and necrosis of the tumor which didn't have fluorescence.

However, the performance of the system on metastasis sites were below expectation. For example, a mouse without visible metastasis (Figure A.4) were subjected to imaging. One fluorescent spot (Figure A.4A, yellow arrow) were detected in the live animal and its correspondent one was found in the autopsy (Figure A.4B, yellow arrow). However, the system missed one fluorescent site (Figure A.4C, green arrowhead). The

fluorescence was visible under Maestro system after the skin was removed, but the system missed during the *in vivo* imaging. The missed lesion was just slightly deeper from skin compared to the detected one. The autopsy showed the real physical lesion was bigger (Figure A.4D green arrowhead). A possible explanation is that part of the metastasis foci was not fluorescent, which was quite often seen during the whole experiment. Even though cells were sorted before injection, more than half of the visible metastatic site did not show fluorescent even in autopsy stage. Metastasis process may select tumor cells against extra fluorescent gene burden. Nevertheless, the presented data was one of the four mice I tested and it is sufficient in telling the story. Overall, the Maestro system prove to be unable to detect fluorescent metastatic foci that are not directly under the skin.

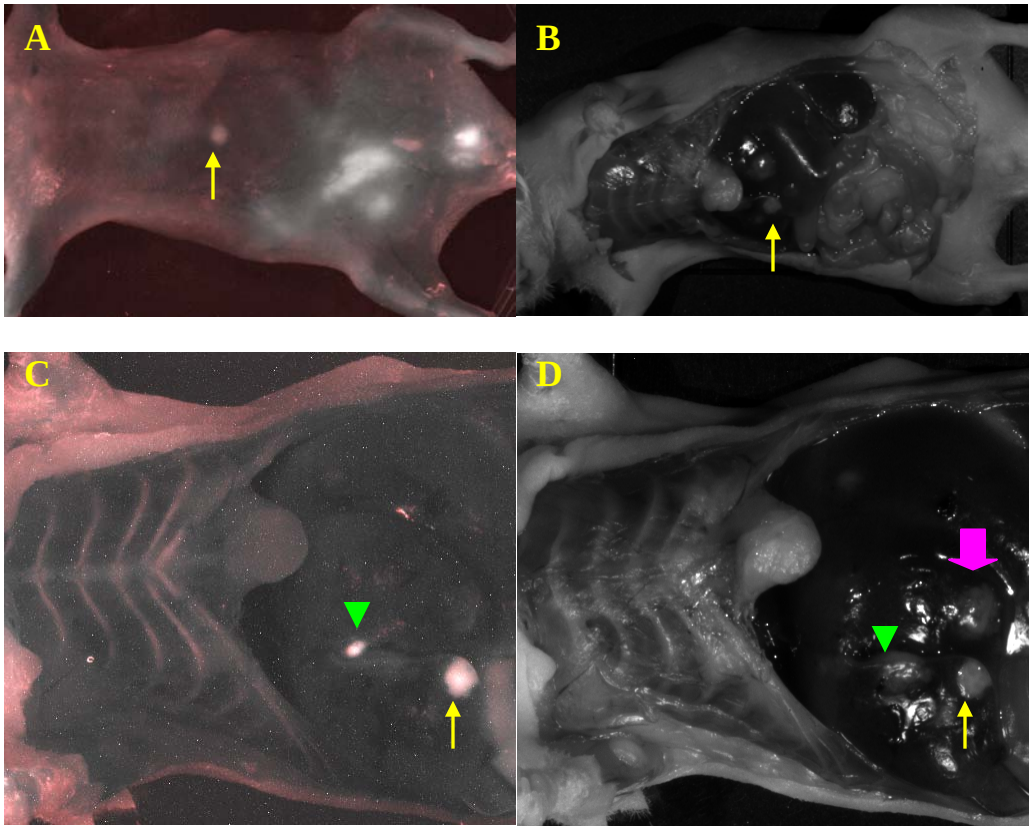

Figure A.4 Maestro system detecting metastatic tumor sites
One fluorescent spot was detected in vivo (A, yellow arrow) and it matched the autopsy result (B, yellow arrow). The same spot can also been seen in the zoom-in view of C and D. However, the system missed the other fluorescent spot which were revealed during autopsy (C, D green arrowhead). There are non-fluorescent foci found (D, purple thick arrow).

3. PROTOCOLS

Isolate tumor cells from mammary tumor tissue

Materials

Dissecting tools

Cotton swabs

Sterile scalpels/ Razor blades

MECL medium (2%ABS)

Collagenase III (Worthington)

Hyaluronidase Sigma #H3506

Pen/Strep Gibco 100×

Gentamycin Gibco

24 well plate or equal surface area 4 well plate

Day 0

Autoclave dissection tools

Day 1

1. Make collagenase solution (Digestion medium)

   DMEM:F12 100ml

   5% FBS

   100u/ml pen/strep (1ml), Stock 10mg/ml

   100μg/ml gentamicine (0.2ml), Stock 50mg/ml

2mg/ml collagenase (200mg)

2. Take tumor sample from mice
3. Use sterile technique, mince tumor tissue into very small pieces (<0.5mm) with two razor blades. Mincing should not take more than 5min. Place minced tissue in digestion medium (0.5g tissue/10ml medium in 15ml conical tube, about rice size) and shake at 37 ºC for approximately 3 hrs. The shaker should be set at 110 to 125 rpm. (Give it a good, hard shake every hour)
4. Centrifuge to collect cells after collagenase digestion. PBS wash once. The result pellet is resuspended in MECL media with 2%ABS, pen/strep and gentamycin. Seed cells in 3-4 wells in 6 well plates (per 0.5g tissue). Change to fresh medium after 6hrs.
5. In the following weeks, passage cells into the same size culture surface until obvious cell growth are observed.
6. Freeze vials along the way.

Immunofluorescence stain (K5, K8/18)

Materials and Solutions

Antibodies

- Anti-cytokeratin 5 (K5, 1:8000, PRB-160P, Covance, Berkeley, CA)
- Anti-cytokeratin 8/18 (Ker8/18, 1:450, GP11, Progen Biotecknik, Heiderlberg, Germany)

Coverslip: 22x22mm, 1 ½, (check the lens to decide optimum thickness)

Sodium citrate 100mM:

29.14g (sodium citrate.$2H_2O$) + 1L H_2O

Blocking buffer:

5%BSA/0.5%Tween-20 in 1X PBS

0.5g BSA + 0.05ml Tween-20 in 10ml PBS (fresh preparation, no more than 1 week old, keep in 4ºC)

Wash solution:

0.1%Tween20 in PBS

0.1ml Tween 20 in 100ml PBS

Equilibrate solution

Mounting medium w/o DABCO

Homemade mounting medium

DABCO/Tris/Glicerol (DTG)

2.5% Dabco (Sigma D2522)

50mM Tris-HCl pH8.0

90% Glycerol

for 50ml use 1.25g DABCO, 45ml glycerol, 2.5ml 1M Tris pH8.0 and 2.5ml H2O. Mix components, dissolve DABCO by warming to 70ºC, mix, aliquot and store at -20ºC. Stable at 4ºC for 1 month (watch for contamination).

Procedure:

1. Deparaffinize and rehydrate sections as follows:

   3 x 3´ Xylene

   3 x 3´ 100% ethanol

   2 x 2´ 95% ethanol

   2 x 2´ 70% ethanol

   1 x 5´ 1x PBS

2. Microwave antigen retrieval:

   - Place slides in a glass slide holder and fill in the rest of the rack with blank slides (10 total).
   - Place the rack in 600 ml of 10 mM Sodium Citrate (pH 6; 100 mM stock) in a glass 2L beaker.
   - Microwave for 20 minutes total, replacing evaporated water after 10 min.
   - Cool the slides 20 min in the beaker.

- Wash 3 x 5´ in ddH_2O, 1 x 5´ in 1x PBS

3. Shake/wipe off excess PBS and circle all sections with a PAP pen. Do not let the sections dry out.
4. Add 50 µl of blocking buffer to each. Incubate 1-4 hours (1hr is sufficient) at room temperature in a humidified chamber.
5. Dilute primary antibody in blocking buffer. Anti-K5 (1:8000), anti-K8/18 (1:400). Add 50 µl of diluted antibody per section and incubate overnight (I didn't try shorter time) at room temperature in a humid chamber (need to be very humid, otherwise slides will dry out, also make a second PAP pen circle if the first one looks weak).
6. Wash 10 times with washing buffer with the aid of a dropper.
7. Apply secondary antibodies (1:200) + DAPI (1ug/ml) in PBS for 2hrs in a humid chamber. PROTECT FROM LIGHT!
8. Wash as in step 6.
9. Equilibrate 2X5min at RT with equilibration solution. This step helps removing salts and switching to mounting compatible buffer.
10. Remove as much remaining fluid as possible.
11. Finish by adding a drop of mounting solution and covering with a coverslip. Squeeze extra mounting solution out with help of bibulous/lens paper otherwise result in insufficient mounting.

12. Seal off with non-fluorescent nail polish. Let the polish dry for 10min. Keep slides at 4ºC at least ON. Take image the day after. Slides can be kept in -20ºC for long term.

Quantification of cell-bound iron using Perls Prussian blue reaction

Materials

K4[Fe(CN)6] (Sigma P9387)

$FeCl_3$

Procedures

Prepare the K4Fe(CN)6, (5% in 2%HCL)

100mg $K_4Fe(CN)_6$ + 2ml H_2O + 40µL saturated HCl, in 50ml Felcon tube. Shake to solve. Use fresh.

Standard curve

Prepare 10mg/L Fe3+ stock solution using FeCl3. Dilute standards as follows.

No	Stock+H2O	Vol(µl)	Fe(µl/L)
1	1500µl + 0µl	1500	10000
2	1200µl + 300µl	1500	8000
3	900µl + 600µl	1500	6000
4	600µl + 900µl	1500	4000
5	450µl + 1050µl	1500	3000
6	300µl + 1200µl	1500	2000
7	150µl + 1350µl	1500	1000
8	0µl + 1500µl	1500	0

Day 0:

Seed HeLa cells in 6 well plates in culture medium, so that each well will reach 95-100% confluency on day 1.

Day 1:

1. Carefully remove the culture medium and load medium containing MNP-A at various concentrations e.g. 0, 0.5, 1, and 2mg/ml.
2. Return the plates to cell culture incubator for 0, 6, 24 or 48hrs.
3. After the treatment is done, wash each well with PBS for 2 times.
4. Digest cells using 300µl 0.05% trypsin for 2 mins.
5. Add 2-3ml culture medium to wash down cells and transfer each well into a 15ml conical tube.
6. Take 10µl cell suspension from each tube for cell counting. Calculate how many cells each well has.
7. Pellet cells down at 1200rpm for 5min.
8. Resuspend cells in 1ml PBS and transfer to 1.5 Eppendorf tubes.
9. Pellet the cells down at 2000rpm for 5min, and aspire the supernatant.
10. Add H2O to each tube to reach 100µl total volume. 100µl from each standards will be treated in the same condition from now on.
11. Add 125µl 6N HCl, mix well (vortex if needed)
12. Incubate O.N at R.T.
13. Centrifuge at 13000rpm for 5min.
14. Transfer supernatant to a new 1.5 eppendorf tube for total iron test.
15. Dilution was needed in all test samples in order to fit in standard curve range.
16. Transfer 225µl diluted supernatant to a well in 96 well plate for total iron test.
17. Add 125µl of 5% K4[Fe(CN)6] into each well and mix.
18. Incubate at RT for 10min.
19. Read the absorbance at 690nm.

4. MSI AUTOMATION SYSTEM

Originally written by Nick Fisher, modified by Haoheng Yan.

The machine need water to cool down when it is running.

No metal in the coil, it will heat up really high and quick.

Turn it on:

1. Turn on the cold water, the gauge will be 30-40
2. Insert the key and turn it on. "→" → "↑"
3. Turn the big red knob to "on" . Should hear the instrument running.
4. Place the sample in the middle of the coil. Don't put any metal around the coil. The space in the coil can fit a 4 well plate well which will get equal heating in the wells.
5. Hit the "NO" (it should have been ON, but the button was installed upside-down)
6. The instrument will start self-checking automatically with the yellow button indicating the steps. If everything is fine, no lights should be on after the checking.
7. Select the Timer|Hand switch for different running mode. Timer will let the magnetic field run under control of the timer, while the hand pedal stands for the pedal control.
8. To change the time on the Timer, first unlock the timer, set the time using the 4 buttons and the green number indicates the time you set. Then hit the reset to

confirm the running time to be one you set. The red number indicates the real time which the machine is going to refer.

9. Use pedal to start the magnetic field. If it is under timer mode, the pedal is a starter, the real running time is according to what has been set on the timer. If it is under hand mode, the magnetic field is only on when the pedal is hit and hold.
10. Use the tuner to adjust the AMP. Don't exceed the max AMP. The FREQ is set to be around 400 kiloHz. Only the company could change it.

Shut it down:

1. Switch to Hand.
2. Make sure the field is off. No bars on AMP and FREQ, "FREQ check" and "heater on" light is off
3. Hit the "off" button.
4. Turn the power off by the red knob.
5. Turn the key and remove it, place it in the drawer.
6. Turn off the water.

Thermometer:

DualLogR thermocouple thermometer with a TEF-30-T thermocouple.

The thermocouple should never touch the coil. The thermometer itself should be place as far away from the inductive heating machine as possible.

Trouble Shooting:

Machine does not pass self-checking

Check cooling water flow. Try restart the machine by strictly following the "Shut it down" and "turn it on" procedures.

On-campus limited support

Chemistry department Electronics Shop

Manufacturer support

DAVE BRINCKERHOFF

MSI AUTOMATION, INC.

4065 N. WOODLAWN BLDG. #4

WICHITA, KANSAS USA 67220

TEL: 316-681-3566

FAX: 316-681-1433

CELL: 316-209-8800

DAVE@MSIAUTOMATION.COM

BIBLIOGRAPHY

Reference List

1. American Cancer Society. Cancer facts & figures 2009. 2009. Atlanta:American Cancer Society.

2. Wellings SR and Jensen HM: On the origin and progression of ductal carcinoma in the human breast. J Natl Cancer Inst 1973, 50:1111-1118

3. Wellings SR, Jensen HM, and Marcum RG: An atlas of subgross pathology of the human breast with special reference to possible precancerous lesions. J Natl Cancer Inst 1975, 55:231-273

4. Allred DC, Wu Y, Mao S, Nagtegaal ID, Lee S, Perou CM, Mohsin SK, O'Connell P, Tsimelzon A, and Medina D: Ductal carcinoma in situ and the emergence of diversity during breast cancer evolution. Clin Cancer Res 2008, 14:370-378

5. Gong G, DeVries S, Chew KL, Cha I, Ljung BM, and Waldman FM: Genetic changes in paired atypical and usual ductal hyperplasia of the breast by comparative genomic hybridization. Clin Cancer Res 2001, 7:2410-2414

6. Amari M, Suzuki A, Moriya T, Yoshinaga K, Amano G, Sasano H, Ohuchi N, Satomi S, and Horii A: LOH analyses of premalignant and malignant lesions of human breast: frequent LOH in 8p, 16q, and 17q in atypical ductal hyperplasia. Oncol Rep 1999, 6:1277-1280

7. O'Connell P, Pekkel V, Fuqua SA, Osborne CK, Clark GM, and Allred DC: Analysis of loss of heterozygosity in 399 premalignant breast lesions at 15 genetic loci. J Natl Cancer Inst 1998, 90:697-703

8. Aldaz CM, Chen T, Sahin A, Cunningham J, and Bondy M: Comparative allelotype of in situ and invasive human breast cancer: high frequency of microsatellite instability in lobular breast carcinomas. Cancer Res 1995, 55:3976-3981

9. Noguchi S, Motomura K, Inaji H, Imaoka S, and Koyama H: Clonal analysis of predominantly intraductal carcinoma and precancerous lesions of the breast by means of polymerase chain reaction. Cancer Res 1994, 54:1849-1853

10. Scott MA, Lagios MD, Axelsson K, Rogers LW, Anderson TJ, and Page DL: Ductal carcinoma in situ of the breast: reproducibility of histological subtype analysis. Hum Pathol 1997, 28:967-973

11. Petersen OW, Hoyer PE, and van DB: Frequency and distribution of estrogen receptor-positive cells in normal, nonlactating human breast tissue. Cancer Res 1987, 47:5748-5751

12. Clarke RB, Howell A, Potten CS, and Anderson E: Dissociation between steroid receptor expression and cell proliferation in the human breast. Cancer Res 1997, 57:4987-4991

13. Shoker BS, Jarvis C, Clarke RB, Anderson E, Hewlett J, Davies MP, Sibson DR, and Sloane JP: Estrogen receptor-positive proliferating cells in the normal and precancerous breast. Am J Pathol 1999, 155:1811-1815

14. Shoker BS, Jarvis C, Sibson DR, Walker C, and Sloane JP: Oestrogen receptor expression in the normal and pre-cancerous breast. J Pathol 1999, 188:237-244

15. Zagouri F, Sergentanis TN, and Zografos GC: Precursors and preinvasive lesions of the breast: the role of molecular prognostic markers in the diagnostic and therapeutic dilemma. World J Surg Oncol 2007, 5:57

16. Lee S, Mohsin SK, Mao S, Hilsenbeck SG, Medina D, and Allred DC: Hormones, receptors, and growth in hyperplastic enlarged lobular units: early potential precursors of breast cancer. Breast Cancer Res 2006, 8:R6

17. Barnes NL, Boland GP, Davenport A, Knox WF, and Bundred NJ: Relationship between hormone receptor status and tumour size, grade and comedo necrosis in ductal carcinoma in situ. Br J Surg 2005, 92:429-434

18. Ariga N, Suzuki T, Moriya T, Kimura M, Inoue T, Ohuchi N, and Sasano H: Progesterone receptor A and B isoforms in the human breast and its disorders. Jpn J Cancer Res 2001, 92:302-308

19. Ross JS and Fletcher JA: HER-2/neu (c-erb-B2) gene and protein in breast cancer. Am J Clin Pathol 1999, 112:S53-S67

20. Heffelfinger SC, Yassin R, Miller MA, and Lower EE: Cyclin D1, retinoblastoma, p53, and Her2/neu protein expression in preinvasive breast pathologies: correlation with vascularity. Pathobiology 2000, 68:129-136

21. Edorh A, Leroux A, N'sossani B, Parache RM, and Rihn B: Detection by immunohistochemistry of c-erbB2 oncoprotein in breast carcinomas and benign mammary lesions. Cell Mol Biol (Noisy -le-grand) 1999, 45:831-840

22. De Potter CR, Van DS, van de Vijver MJ, Pauwels C, Maertens G, De BJ, Vandekerckhove D, and Roels H: The expression of the neu oncogene product in breast lesions and in normal fetal and adult human tissues. Histopathology 1989, 15:351-362

23. Lee S, Mohsin SK, Mao S, Hilsenbeck SG, Medina D, and Allred DC: Hormones, receptors, and growth in hyperplastic enlarged lobular units: early potential precursors of breast cancer. Breast Cancer Res 2006, 8:R6

24. Tsuda H and Hirohashi S: Multiple developmental pathways of highly aggressive breast cancers disclosed by comparison of histological grades and c-erbB-2 expression patterns in both the non-invasive and invasive portions. Pathol Int 1998, 48:518-525

25. Horak E, Smith K, Bromley L, LeJeune S, Greenall M, Lane D, and Harris AL: Mutant p53, EGF receptor and c-erbB-2 expression in human breast cancer. Oncogene 1991, 6:2277-2284

26. Perou CM, Sorlie T, Eisen MB, van de RM, Jeffrey SS, Rees CA, Pollack JR, Ross DT, Johnsen H, Akslen LA, Fluge O, Pergamenschikov A, Williams C, Zhu SX, Lonning PE, Borresen-Dale AL, Brown PO, and Botstein D: Molecular portraits of human breast tumours. Nature 2000, 406:747-752

27. Sorlie T, Perou CM, Tibshirani R, Aas T, Geisler S, Johnsen H, Hastie T, Eisen MB, van de RM, Jeffrey SS, Thorsen T, Quist H, Matese JC, Brown PO, Botstein D, Eystein LP, and Borresen-Dale AL: Gene expression patterns of breast carcinomas distinguish tumor subclasses with clinical implications. Proc Natl Acad Sci U S A 2001, 98:10869-10874

28. Yu K, Lee CH, Tan PH, and Tan P: Conservation of breast cancer molecular subtypes and transcriptional patterns of tumor progression across distinct ethnic populations. Clin Cancer Res 2004, 10:5508-5517

29. Jackson RB and Little CC: THE EXISTENCE OF NON-CHROMOSOMAL INFLUENCE IN THE INCIDENCE OF MAMMARY TUMORS IN MICE. Science 1933, 78:465-466

30. Stewart TA, Pattengale PK, and Leder P: Spontaneous mammary adenocarcinomas in transgenic mice that carry and express MTV/myc fusion genes. Cell 1984, 38:627-637

31. Guy CT, Webster MA, Schaller M, Parsons TJ, Cardiff RD, and Muller WJ: Expression of the neu protooncogene in the mammary epithelium of transgenic mice induces metastatic disease. Proc Natl Acad Sci U S A 1992, 89:10578-10582

32. Muller WJ, Sinn E, Pattengale PK, Wallace R, and Leder P: Single-step induction of mammary adenocarcinoma in transgenic mice bearing the activated c-neu oncogene. Cell 1988, 54:105-115

33. Sinn E, Muller W, Pattengale P, Tepler I, Wallace R, and Leder P: Coexpression of MMTV/v-Ha-ras and MMTV/c-myc genes in transgenic mice: synergistic action of oncogenes in vivo. Cell 1987, 49:465-475

34. Xu X, Wagner KU, Larson D, Weaver Z, Li C, Ried T, Hennighausen L, Wynshaw-Boris A, and Deng CX: Conditional mutation of Brca1 in mammary epithelial cells results in blunted ductal morphogenesis and tumour formation. Nat Genet 1999, 22:37-43

35. Lin SC, Lee KF, Nikitin AY, Hilsenbeck SG, Cardiff RD, Li A, Kang KW, Frank SA, Lee WH, and Lee EY: Somatic mutation of p53 leads to estrogen receptor alpha-positive and -negative mouse mammary tumors with high frequency of metastasis. Cancer Res 2004, 64:3525-3532

36. Cardiff RD, Anver MR, Gusterson BA, Hennighausen L, Jensen RA, Merino MJ, Rehm S, Russo J, Tavassoli FA, Wakefield LM, Ward JM, and Green JE: The mammary pathology of genetically engineered mice: the consensus report and recommendations from the Annapolis meeting. Oncogene 2000, 19:968-988

37. Herschkowitz JI, Simin K, Weigman VJ, Mikaelian I, Usary J, Hu Z, Rasmussen KE, Jones LP, Assefnia S, Chandrasekharan S, Backlund MG, Yin Y, Khramtsov AI, Bastein R, Quackenbush J, Glazer RI, Brown PH, Green JE, Kopelovich L, Furth PA, Palazzo JP, Olopade OI, Bernard PS, Churchill GA, Van DT, and Perou CM: Identification of conserved gene expression features between murine mammary carcinoma models and human breast tumors. Genome Biol 2007, 8:R76

38. Ben Porath I, Thomson MW, Carey VJ, Ge R, Bell GW, Regev A, and Weinberg RA: An embryonic stem cell-like gene expression signature in poorly differentiated aggressive human tumors. Nat Genet 2008, 40:499-507

39. Stingl J and Caldas C: Molecular heterogeneity of breast carcinomas and the cancer stem cell hypothesis. Nat Rev Cancer 2007, 7:791-799

40. Enver T, Pera M, Peterson C, and Andrews PW: Stem cell states, fates, and the rules of attraction. Cell Stem Cell 2009, 4:387-397

41. Smalley M and Ashworth A: Stem cells and breast cancer: A field in transit. Nat Rev Cancer 2003, 3:832-844

42. Clarke MF and Fuller M: Stem cells and cancer: two faces of eve. Cell 2006, 124:1111-1115

43. Bonnet D and Dick JE: Human acute myeloid leukemia is organized as a hierarchy that originates from a primitive hematopoietic cell. Nat Med 1997, 3:730-737

44. Reya T and Clevers H: Wnt signalling in stem cells and cancer. Nature 2005, 434:843-850

45. Dontu G, Jackson KW, McNicholas E, Kawamura MJ, Abdallah WM, and Wicha MS: Role of Notch signaling in cell-fate determination of human mammary stem/progenitor cells. Breast Cancer Res 2004, 6:R605-R615

46. Liu S, Dontu G, Mantle ID, Patel S, Ahn NS, Jackson KW, Suri P, and Wicha MS: Hedgehog signaling and Bmi-1 regulate self-renewal of normal and malignant human mammary stem cells. Cancer Res 2006, 66:6063-6071

47. Li Y, Welm B, Podsypanina K, Huang S, Chamorro M, Zhang X, Rowlands T, Egeblad M, Cowin P, Werb Z, Tan LK, Rosen JM, and Varmus HE: Evidence that transgenes encoding components of the Wnt signaling pathway preferentially induce mammary cancers from progenitor cells. Proc Natl Acad Sci U S A 2003, 100:15853-15858

48. Liu BY, McDermott SP, Khwaja SS, and Alexander CM: The transforming activity of Wnt effectors correlates with their ability to induce the accumulation of mammary progenitor cells. Proc Natl Acad Sci U S A 2004, 101:4158-4163

49. Teuliere J, Faraldo MM, Deugnier MA, Shtutman M, Ben-Ze'ev A, Thiery JP, and Glukhova MA: Targeted activation of beta-catenin signaling in basal mammary epithelial cells affects mammary development and leads to hyperplasia. Development 2005, 132:267-277

50. Barker N, Ridgway RA, van Es JH, van de WM, Begthel H, van den BM, Danenberg E, Clarke AR, Sansom OJ, and Clevers H: Crypt stem cells as the cells-of-origin of intestinal cancer. Nature 2009, 457:608-611

51. Al-Hajj M, Wicha MS, ito-Hernandez A, Morrison SJ, and Clarke MF: Prospective identification of tumorigenic breast cancer cells. Proc Natl Acad Sci U S A 2003, 100:3983-3988

52. O'Brien CA, Pollett A, Gallinger S, and Dick JE: A human colon cancer cell capable of initiating tumour growth in immunodeficient mice. Nature 2007, 445:106-110

53. Zhang S, Balch C, Chan MW, Lai HC, Matei D, Schilder JM, Yan PS, Huang TH, and Nephew KP: Identification and characterization of ovarian cancer-initiating cells from primary human tumors. Cancer Res 2008, 68:4311-4320

54. Maitland NJ and Collins AT: Prostate cancer stem cells: a new target for therapy. J Clin Oncol 2008, 26:2862-2870

55. Li C, Heidt DG, Dalerba P, Burant CF, Zhang L, Adsay V, Wicha M, Clarke MF, and Simeone DM: Identification of pancreatic cancer stem cells. Cancer Res 2007, 67:1030-1037

56. Lang SH, Frame FM, and Collins AT: Prostate cancer stem cells. J Pathol 2009, 217:299-306

57. Petitjean A, Mathe E, Kato S, Ishioka C, Tavtigian SV, Hainaut P, and Olivier M: Impact of mutant p53 functional properties on TP53 mutation patterns and tumor phenotype: lessons from recent developments in the IARC TP53 database. Hum Mutat 2007, 28:622-629

58. Wood LD, Parsons DW, Jones S, Lin J, Sjoblom T, Leary RJ, Shen D, Boca SM, Barber T, Ptak J, Silliman N, Szabo S, Dezso Z, Ustyanksky V, Nikolskaya T, Nikolsky Y, Karchin R, Wilson PA, Kaminker JS, Zhang Z, Croshaw R, Willis J, Dawson D, Shipitsin M, Willson JK, Sukumar S, Polyak K, Park BH, Pethiyagoda CL, Pant PV, Ballinger DG, Sparks AB, Hartigan J, Smith DR, Suh E, Papadopoulos N, Buckhaults P, Markowitz SD, Parmigiani G, Kinzler KW, Velculescu VE, and Vogelstein B: The genomic landscapes of human breast and colorectal cancers. Science 2007, 318:1108-1113

59. Vogelstein B, Lane D, and Levine AJ: Surfing the p53 network. Nature 2000, 408:307-310

60. Bensaad K and Vousden KH: p53: new roles in metabolism. Trends Cell Biol 2007, 17:286-291

61. Bertrand P, Saintigny Y, and Lopez BS: p53's double life: transactivation-independent repression of homologous recombination. Trends Genet 2004, 20:235-243

62. Gatz SA and Wiesmuller L: p53 in recombination and repair. Cell Death Differ 2006, 13:1003-1016

63. Sugrue MM, Shin DY, Lee SW, and Aaronson SA: Wild-type p53 triggers a rapid senescence program in human tumor cells lacking functional p53. Proc Natl Acad Sci U S A 1997, 94:9648-9653

64. Tasdemir E, Maiuri MC, Galluzzi L, Vitale I, Djavaheri-Mergny M, D'Amelio M, Criollo A, Morselli E, Zhu C, Harper F, Nannmark U, Samara C, Pinton P, Vicencio JM, Carnuccio R, Moll UM, Madeo F, Paterlini-Brechot P, Rizzuto R, Szabadkai G, Pierron G, Blomgren K, Tavernarakis N, Codogno P, Cecconi F, and Kroemer G: Regulation of autophagy by cytoplasmic p53. Nat Cell Biol 2008,

65. Suzuki HI, Yamagata K, Sugimoto K, Iwamoto T, Kato S, and Miyazono K: Modulation of microRNA processing by p53. Nature 2009, 460:529-533

66. Shenghui H, Nakada D, and Morrison SJ: Mechanisms of stem cell self-renewal. Annu Rev Cell Dev Biol 2009, 25:377-406

67. Lin T, Chao C, Saito S, Mazur SJ, Murphy ME, Appella E, and Xu Y: p53 induces differentiation of mouse embryonic stem cells by suppressing Nanog expression. Nat Cell Biol 2005, 7:165-171

68. Pan G and Thomson JA: Nanog and transcriptional networks in embryonic stem cell pluripotency. Cell Res 2007, 17:42-49

69. Qin H, Yu T, Qing T, Liu Y, Zhao Y, Cai J, Li J, Song Z, Qu X, Zhou P, Wu J, Ding M, and Deng H: Regulation of apoptosis and differentiation by p53 in human embryonic stem cells. J Biol Chem 2007, 282:5842-5852

70. Chambers SM, Shaw CA, Gatza C, Fisk CJ, Donehower LA, and Goodell MA: Aging hematopoietic stem cells decline in function and exhibit epigenetic dysregulation. PLoS Biol 2007, 5:e201

71. Dumble M, Moore L, Chambers SM, Geiger H, Van ZG, Goodell MA, and Donehower LA: The impact of altered p53 dosage on hematopoietic stem cell dynamics during aging. Blood 2007, 109:1736-1742

72. Medrano S, Burns-Cusato M, Atienza MB, Rahimi D, and Scrable H: Regenerative capacity of neural precursors in the adult mammalian brain is under the control of p53. Neurobiol Aging 2009, 30:483-497

73. Meletis K, Wirta V, Hede SM, Nister M, Lundeberg J, and Frisen J: p53 suppresses the self-renewal of adult neural stem cells. Development 2006, 133:363-369

74. Cicalese A, Bonizzi G, Pasi CE, Faretta M, Ronzoni S, Giulini B, Brisken C, Minucci S, Di Fiore PP, and Pelicci PG: The tumor suppressor p53 regulates polarity of self-renewing divisions in mammary stem cells. Cell 2009, 138:1083-1095

75. Gatza CE, Dumble M, Kittrell F, Edwards DG, Dearth RK, Lee AV, Xu J, Medina D, and Donehower LA: Altered mammary gland development in the p53+/m mouse, a model of accelerated aging. Dev Biol 2008, 313:130-141

76. Kawamura T, Suzuki J, Wang YV, Menendez S, Morera LB, Raya A, Wahl GM, and Belmonte JC: Linking the p53 tumour suppressor pathway to somatic cell reprogramming. Nature 2009, 460:1140-1144

77. Li H, Collado M, Villasante A, Strati K, Ortega S, Canamero M, Blasco MA, and Serrano M: The Ink4/Arf locus is a barrier for iPS cell reprogramming. Nature 2009, 460:1136-1139

78. Marion RM, Strati K, Li H, Murga M, Blanco R, Ortega S, Fernandez-Capetillo O, Serrano M, and Blasco MA: A p53-mediated DNA damage response limits reprogramming to ensure iPS cell genomic integrity. Nature 2009, 460:1149-1153

79. Utikal J, Polo JM, Stadtfeld M, Maherali N, Kulalert W, Walsh RM, Khalil A, Rheinwald JG, and Hochedlinger K: Immortalization eliminates a roadblock during cellular reprogramming into iPS cells. Nature 2009, 460:1145-1148

80. Hong H, Takahashi K, Ichisaka T, Aoi T, Kanagawa O, Nakagawa M, Okita K, and Yamanaka S: Suppression of induced pluripotent stem cell generation by the p53-p21 pathway. Nature 2009, 460:1132-1135

81. Birch JM, Alston RD, McNally RJ, Evans DG, Kelsey AM, Harris M, Eden OB, and Varley JM: Relative frequency and morphology of cancers in carriers of germline TP53 mutations. Oncogene 2001, 20:4621-4628

82. Kleihues P, Schauble B, zur HA, Esteve J, and Ohgaki H: Tumors associated with p53 germline mutations: a synopsis of 91 families. Am J Pathol 1997, 150:1-13

83. Nichols KE, Malkin D, Garber JE, Fraumeni JF, Jr., and Li FP: Germ-line p53 mutations predispose to a wide spectrum of early-onset cancers. Cancer Epidemiol Biomarkers Prev 2001, 10:83-87

84. Jerry DJ, Kittrell FS, Kuperwasser C, Laucirica R, Dickinson ES, Bonilla PJ, Butel JS, and Medina D: A mammary-specific model demonstrates the role of the p53 tumor suppressor gene in tumor development. Oncogene 2000, 19:1052-1058

85. Rodriguez R, Rubio R, Masip M, Catalina P, Nieto A, de la CT, Arriero M, San MN, de la CE, Balomenos D, Menendez P, and Garcia-Castro J: Loss of p53 induces tumorigenesis in p21-deficient mesenchymal stem cells. Neoplasia 2009, 11:397-407

86. Alcantara LS, Chen J, Kwon CH, Jackson EL, Li Y, Burns DK, varez-Buylla A, and Parada LF: Malignant astrocytomas originate from neural stem/progenitor cells in a somatic tumor suppressor mouse model. Cancer Cell 2009, 15:45-56

87. Berman SD, Calo E, Landman AS, Danielian PS, Miller ES, West JC, Fonhoue BD, Caron A, Bronson R, Bouxsein ML, Mukherjee S, and Lees JA: Metastatic osteosarcoma induced by inactivation of Rb and p53 in the osteoblast lineage. Proc Natl Acad Sci U S A 2008,

88. Blackburn AC, Mclary SC, Naeem R, Luszcz J, Stockton DW, Donehower LA, Mohammed M, Mailhes JB, Soferr T, Naber SP, Otis CN, and Jerry DJ: Loss of heterozygosity occurs via mitotic recombination in Trp53(+/-) mice and associates with mammary tumor susceptibility of the BALB/c strain. Cancer Research 2004, 64:5140-5147

89. Kuperwasser C, Hurlbut GD, Kittrell FS, Dickinson ES, Laucirica R, Medina D, Naber SP, and Jerry DJ: Development of spontaneous mammary tumors in BALB/c p53 heterozygous mice - A model for Li-Fraumeni syndrome. American Journal of Pathology 2000, 157:2151-2159

90. Dunphy KA, Blackburn AC, Yan H, O'Connell LR, and Jerry DJ: Estrogen and progesterone induce persistent increases in p53-dependent apoptosis and suppress mammary tumors in BALB/c-Trp53+/- mice. Breast Cancer Res 2008, 10:R43

91. Lu X, Lozano G, and Donehower LA: Activities of wildtype and mutant p53 in suppression of homologous recombination as measured by a retroviral vector system. Mutat Res 2003, 522:69-83

92. Lynch CJ and Milner J: Loss of one p53 allele results in four-fold reduction of p53 mRNA and protein: a basis for p53 haplo-insufficiency. Oncogene 2006,

93. Blackburn AC, Hill LZ, Roberts AL, Wang J, Aud D, Jung J, Nikolcheva T, Allard J, Peltz G, Otis CN, Cao QJ, Ricketts RS, Naber SP, Mollenhauer J, Poustka A, Malamud D, and Jerry DJ: Genetic mapping in mice identifies DMBT1 as a candidate modifier of mammary tumors and breast cancer risk. Am J Pathol 2007, 170:2030-2041

94. Singletary SE: Rating the risk factors for breast cancer. Ann Surg 2003, 237:474-482

95. MacMahon B, Cole P, Lin TM, Lowe CR, Mirra AP, Ravnihar B, Salber EJ, Valaoras VG, and Yuasa S: Age at first birth and breast cancer risk. Bull World Health Organ 1970, 43:209-221

96. Ahmed M and Rahman N: ATM and breast cancer susceptibility. Oncogene 2006, 25:5906-5911

97. Bond GL, Hirshfield KM, Kirchhoff T, Alexe G, Bond EE, Robins H, Bartel F, Taubert H, Wuerl P, Hait W, Toppmeyer D, Offit K, and Levine AJ: MDM2 SNP309 accelerates tumor formation in a gender-specific and hormone-dependent manner. Cancer Res 2006, 66:5104-5110

98. Meijers-Heijboer H, Van Den OA, Klijn J, Wasielewski M, De Snoo A, Oldenburg R, Hollestelle A, Houben M, Crepin E, Veghel-Plandsoen M, Elstrodt F, Van Duijn C, Bartels C, Meijers C, Schutte M, McGuffog L, Thompson D, Easton DF, Sodha N, Seal S, Barfoot R, Mangion J, Chang-Claude J, Eccles D, Eeles R, Evans DG, Houlston R, Murday V, Narod S, Peretz T, Peto J, Phelan C, Zhang HX, Szabo C, Devilee P, Goldgar D, Futreal PA, Nathanson KL, Weber BL, Rahman N, and Stratton MR: Low-penetrance susceptibility to breast cancer due to CHEK2(*)1100delC in noncarriers of BRCA1 or BRCA2 mutations. Nat Genet 2002, 31:55-59

99. Sivaraman L, Stephens LC, Markaverich BM, Clark JA, Krnacik S, Conneely OM, O'Malley BW, and Medina D: Hormone-induced refractoriness to mammary carcinogenesis in Wistar-Furth rats. Carcinogenesis 1998, 19:1573-1581

100. Medina D and Kittrell FS: p53 function is required for hormone-mediated protection of mouse mammary tumorigenesis. Cancer Res 2003, 63:6140-6143

101. Siwko SK, Dong J, Lewis MT, Liu H, Hilsenbeck SG, and Li Y: Evidence that an early pregnancy causes a persistent decrease in the number of functional mammary epithelial stem cells--implications for pregnancy-induced protection against breast cancer. Stem Cells 2008, 26:3205-3209

102. Britt KL, Kendrick H, Regan JL, Molyneux G, Magnay FA, Ashworth A, and Smalley MJ: Pregnancy in the mature adult mouse does not alter the proportion of mammary epithelial stem/progenitor cells. Breast Cancer Res 2009, 11:R20

103. Smith GH, Salomon DS, and Vonderhar BK: Re: "Evidence that an early pregnancy causes a persistent decrease in the number of functional mammary epithelial stem cells-implications for pregnancy-induced protection against breast cancer" by Siwko et al. Stem Cells 2009, 27:1223-1225

104. Petitjean A, Achatz MI, Borresen-Dale AL, Hainaut P, and Olivier M: TP53 mutations in human cancers: functional selection and impact on cancer prognosis and outcomes. Oncogene 2007, 26:2157-2165

105. Ahmed M and Rahman N: ATM and breast cancer susceptibility. Oncogene 2006, 25:5906-5911

106. Bond GL, Hirshfield KM, Kirchhoff T, Alexe G, Bond EE, Robins H, Bartel F, Taubert H, Wuerl P, Hait W, Toppmeyer D, Offit K, and Levine AJ: MDM2 SNP309 accelerates tumor formation in a gender-specific and hormone-dependent manner. Cancer Res 2006, 66:5104-5110

107. Meijers-Heijboer H, Van Den OA, Klijn J, Wasielewski M, De Snoo A, Oldenburg R, Hollestelle A, Houben M, Crepin E, Veghel-Plandsoen M, Elstrodt F, Van Duijn C, Bartels C, Meijers C, Schutte M, McGuffog L, Thompson D, Easton DF, Sodha N, Seal S, Barfoot R, Mangion J, Chang-Claude J, Eccles D, Eeles R, Evans DG, Houlston R, Murday V, Narod S, Peretz T, Peto J, Phelan C, Zhang HX, Szabo C, Devilee P, Goldgar D, Futreal PA, Nathanson KL, Weber BL, Rahman N, and Stratton MR: Low-penetrance susceptibility to breast cancer due to CHEK2(*)1100delC in noncarriers of BRCA1 or BRCA2 mutations. Nat Genet 2002, 31:55-59

108. Sivaraman L, Stephens LC, Markaverich BM, Clark JA, Krnacik S, Conneely OM, O'Malley BW, and Medina D: Hormone-induced refractoriness to mammary carcinogenesis in Wistar-Furth rats. Carcinogenesis 1998, 19:1573-1581

109. Medina D and Kittrell FS: p53 function is required for hormone-mediated protection of mouse mammary tumorigenesis. Cancer Res 2003, 63:6140-6143

110. Birch JM, Alston RD, McNally RJ, Evans DG, Kelsey AM, Harris M, Eden OB, and Varley JM: Relative frequency and morphology of cancers in carriers of germline TP53 mutations. Oncogene 2001, 20:4621-4628

111. Kleihues P, Schauble B, zur HA, Esteve J, and Ohgaki H: Tumors associated with p53 germline mutations: a synopsis of 91 families. Am J Pathol 1997, 150:1-13

112. Nichols KE, Malkin D, Garber JE, Fraumeni JF, Jr., and Li FP: Germ-line p53 mutations predispose to a wide spectrum of early-onset cancers. Cancer Epidemiol Biomarkers Prev 2001, 10:83-87

113. Bertrand P, Saintigny Y, and Lopez BS: p53's double life: transactivation-independent repression of homologous recombination. Trends Genet 2004, 20:235-243

114. Gatz SA and Wiesmuller L: p53 in recombination and repair. Cell Death Differ 2006, 13:1003-1016

115. Sugrue MM, Shin DY, Lee SW, and Aaronson SA: Wild-type p53 triggers a rapid senescence program in human tumor cells lacking functional p53. Proc Natl Acad Sci U S A 1997, 94:9648-9653

116. Suzuki HI, Yamagata K, Sugimoto K, Iwamoto T, Kato S, and Miyazono K: Modulation of microRNA processing by p53. Nature 2009, 460:529-533

117. Qin H, Yu T, Qing T, Liu Y, Zhao Y, Cai J, Li J, Song Z, Qu X, Zhou P, Wu J, Ding M, and Deng H: Regulation of apoptosis and differentiation by p53 in human embryonic stem cells. J Biol Chem 2007, 282:5842-5852

118. Godar S, Ince TA, Bell GW, Feldser D, Donaher JL, Bergh J, Liu A, Miu K, Watnick RS, Reinhardt F, McAllister SS, Jacks T, and Weinberg RA: Growth-inhibitory and tumor- suppressive functions of p53 depend on its repression of CD44 expression. Cell 2008, 134:62-73

119. Zhang M, Behbod F, Atkinson RL, Landis MD, Kittrell F, Edwards D, Medina D, Tsimelzon A, Hilsenbeck S, Green JE, Michalowska AM, and Rosen JM: Identification of tumor-initiating cells in a p53-null mouse model of breast cancer. Cancer Res 2008, 68:4674-4682

120. Schmitt CA, Fridman JS, Yang M, Baranov E, Hoffman RM, and Lowe SW: Dissecting p53 tumor suppressor functions in vivo. Cancer Cell 2002, 1:289-298

121. Xue W, Zender L, Miething C, Dickins RA, Hernando E, Krizhanovsky V, Cordon-Cardo C, and Lowe SW: Senescence and tumour clearance is triggered by p53 restoration in murine liver carcinomas. Nature 2007, 445:656-660

122. Ventura A, Kirsch DG, McLaughlin ME, Tuveson DA, Grimm J, Lintault L, Newman J, Reczek EE, Weissleder R, and Jacks T: Restoration of p53 function leads to tumour regression in vivo. Nature 2007, 445:661-665

123. Walsh T and King MC: Ten genes for inherited breast cancer. Cancer Cell 2007, 11:103-105

124. Jerry DJ, Kuperwasser C, Downing SR, Pinkas J, He C, Dickinson E, Marconi S, and Naber SP: Delayed involution of the mammary epithelium in BALB/c-p53null mice. Oncogene 1998, 17:2305-2312

125. Jacks T, Remington L, Williams BO, Schmitt EM, Halachmi S, Bronson RT, and Weinberg RA: Tumor spectrum analysis in p53-mutant mice. Curr Biol 1994, 4:1-7

126. Medina D: The mammary gland: a unique organ for the study of development and tumorigenesis. J Mammary Gland Biol Neoplasia 1996, 1:5-19

127. Medina D, Kittrell FS, Shepard A, Stephens LC, Jiang C, Lu J, Allred DC, McCarthy M, and Ullrich RL: Biological and genetic properties of the p53 null preneoplastic mammary epithelium. FASEB J 2002, 16:881-883

128. Gomm JJ, Browne PJ, Coope RC, Liu QY, Buluwela L, and Coombes RC: Isolation of pure populations of epithelial and myoepithelial cells from the normal human mammary gland using immunomagnetic separation with Dynabeads. Anal Biochem 1995, 226:91-99

129. Gomm JJ, Browne PJ, Coope RC, Liu QY, Buluwela L, and Coombes RC: Isolation of pure populations of epithelial and myoepithelial cells from the normal human mammary gland using immunomagnetic separation with Dynabeads. Anal Biochem 1995, 226:91-99

130. Laws AM and Osborne BA: p53 regulates thymic Notch1 activation. Eur J Immunol 2004, 34:726-734

131. Lefort K, Mandinova A, Ostano P, Kolev V, Calpini V, Kolfschoten I, Devgan V, Lieb J, Raffoul W, Hohl D, Neel V, Garlick J, Chiorino G, and Dotto GP: Notch1 is a p53 target gene involved in human keratinocyte tumor suppression through negative regulation of ROCK1/2 and MRCKalpha kinases. Genes Dev 2007, 21:562-577

132. Smith GH, Mehrel T, and Roop DR: Differential keratin gene expression in developing, differentiating, preneoplastic, and neoplastic mouse mammary epithelium. Cell Growth Differ 1990, 1:161-170

133. Livasy CA, Karaca G, Nanda R, Tretiakova MS, Olopade OI, Moore DT, and Perou CM: Phenotypic evaluation of the basal-like subtype of invasive breast carcinoma. Mod Pathol 2006, 19:264-271

134. Sotgia F, Williams TM, Cohen AW, Minetti C, Pestell RG, and Lisanti MP: Caveolin-1-deficient mice have an increased mammary stem cell population with upregulation of Wnt/beta-catenin signaling. Cell Cycle 2005, 4:1808-1816

135. Farnie G and Clarke RB: Mammary stem cells and breast cancer--role of Notch signalling. Stem Cell Rev 2007, 3:169-175

136. Woodward WA, Chen MS, Behbod F, Alfaro MP, Buchholz TA, and Rosen JM: WNT/beta-catenin mediates radiation resistance of mouse mammary progenitor cells. Proc Natl Acad Sci U S A 2007, 104:618-623

137. Colombel M, Radvanyi F, Blanche M, Abbou C, Buttyan R, Donehower LA, Chopin D, and Thiery JP: Androgen suppressed apoptosis is modified in p53 deficient mice. Oncogene 1994, 10:1269-1274

138. Borresen-Dale AL: TP53 and breast cancer. Hum Mutat 2003, 21:292-300

139. Varley JM, Thorncroft M, McGown G, Appleby J, Kelsey AM, Tricker KJ, Evans DG, and Birch JM: A detailed study of loss of heterozygosity on chromosome 17 in tumours from Li-Fraumeni patients carrying a mutation to the TP53 gene. Oncogene 1997, 14:865-871

140. Liu X, Holstege H, van der GH, Treur-Mulder M, Zevenhoven J, Velds A, Kerkhoven RM, van Vliet MH, Wessels LF, Peterse JL, Berns A, and Jonkers J: Somatic loss of BRCA1 and p53 in mice induces mammary tumors with features of human BRCA1-mutated basal-like breast cancer. Proc Natl Acad Sci U S A 2007, 104:12111-12116

141. Halazonetis TD, Gorgoulis VG, and Bartek J: An oncogene-induced DNA damage model for cancer development. Science 2008, 319:1352-1355

142. Andrechek ER, Hardy WR, Siegel PM, Rudnicki MA, Cardiff RD, and Muller WJ: Amplification of the neu/erbB-2 oncogene in a mouse model of mammary tumorigenesis. Proc Natl Acad Sci U S A 2000, 97:3444-3449

143. Derksen PW, Liu X, Saridin F, van der GH, Zevenhoven J, Evers B, van B, Jr., Griffioen AW, Vink J, Krimpenfort P, Peterse JL, Cardiff RD, Berns A, and Jonkers J: Somatic inactivation of E-cadherin and p53 in mice leads to metastatic lobular mammary carcinoma through induction of anoikis resistance and angiogenesis. Cancer Cell 2006, 10:437-449

144. Wijnhoven SW, Zwart E, Speksnijder EN, Beems RB, Olive KP, Tuveson DA, Jonkers J, Schaap MM, van den BJ, Jacks T, van Steeg H, and de Vries A: Mice expressing a mammary gland-specific R270H mutation in the p53 tumor suppressor gene mimic human breast cancer development. Cancer Res 2005, 65:8166-8173

145. Medrano S, Burns-Cusato M, Atienza MB, Rahimi D, and Scrable H: Regenerative capacity of neural precursors in the adult mammalian brain is under the control of p53. Neurobiol Aging 2009, 30:483-497

146. Godar S, Ince TA, Bell GW, Feldser D, Donaher JL, Bergh J, Liu A, Miu K, Watnick RS, Reinhardt F, McAllister SS, Jacks T, and Weinberg RA: Growth-inhibitory and tumor- suppressive functions of p53 depend on its repression of CD44 expression. Cell 2008, 134:62-73

147. Foulkes WD, Stefansson IM, Chappuis PO, Begin LR, Goffin JR, Wong N, Trudel M, and Akslen LA: Germline BRCA1 mutations and a basal epithelial phenotype in breast cancer. J Natl Cancer Inst 2003, 95:1482-1485

148. Sorlie T, Tibshirani R, Parker J, Hastie T, Marron JS, Nobel A, Deng S, Johnsen H, Pesich R, Geisler S, Demeter J, Perou CM, Lonning PE, Brown PO, Borresen-Dale AL, and Botstein D: Repeated observation of breast tumor subtypes in independent gene expression data sets. Proc Natl Acad Sci U S A 2003, 100:8418-8423

149. Schuyer M and Berns EM: Is TP53 dysfunction required for BRCA1-associated carcinogenesis? Mol Cell Endocrinol 1999, 155:143-152

150. Milne RL, Osorio A, Cajal T, Baiget M, Lasa A, az-Rubio E, de la HM, Caldes T, Teule A, Lazaro C, Blanco I, Balmana J, Sanchez-Olle G, Vega A, Blanco A, Chirivella I, Esteban CE, Duran M, Velasco E, Martinez de DE, Tejada MI, Miramar MD, Calvo MT, Guillen-Ponce C, Salazar R, San RC, Urioste M, and Benitez J: Parity and the risk of breast and ovarian cancer in BRCA1 and BRCA2 mutation carriers. Breast Cancer Res Treat 2010, 119:221-232

151. Liu S, Ginestier C, Charafe-Jauffret E, Foco H, Kleer CG, Merajver SD, Dontu G, and Wicha MS: BRCA1 regulates human mammary stem/progenitor cell fate. Proc Natl Acad Sci U S A 2008, 105:1680-1685

152. van der ZJ: Heating the patient: a promising approach? Ann Oncol 2002, 13:1173-1184

153. Yatvin MB and Cramp WA: Role of cellular membranes in hyperthermia: some observations and theories reviewed. Int J Hyperthermia 1993, 9:165-185

154. Wust P, Hildebrandt B, Sreenivasa G, Rau B, Gellermann J, Riess H, Felix R, and Schlag PM: Hyperthermia in combined treatment of cancer. Lancet Oncol 2002, 3:487-497

155. Wust P, Stahl H, Loffel J, Seebass M, Riess H, and Felix R: Clinical, physiological and anatomical determinants for radiofrequency hyperthermia. Int J Hyperthermia 1995, 11:151-167

156. Perez CA, Scott C, Emami B, Hornback NB, Sneed PK, Asbell SO, and Janjan NA: Evaluation of 45 degrees C hyperthermia and irradiation. II. A phase I clinical trial in humans by the Radiation Therapy Oncology Group. Am J Clin Oncol 1993, 16:477-481

157. Castren-Persons M, Lipasti J, Puolakkainen P, and Schroder T: Laser-induced hyperthermia: comparison of two different methods. Lasers Surg Med 1992, 12:665-668

158. Clement GT and Hynynen K: A non-invasive method for focusing ultrasound through the human skull. Phys Med Biol 2002, 47:1219-1236

159. Mitsumori M, Hiraoka M, Okuno Y, Nishimura Y, Li YP, Fujishiro S, Nagata Y, Abe M, Koishi M, Sano T, Marume T, and Takayama N: A phase I and II clinical trial of a newly developed ultrasound hyperthermia system with an improved planar transducer. Int J Radiat Oncol Biol Phys 1996, 36:1169-1175

160. Deger S, Boehmer D, Turk I, Roigas J, Budach V, and Loening SA: Interstitial hyperthermia using self-regulating thermoseeds combined with conformal radiation therapy. Eur Urol 2002, 42:147-153

161. Park BH, Koo BS, Kim YK, and Kim MK: The induction of hyperthermia in rabbit liver by means of duplex stainless steel thermoseeds. Korean J Radiol 2002, 3:98-104

162. Hirsch LR, Stafford RJ, Bankson JA, Sershen SR, Rivera B, Price RE, Hazle JD, Halas NJ, and West JL: Nanoshell-mediated near-infrared thermal therapy of tumors under magnetic resonance guidance. Proc Natl Acad Sci U S A 2003, 100:13549-13554

163. Loo C, Lowery A, Halas N, West J, and Drezek R: Immunotargeted nanoshells for integrated cancer imaging and therapy. Nano Lett 2005, 5:709-711

164. Huang X, El-Sayed IH, Qian W, and El-Sayed MA: Cancer cell imaging and photothermal therapy in the near-infrared region by using gold nanorods. J Am Chem Soc 2006, 128:2115-2120

165. Kam NW, O'Connell M, Wisdom JA, and Dai H: Carbon nanotubes as multifunctional biological transporters and near-infrared agents for selective cancer cell destruction. Proc Natl Acad Sci U S A 2005, 102:11600-11605

166. Hilger I, Hergt R, and Kaiser WA: Use of magnetic nanoparticle heating in the treatment of breast cancer. IEE Proc Nanobiotechnol 2005, 152:33-39

167. Lin MM, Kim dK, El Haj AJ, and Dobson J: Development of superparamagnetic iron oxide nanoparticles (SPIONS) for translation to clinical applications. IEEE Trans Nanobioscience 2008, 7:298-305

168. Duguet E, Vasseur S, Mornet S, and Devoisselle JM: Magnetic nanoparticles and their applications in medicine. Nanomed 2006, 1:157-168

169. Ito A, Tanaka K, Kondo K, Shinkai M, Honda H, Matsumoto K, Saida T, and Kobayashi T: Tumor regression by combined immunotherapy and hyperthermia using magnetic nanoparticles in an experimental subcutaneous murine melanoma. Cancer Sci 2003, 94:308-313

170. Hilger I, Andra W, Hergt R, Hiergeist R, Schubert H, and Kaiser WA: Electromagnetic heating of breast tumors in interventional radiology: in vitro and in vivo studies in human cadavers and mice. Radiology 2001, 218:570-575

171. Minamimura T, Sato H, Kasaoka S, Saito T, Ishizawa S, Takemori S, Tazawa K, and Tsukada K: Tumor regression by inductive hyperthermia combined with hepatic embolization using dextran magnetite-incorporated microspheres in rats. Int J Oncol 2000, 16:1153-1158

172. Jordan A, Scholz R, Wust P, Schirra H, Schiestel T, Schmidt H, and Felix R: Endocytosis of dextran and silan-coated magnetite nanoparticles and the effect of intracellular hyperthermia on human mammary carcinoma cells in vitro. Journal of Magnetism and Magnetic Materials 1999, 194:185-196

173. Johannsen M, Thiesen B, Gneveckow U, Taymoorian K, Waldofner N, Scholz R, Deger S, Jung K, Loening SA, and Jordan A: Thermotherapy using magnetic nanoparticles combined with external radiation in an orthotopic rat model of prostate cancer. Prostate 2006, 66:97-104

174. DeNardo SJ, DeNardo GL, Miers LA, Natarajan A, Foreman AR, Gruettner C, Adamson GN, and Ivkov R: Development of tumor targeting bioprobes ((111)In-chimeric L6 monoclonal antibody nanoparticles) for alternating magnetic field cancer therapy. Clin Cancer Res 2005, 11:7087s-7092s

175. Ivkov R, DeNardo SJ, Daum W, Foreman AR, Goldstein RC, Nemkov VS, and DeNardo GL: Application of high amplitude alternating magnetic fields for heat induction of nanoparticles localized in cancer. Clin Cancer Res 2005, 11:7093s-7103s

176. Rosensweig RE: Heating magnetic fluid with alternating magnetic field. Journal of Magnetism and Magnetic Materials 2002, 252:370-374

177. Grant ER, Errico MA, Emanuel SL, Benjamin D, McMillian MK, Wadsworth SA, Zivin RA, and Zhong Z: Protection against glutamate toxicity through inhibition of the p44/42 mitogen-activated protein kinase pathway in neuronally differentiated P19 cells. Biochem Pharmacol 2001, 62:283-296

178. Liu S, Kawai K, Tyurin VA, Tyurina YY, Borisenko GG, Fabisiak JP, Quinn PJ, Pitt BR, and Kagan VE: Nitric oxide-dependent pro-oxidant and pro-apoptotic effect of metallothioneins in HL-60 cells challenged with cupric nitrilotriacetate. Biochem J 2001, 354:397-406

179. Cengelli F, Maysinger D, Tschudi-Monnet F, Montet X, Corot C, Petri-Fink A, Hofmann H, and Juillerat-Jeanneret L: Interaction of functionalized superparamagnetic iron oxide nanoparticles with brain structures. J Pharmacol Exp Ther 2006, 318:108-116

180. Samanta B, Yan H, Fischer NO, Shi J, Jerry DJ, and Rotello VM: Protein-passivated Fe(3)O(4) nanoparticles: low toxicity and rapid heating for thermal therapy. J Mater Chem 2008, 18:1204-1208

181. Zhang Y, Kohler N, and Zhang M: Surface modification of superparamagnetic magnetite nanoparticles and their intracellular uptake. Biomaterials 2002, 23:1553-1561

182. Jordan A, Wust P, Fahling H, John W, Hinz A, and Felix R: Inductive heating of ferrimagnetic particles and magnetic fluids: physical evaluation of their potential for hyperthermia. Int J Hyperthermia 1993, 9:51-68

183. Jordan A, Wust P, Scholz R, Tesche B, Fahling H, Mitrovics T, Vogl T, Cervos-Navarro J, and Felix R: Cellular uptake of magnetic fluid particles and their effects on human adenocarcinoma cells exposed to AC magnetic fields in vitro. Int J Hyperthermia 1996, 12:705-722

184. Choi H, Choi SR, Zhou R, Kung HF, and Chen IW: Iron oxide nanoparticles as magnetic resonance contrast agent for tumor imaging via folate receptor-targeted delivery. Acad Radiol 2004, 11:996-1004

185. Simberg D, Duza T, Park JH, Essler M, Pilch J, Zhang L, Derfus AM, Yang M, Hoffman RM, Bhatia S, Sailor MJ, and Ruoslahti E: Biomimetic amplification of nanoparticle homing to tumors. Proc Natl Acad Sci U S A 2007, 104:932-936

186. Kikumori T, Kobayashi T, Sawaki M, and Imai T: Anti-cancer effect of hyperthermia on breast cancer by magnetite nanoparticle-loaded anti-HER2 immunoliposomes. Breast Cancer Res Treat 2008,

187. Gupta AK and Gupta M: Synthesis and surface engineering of iron oxide nanoparticles for biomedical applications. Biomaterials 2005, 26:3995-4021

188. Alexiou C, Schmid RJ, Jurgons R, Kremer M, Wanner G, Bergemann C, Huenges E, Nawroth T, Arnold W, and Parak FG: Targeting cancer cells: magnetic nanoparticles as drug carriers. Eur Biophys J 2006, 35:446-450

189. Scarberry KE, Dickerson EB, McDonald JF, and Zhang ZJ: Magnetic Nanoparticle-Peptide Conjugates for in Vitro and in Vivo Targeting and Extraction of Cancer Cells. J Am Chem Soc 2008,

190. Dontu G, El Ashry D, and Wicha MS: Breast cancer, stem/progenitor cells and the estrogen receptor. Trends Endocrinol Metab 2004, 15:193-197

191. Dontu G, Abdallah WM, Foley JM, Jackson KW, Clarke MF, Kawamura MJ, and Wicha MS: In vitro propagation and transcriptional profiling of human mammary stem/progenitor cells. Genes Dev 2003, 17:1253-1270

192. Hochedlinger K and Jaenisch R: Nuclear reprogramming and pluripotency. Nature 2006, 441:1061-1067

193. Takahashi K and Yamanaka S: Induction of pluripotent stem cells from mouse embryonic and adult fibroblast cultures by defined factors. Cell 2006, 126:663-676

194. Takahashi K, Tanabe K, Ohnuki M, Narita M, Ichisaka T, Tomoda K, and Yamanaka S: Induction of pluripotent stem cells from adult human fibroblasts by defined factors. Cell 2007, 131:861-872